AD-A152 346 AN ASSESSMENT OF ATMOSPHERIC REFRACTIVITY IN THE NORTHERN MARGINAL ICE ZONE(U) NAVAL POSTGRADUATE SCHOOL MONTEREY CA C T SUTHERLIN SEP 84 1/2

UNCLASSIFIED F/G 4/1 NL

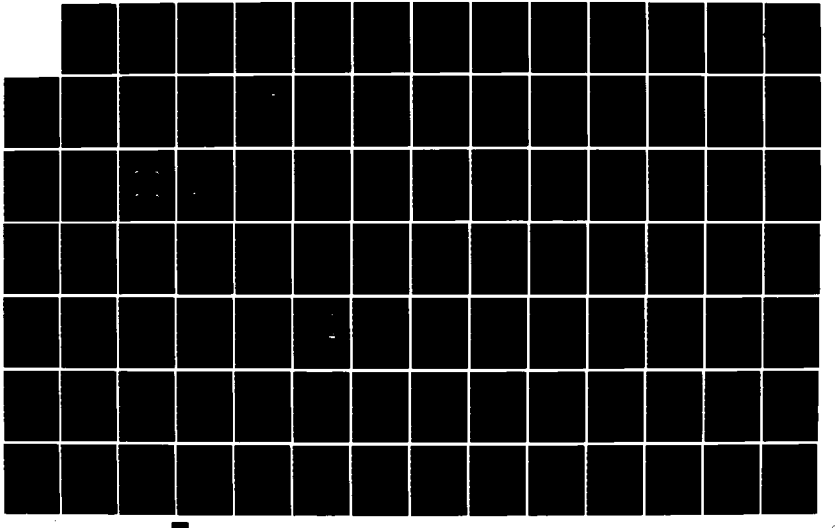

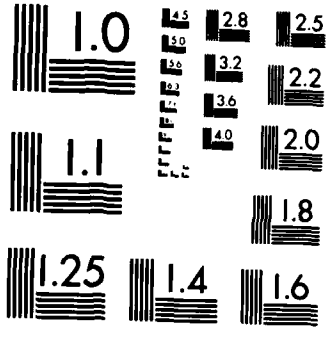

MICROCOPY RESOLUTION TEST CHART
NATIONAL BUREAU OF STANDARDS-1963-A

NAVAL POSTGRADUATE SCHOOL
Monterey, California

THESIS

AN ASSESSMENT OF ATMOSPHERIC REFRACTIVITY
IN THE NORTHERN MARGINAL ICE ZONE

by

Charles Thomas Sutherlin

September 1984

Thesis Advisor: William J. Shaw

Approved for public release; distribution unlimited

UNCLASSIFIED

SECURITY CLASSIFICATION OF THIS PAGE (When Data Entered)

REPORT DOCUMENTATION PAGE		READ INSTRUCTIONS BEFORE COMPLETING FORM
1. REPORT NUMBER	2. GOVT ACCESSION NO.	3. RECIPIENT'S CATALOG NUMBER
4. TITLE (and Subtitle) An Assessment of Atmospheric Refractivity in the Northern Marginal Ice Zone		5. TYPE OF REPORT & PERIOD COVERED Master's Thesis September 1984 6. PERFORMING ORG. REPORT NUMBER
7. AUTHOR(s) Charles Thomas Sutherlin		8. CONTRACT OR GRANT NUMBER(s)
9. PERFORMING ORGANIZATION NAME AND ADDRESS Naval Postgraduate School Monterey, California 93943		10. PROGRAM ELEMENT, PROJECT, TASK AREA & WORK UNIT NUMBERS
11. CONTROLLING OFFICE NAME AND ADDRESS Naval Postgraduate School Monterey, California 93943		12. REPORT DATE September 1984 13. NUMBER OF PAGES 118
14. MONITORING AGENCY NAME & ADDRESS(if different from Controlling Office)		15. SECURITY CLASS. (of this report) 15a. DECLASSIFICATION/ DOWNGRADING SCHEDULE

16. DISTRIBUTION STATEMENT (of this Report)

Approved for public release, distribution unlimited

17. DISTRIBUTION STATEMENT (of the abstract entered in Block 20, if different from Report)

18. SUPPLEMENTARY NOTES

19. KEY WORDS (Continue on reverse side if necessary and identify by block number)

Marginal Ice Zone
MIZEX-83
Electromagnetic Wave Propagation
Atmospheric Refractivity
Atmospheric Duct
Ducting
IREPS

20. ABSTRACT (Continue on reverse side if necessary and identify by block number)

This thesis presents an analysis of atmospheric refractivity conditions in the Arctic Marginal Ice Zone. The fundamental principles of atmospheric effects on electromagnetic wave propagation are presented along with methods to assess these effects. Using these principles, a determination of the occurrence of atmospheric ducts is made from meteorological data gathered during the Arctic Marginal Ice Zone Exercise, 1983, MIZEX-83. The optimum coupling height, thickness and intensity

DD FORM 1 JAN 73 1473 EDITION OF 1 NOV 65 IS OBSOLETE

S N 0102-LF-014-6601

of each duct are calculated and statistically compared. Duct occurrence is related to area meteorological conditions. Based on area refractivity, the potential for enhanced electronic warfare operations is evaluated.

Approved for public release; distribution unlimited

A Study of Ducting Conditions in the Northern Marginal Ice Zone

by

Charles Thomas Sutherlin
Lieutenant Commander, United States Navy
B.S., North Carolina State University, 1970

Submitted in partial fulfillment of the
requirements for the degree of

MASTER OF SCIENCE IN SYSTEM ENGINEERING
(ELECTRONIC WARFARE)

from the

NAVAL POSTGRADUATE SCHOOL
September, 1984

Author: _____
Charles T. Sutherlin, LCDR, USN

Approved by: _____
Professor William J. Shaw, Thesis Advisor

_____
Professor K.L. Davidson, Second Reader

_____
Professor John M. Bouldry
Chairman, Electronic Warfare Academic Group

_____
Dr. David A. Schrady, Academic Dean

ABSTRACT

This thesis presents an analysis of atmospheric refractivity conditions in the arctic Marginal Ice Zone. The fundamental principles of atmospheric effects on electromagnetic wave propagation are presented along with methods to assess these effects. Using these principles, a determination of the occurrence of atmospheric ducts is made from meteorological data gathered during the Arctic Marginal Ice Zone Exercise, 1983 (MIZEX-83). The optimum coupling height, thickness and intensity for all ducts are calculated and statistically analyzed. Duct occurrence is related to area meteorological conditions. Based on area refractivity, the potential for enhanced area electronic warfare operations is evaluated.

TABLE OF CONTENTS

LIST OF FIGURES

LIST OF TABLES

ACKNOWLEDGEMENT

I wish to express my sincere appreciation to Professor William J. Shaw for his guidance and assistance during the preparation of this thesis. I am also very grateful to the people who conducted MIZEX-83 for providing the data used in this analysis.

I wish to dedicate this thesis to my wife, Theresa, who made the greatest sacrifice for this project. For, without her love, devotion and understanding, this work would not have been possible.

I. INTRODUCTION

A. BACKGROUND

Modern Naval warfare will rely heavily on command and control communications (C^3), command and control communications countermeasures (C^3CM) as well as weapons guidance and other electronic warfare support systems. All systems employed for these purposes propagate electromagnetic energy in the electromagnetic frequency spectrum (Table 1), and all are affected, to some extent, by the meteorological environment in which they are operated. A more detailed description of the electromagnetic spectrum can be found in Tipler (1976). Task force commanders will be able to gain a decided advantage if they can determine which systems will be enhanced and which will be degraded and use this information in making their tactical decisions.

Various projects to study meteorological conditions and document atmospheric anomalies that affect electromagnetic wave propagation have been conducted in the more common Naval operating areas of the world such as the Mediterranean and Indian oceans. Throughout the world, meteorological data are gathered daily. A comprehensive statistical analysis of this data has been conducted by Leigh N. Orthenburger of GTE Sylvania (Orthenburger, et al., 1978). Meteorological conditions in the area around the northern ice pack have just recently gained interest. An experiment

III. ATMOSPHERIC EFFECTS ON ELECTROMAGNETIC WAVE PROPAGATION

The atmosphere contains two specific regions, the troposphere and the ionosphere, that have a dramatic effect on electromagnetic wave propagation. The ionosphere extends from approximately 31 km to 400 km above the Earth's surface and is composed of layers of ionized molecules that refract electromagnetic waves in the high frequency portion of the spectrum (3 to 30 MHz). Between the surface of the Earth and the upper atmosphere, extending up to about 12 km, is the troposphere. Refractive conditions in the troposphere primarily affect signals at frequencies above the high frequency band. The troposphere is an inhomogeneous dielectric medium made up of various constituents. Concentrations of permanent gases, such as oxygen and nitrogen, remain relatively constant; however, concentrations water vapor and aerosols such as suspended organic and inorganic matter vary greatly. Also, fog, rain, snow, smoke and dust can frequently be present. These molecules all have their particular resonant frequencies and dipole characteristics. Electromagnetic waves coming in contact with or in close proximity to these molecules can be absorbed, scattered or refracted depending upon the frequency of the electromagnetic wave and the characteristics of the molecule. As such, electromagnetic waves transmitted in or entering the troposphere are

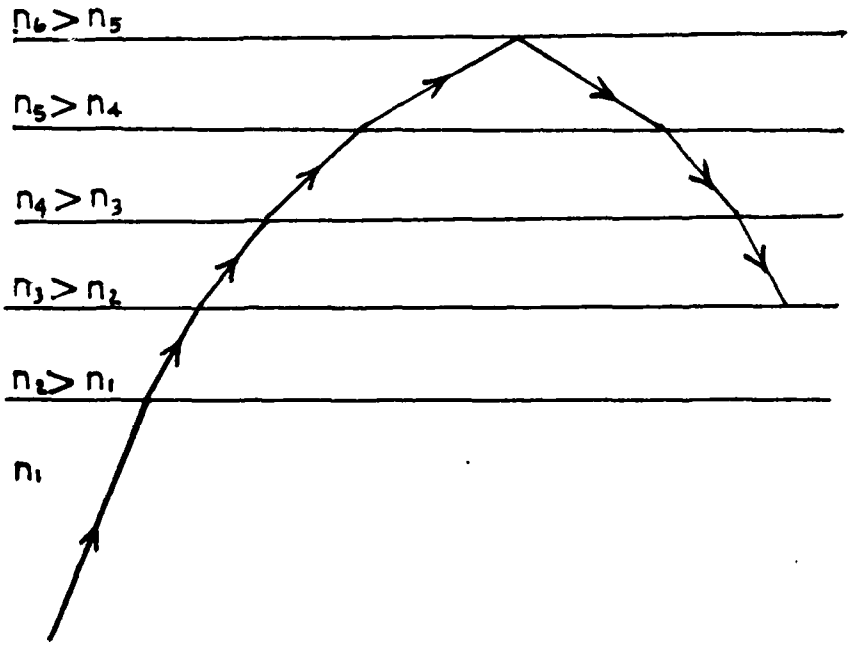

FIGURE 5

Continuous Refraction of a Wave when Encountering a Refractive Gradient of Successive Dielectric Layers with Increasing Indices of Refraction

the angle of refraction θ_c equal to 90 degrees (Tipler 1976).

$$\text{SIN } \theta_c = n_2/n_1 \qquad (5.6)$$

Thus far, only the case of a wave encountering a single discontinuity in the index of refraction has been considered. However, if successive dielectric layers, each constituting a discontinuity, are stacked one upon the other, a refractive gradient can be approximated as shown in figure 5. As these layers become differentially small, the wave can be refracted , in the example in figure 5, downward. Further, if the wave is propagated within the critical acceptance angle, it can be trapped within the gradient.

The basic concepts of electromagnetic wave propagation in a homogeneous dielectric medium can also be used to describe propagation in an inhomogeneous dielectric medium like the atmosphere. However, unlike a homogeneous, isotropic dielectric medium, the atmosphere can be characterized by continuously changing values of refractive gradient throughout a given vertical cross section. This property of the atmosphere where refractive index changes with altitude gives rise to atmospheric phenomena having unique effects on electromagnetic wave propagation. These effects and the meteorological conditions that cause them will be described in chapter III.

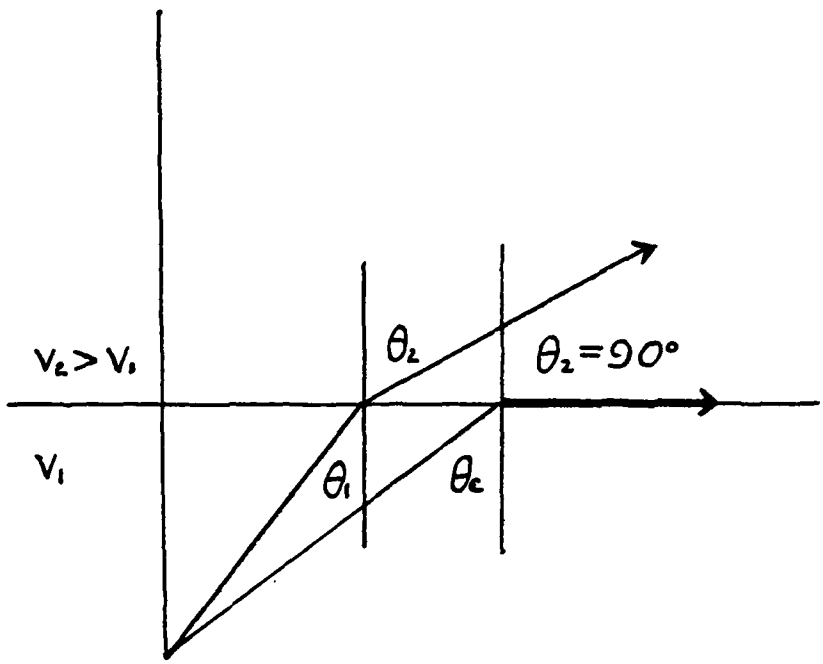

FIGURE 4

Total Internal Reflection
Critical Angle

toward the greater n. Air, in this example, has an index of refraction which limits the speed of the propagating ray to a velocity v_1. Likewise, the water has a different index of refraction which limits the speed of the ray to a slower velocity v_2. Consequently, distances traveled by the ray in the two media in the same time are not the same, resulting in a change in the direction of the wave as the wavefront passes through the discontinuity boundary. The following equation, which is Snell's law, can be derived by applying geometric arguments to the drawing in figure 3 (Tipler 1976).

$$n_1 \text{ SIN } \theta_1 = n_2 \text{ SIN } \theta_2 \qquad (2.4)$$

Equation (2.12) can be solved for θ_2 yielding

$$\text{SIN } \theta_2 = n_1/n_2 \text{ SIN } \theta_1 \qquad (2.5)$$

If n_2 is greater than n_1, equation (2.5) can be solved for the angle of refraction θ_2 for any angle of incidence θ_1. If n_2 is less than n_1, equation (2.13) gives values for sine greater than 1 if the angle of incidence is greater than some critical angle θ_c. Since the value of the sine function cannot be greater than 1, this implies that there is an angle of incidence, beyond which, the wave will be totally reflected into the incident medium. The critical angle, as shown in figure 4, is defined as the angle which makes

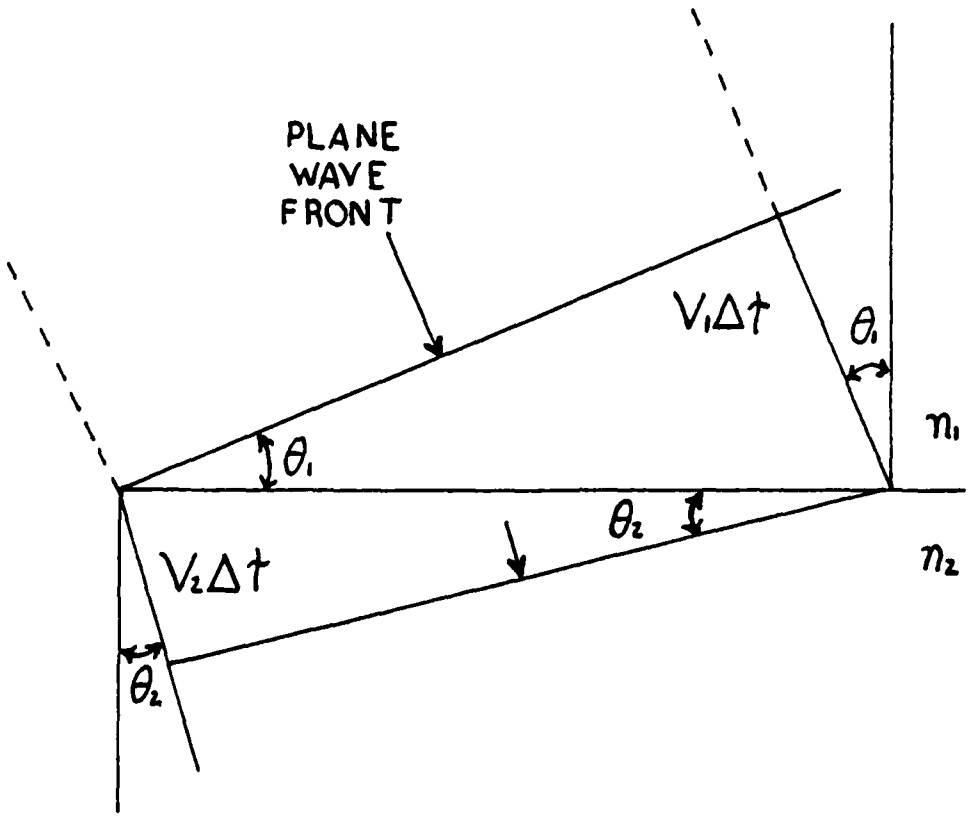

FIGURE 3

Refraction of Plane Waves at the Surface of an Index of Refraction Discontinuity

2. Description of Refraction

The ratio of the speed of an electromagnetic wave in free space to that in a dielectric medium is known as the absolute index of refraction n. The index of refraction is also equal to the square root of the dielectric constant (Hecht and Zajac, 1979).

$$n = C/V = (K)^{1/2} \qquad (2.3)$$

Where:

C = The speed of light
V = Speed in the medium

Since the speed of propagation in a dielectric medium cannot be greater than that in free space, n will always be greater than or equal to 1.0. According to Hecht and Zajac (1979), the index of refraction for air varies between 1.0003 and 1.0005.

When an electromagnetic wave encounters a discontinuity in n like a light ray going from air to water, the path of the incident wave will be bent or refracted. Figure 3 depicts a light wave passing from air into water. Since light propagates as an electromagnetic wave, a wave front is used here to illustrate the refractive process. Similar refractive conditions can exist between any two dielectric media with differing indices of refraction, such as two differing air masses. As the index of refraction for water is greater than for air (1.33 as opposed to 1.0003), n_2 is greater than n_1 and it can be seen that the wave bends

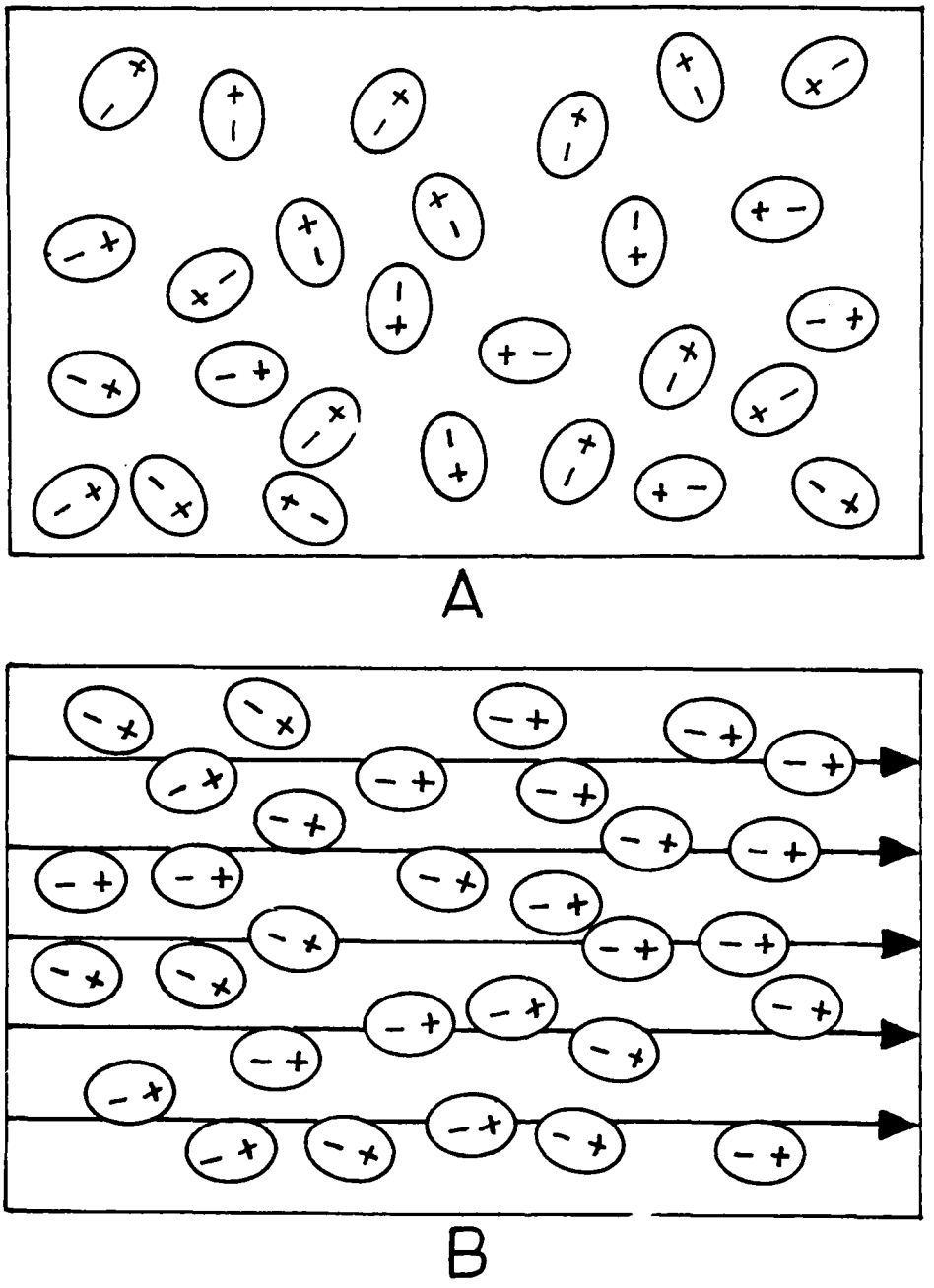

FIGURE 2

(a) Randomly Oriented Polar Molecules in a Dielectric Medium. (b) Polar Molecules Oriented in Direction of Propagation in the Presence of an Electromagnetic Wave

dipole moment as a result of unequal sharing of valence electrons (Figure 2a). When a dielectric medium is subject to an applied electric field, the internal charge distribution distorts under its influence. This corresponds to the generation of electric dipole moments. These dipole moments experience a torque, which tends to align them in the direction of the field (Figure 2b). This alignment of the molecular dipoles produces an additional electric field due to the dipoles which is in the direction opposite the original field. The original field is weakened in this way. Even if the molecules of the dielectric medium are nonpolar, they will experience an induced dipole moment (in the direction of the original field) in the presence of the electric field of the propagating wave. Here again, the additional electric field due to these induced moments weakens the original field (Tipler, 1976).

The interaction of a dielectric medium with a propagating electromagnetic wave is described by the dielectric constant K of the medium. If E_0 is the original field without the dielectric, the new field E is

$$E = E_0/K \qquad (2.1)$$

The dielectric constant is the ratio of the magnitude of the field in free space to the field in the dielectric medium.

$$K = E_0/E \qquad (2.2)$$

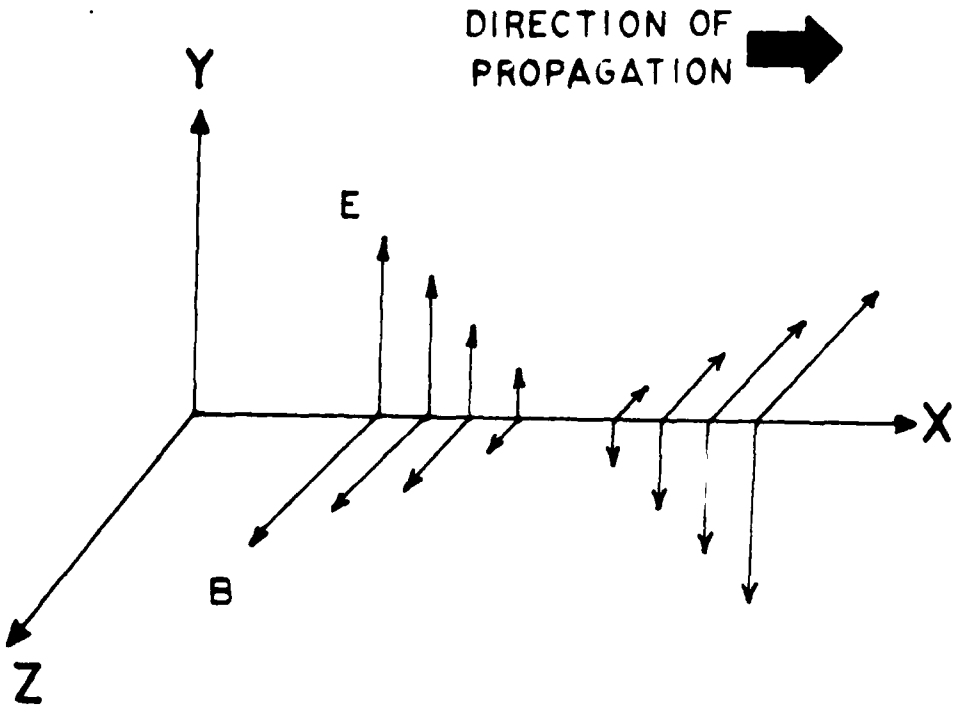

FIGURE 1

Electric and Magnetic Field Vectors in a Plane Electromagnetic Wave

II. ELECTROMAGNETIC WAVE PROPAGATION

A. PROPAGATION IN FREE SPACE

James Clerk Maxwell demonstrated that electromagnetic waves, in free space, propagate in a straight line at the speed of light (Tipler, 1976).

Maxwell showed that electromagnetic wave propagation can be graphically displayed on a three dimensional (XYZ) plot as shown in figure 1. Note that the electric field (Ey) and the magnetic field (B_Z) are orthogonal to each other and that the direction of propagation is parallel to the vector ($\bar{E}$ X $\bar{B}$) and is in the X direction.

This property of propagation in a straight line and at the speed of light is common to electromagnetic waves of all wavelengths as long as the propagation path is in a vacuum. Electromagnetic waves can also be propagated in media such as water, glass and the Earth's atmosphere. However, when this happens, the propagation path can be altered by the medium.

B. EFFECTS OF A DIELECTRIC MEDIUM ON PROPAGATION

1. Description of a Dielectric Medium

When an electromagnetic wave is transmitted in a homogeneous, isotropic dielectric medium, the medium tends to resist the wave and the net effect is to reduce the propagation speed. The medium can be modeled as consisting of numerous randomly oriented molecules which have a

electromagnetic wave propagation exist and to correlate these findings to the overall meteorological conditions in the area. This "area refractivity summary" can then be used by tactical commanders operating in the area.

C. ORGANIZATION

The first portion of this thesis (Chapters II and III) describes the basic concepts necessary to understand the data analysis process. Chapter II deals with basic electromagnetic wave propagation in free space and how these waves can be refracted in a generic, homogeneous dielectric medium such as glass or water. Chapter III covers the atmosphere. Atmospheric refractivity is introduced and related to atmospheric temperature, pressure and humidity. The concept of changing refractivity with altitude or refractivity gradients is presented here and it is shown how to use these gradients to detect atmospheric anomalies that can affect propagation. Chapter III also describes refractivity assessment methods.

The final portion of this thesis deals with data analysis and conclusions. In chapter IV, data acquisition and analysis methods are described. A compilation of the data is presented along with results. Chapter V consists of an area refractivity summary, an application of this summary to electronic warfare and recommendations. Data are contained in the appendices.

was begun in the summer of 1983 to determine and evaluate those meteorological factors which significantly affect or are affected by the position of the ice edge. The Marginal Ice Zone Experiment, 1983 (MIZEX-83) is the first large scale effort to assess meteorological conditions in the northern marginal ice zone (MIZ). Now that interest and the level of research in the MIZ has risen, the U.S. Army Cold Regions Research and Engineering Laboratory publishes the MIZEX Bulletin series which consists of articles on the results of meteorological and oceanographic research being done in the area. Interest in the MIZ has led to the development of an area atmospheric boundary layer model by J.E. Overland (Overland, et al., 1983) and a wind drag coefficient study by S.A. Macklin (Macklin, 1983). These and other related reports can be found in the March 30, 1983 issue of the Journal of Geophysical Research which is a special issue on the marginal ice zone. Data gathered during MIZEX-83 will be the basis of this thesis.

B. PURPOSE

Thus far, research on the MIZ has dealt with the climatology of the area. Minimal work has been done to correlate area meteorological conditions and atmospheric refractivity. The purpose of this thesis is to analyze meteorological data gathered during MIZEX-83; to report findings on the degree to which atmospheric anomalies that affect

TABLE 1

ELECTROMAGNETIC SPECTRUM SUMMARY

FREQUENCY BAND	FREQUENCY	PRIMARY METHOD OF PROPAGATION	TYPICAL MAXIMUM DISTANCE IN (NAUTICAL MILES)
Very Low (VLF)	3-30 KHz	Ground Wave	5000
Low (LF)	30-300 KHz	Ground Wave Sky Wave	1000-5000
Medium (MF)	300-3000 KHz	Ground Wave Sky Wave	100-1000 1000-3000
High (HF)	3-30 MHz	Ground Wave	10-100 100-250 (1 hop) 100-1200 (>1 hop)
Very High (VHF)	30-300 MHz	Scatter Line of Sight	600-1200 100 (comm) 300 (radar)
Ultra-High (UHF)	.3-3 GHz	Scatter Line of Sight	30-400 100 (comm) 300 (radar)
Super-High (SHF)	3-30 GHz	Line of Sight	100 (comm) 300 (radar)
Extremely-High (EHF)	30-300 GHz	Line of Sight	100
Infrared (IR)	1-400 THz	Line of Sight	5
Optical	400-800 THz	Line of Sight	0-100

subject to the classical dielectric effects described in chapter II.

The troposphere is constantly in a state of change with different layers, air masses, wind conditions, and temperature and pressure levels. Generally, humidity, temperature and pressure change with altitude and so does the index of refraction. It will be shown later in this chapter how the index of refraction can be redefined in terms of humidity, temperature and pressure. Within the troposphere, layers with different indices of refraction can form because of variations in humidity, temperature and pressure. If, because of changes in these conditions, refraction decreases with altitude much faster than normal, an atmospheric duct can be formed. Variations in humidity, temperature and pressure sufficient to cause a duct are a direct product of the existing weather conditions.

This chapter will present a description of the atmospheric parameters and mechanisms involved in duct formation and will describe how vertical measurements of tropospheric humidity, temperature and pressure can be used to calculate refractive gradients. Finally, it will be shown how analysis of these gradients can provide predictions of atmospheric effects on electromagnetic wave propagation.

A. DUCTING AND REFRACTION

1. Duct Formation

As stated, electromagnetic waves in the high frequency band can be refracted back to the Earth by the ionosphere. These waves can then be reflected from the Earth's surface back to the ionosphere to be refracted again. As this process is repeated, these waves can propagate for thousands of miles. Electromagnetic waves in the VHF, UHF and SHF frequency bands (see table 1) are unaffected by the ionosphere. However, if an electromagnetic wave in one of these frequency bands encounters a gradient of refractive index and is within a critical angle, it can be refracted back toward the surface of the Earth. In this way, the wave can be channeled along the curvature of the Earth. This region is called an atmospheric duct and the preceding case was an example of an elevated duct. Duct types will be covered in detail later in this chapter. Electromagnetic waves in a duct are directed much like electromagnetic waves in a wave guide and ranges can be extended far beyond the horizon as shown in figure 6. Ducts are primarily caused by warm dry air overriding cool moist air resulting in a temperature inversion. It can be seen from figure 7 (Helvey and Rosenthal, 1983, adapted from the GTE Sylvania Report) that this happens with regularity throughout the ocean areas of the world.

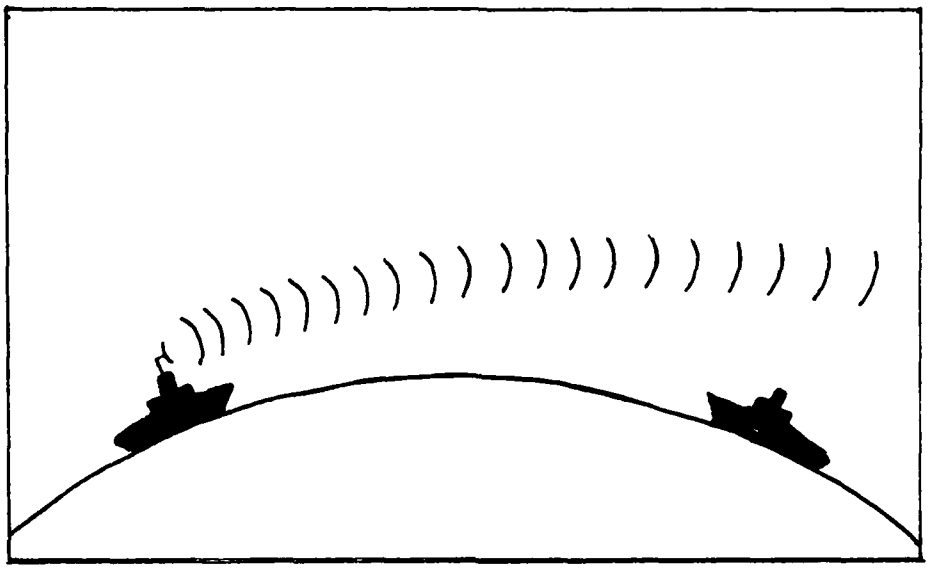

A

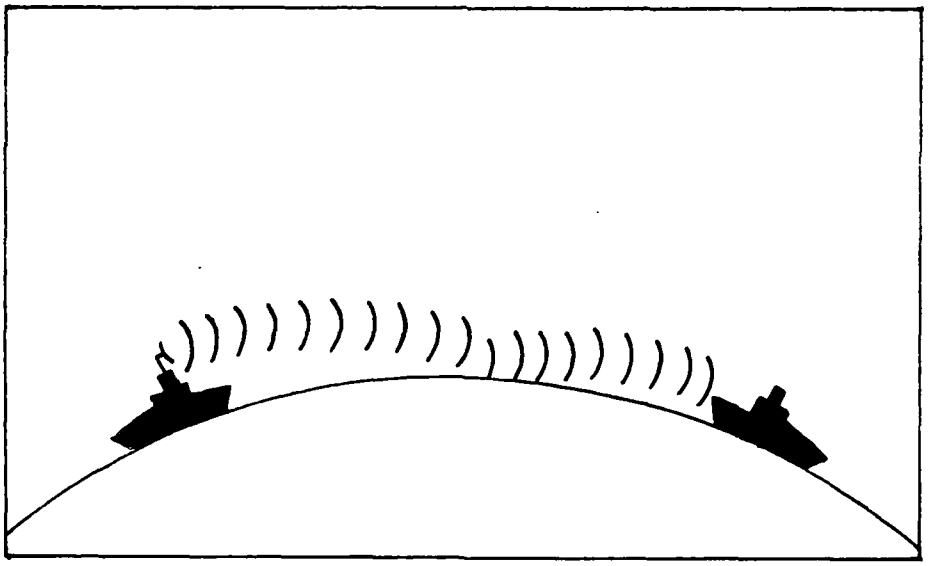

B

FIGURE 6

(a) Radar Wave Propagation under "Standard" Atmospheric Conditions. (b) Radar Wave Propagation Path in a Surface Duct. Reproduced from IREPS Manual

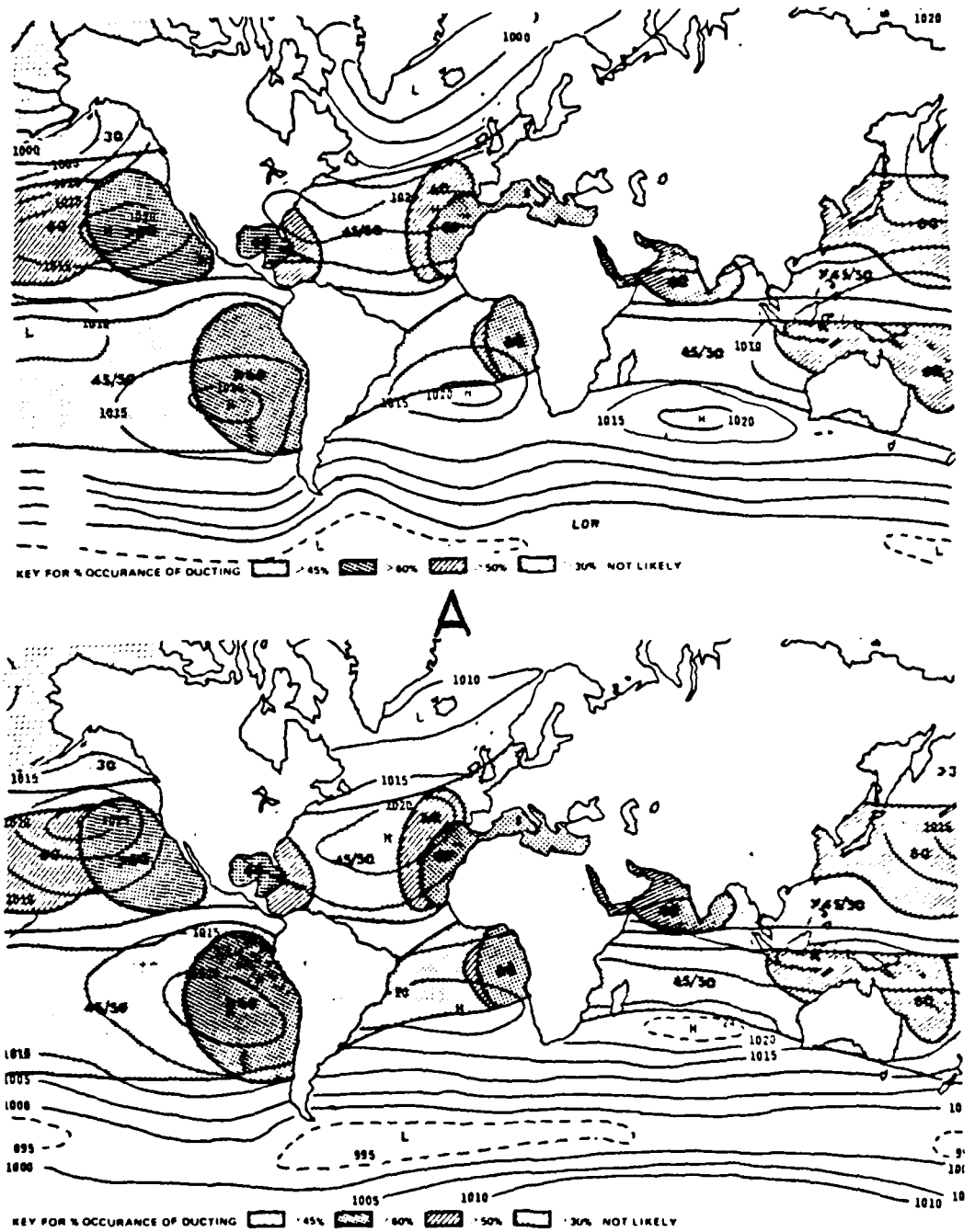

FIGURE 7

Mean Annual Frequency of Ducting (a) Winter, (b) Summer
From GTE Sylvania Report

2. Refractivity

The index of refraction can be scaled to yield atmospheric refractivity N. N is related to n by:

$$N = (n-1) \times 10^6 \qquad (3.1)$$

When expressed in terms of the atmospheric parameters pressure P in millibars, temperature T in degrees Kelvin and water vapor pressure e in millibars, N becomes (Kerr, 1951):

$$N = [(77.6\ P/T) + (3.73 \times 10^5\ e/T^2)] \qquad (3.2)$$

Refractivity can be directly calculated from humidity, temperature and pressure. But, refractivity at any given altitude is not an important parameter by itself. A vertical profile of N , N values plotted against altitude, or a plot of the change in N with respect to the change in altitude (dN/dz) provides a graphic method by which a duct can be identified. However, identifying a duct and defining its boundaries using the N profile requires the use of an overlay and is a cumbersome technique. To make the determination of duct occurrence more convenient, modified refractivity has been developed.

3. Modified Refractivity

Modified refractivity M takes the Earth's curvature into account and allows quick identification of

ducting whenever M values decrease with altitude. M is related to N by:

$$M = N + (z/a) \times 10^6 \qquad (3.3)$$

where z is equal to altitude in kilometers and a is the mean Earth radius in kilometers. Using a mean Earth radius of 6.37×10^3 KM, $10^6/a$ equals 157 KM^{-1}. Now M can be expressed as

$$M = N + 157z \text{ for } z \text{ in kilometers} \qquad (3.4)$$

For the Standard Atmosphere where there are no well defined layers or inversions, temperature and pressure decrease with altitude. As shown in figure 8, N decreases and M increases in these standard conditions. A complete derivation of the refractivity and modified refractivity formulae is given by Kerr (1951).

4. Trapping

A trapping layer exists when dN/dz is less than -157 or dM/dz is less than zero. Figure 9 shows representative M and N profiles for an elevated trapping layer. Under these conditions the electromagnetic wave will be bent down relative to the Earth. For a wave to be trapped, a ducting condition must exist where the wave is trapped between the upper and lower boundaries of the duct. Trapped means the energy transmitted within the critical

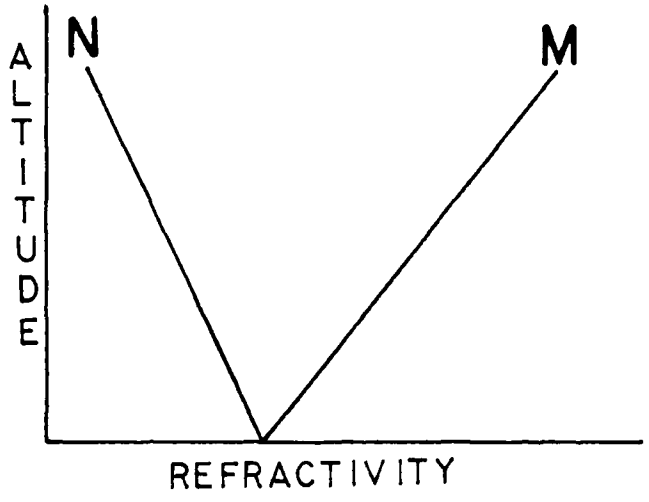

FIGURE 8

M and N Profiles for Standard Atmosphere

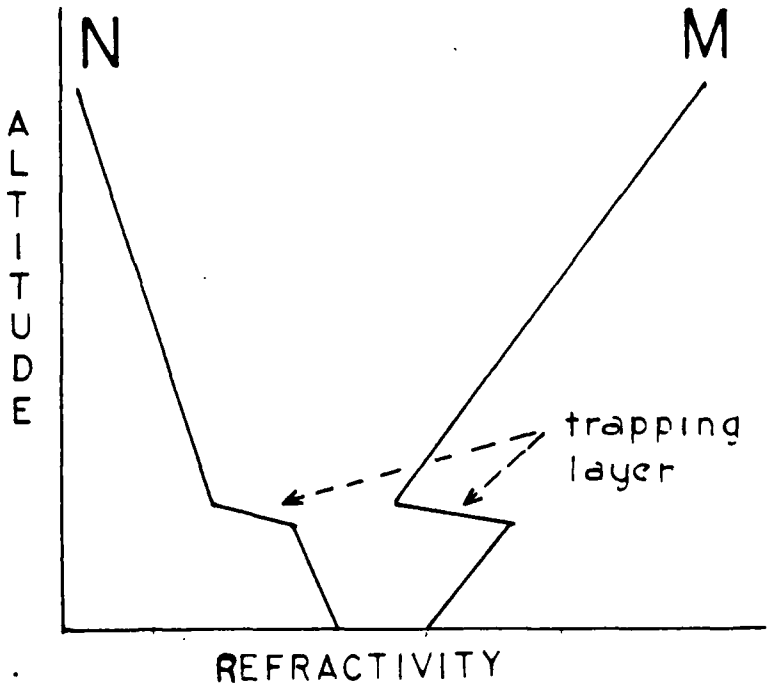

FIGURE 9

M and N Ducting Profiles

acceptance angle will be partially confined within the duct with very little loss. In the atmosphere n varies between 1.0003 and 1.0005. Using equation 5.6 with n_1 equal to 1.0005 and n_2 equal to 1.0003, n_2/n_1 is approximately equal to 0.9998. By inserting this figure in equation 5.6, the critical angle for trapping is [90 - ARCSINE (0.9998)] degrees which is approximately equal to (90 - 89) degrees or one degree. Since the wave front is assumed to be spherical, the entire wave front will not meet this requirement and not all of the energy in the wave will be trapped. Some will pass through the layer leading to the formation of radar or radio holes as shown in figure 10. However, for the wave to be trapped, the emitter must be within the trapping layer to meet the one degree critical acceptance angle requirement.

Hitney and Paulus (1979) describe refractive conditions in terms of the refractive gradient found in the Standard Atmosphere. Under standard conditions, values for the M gradient range between 79 and 157 M units/km. Under these conditions, an electromagnetic wave propagating in the troposphere will be refracted down, but with a curvature less than that of the Earth. Subrefraction describes an M gradient weaker than the standard gradient or greater than 157 M units/km. Subrefracted waves will be refracted upward away from the Earth's surface. Superrefraction describes an M gradient stronger than the standard gradient or 0 to 79 M

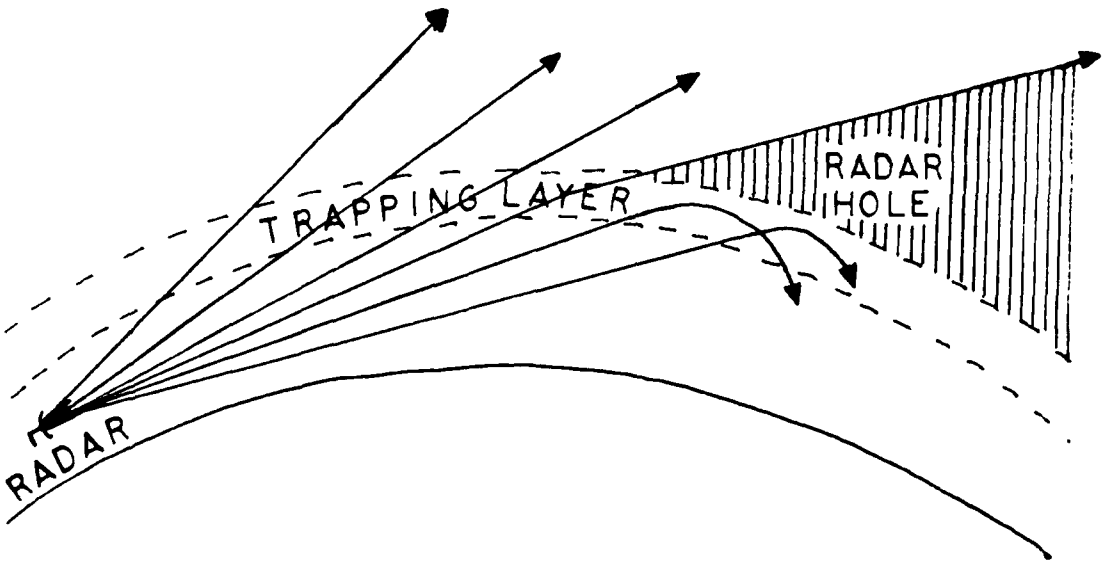

FIGURE 10

Radar Holes

units/km. Superrefracted waves will be bent downward but not trapped. Trapping, of course, occurs when the M gradient is less than zero or M decreases with height.

B. SURFACE AND ELEVATED DUCTS

Ducts are also described according to the location of their lower boundaries. A duct with its lower boundary at the surface is called a surface duct; however, a surface duct may extend to a rather high altitude (300 meters to 1 kilometer). A duct with its lower boundary above the surface is called an elevated duct. The thickness of the duct is determined by extending a vertical line down from the top of the trapping layer (the point where the slope of the M profile changes from negative to positive) to the intersection of the M curve as shown in figure 11. The size of the duct governs frequencies which will be trapped. Basically, the thicker the duct, the lower the minimum trapped frequency will be.

C. EVAPORATION DUCT

Evaporation at the surface of the sea leads to near 100% relative humidity in the air immediately above the surface. A rapid decrease to 80% to 90% relative humidity a few meters above the surface leads to a refractive gradient change sufficient to bring about a duct. This is known as the evaporation duct and exists almost all the time over all oceanic areas.

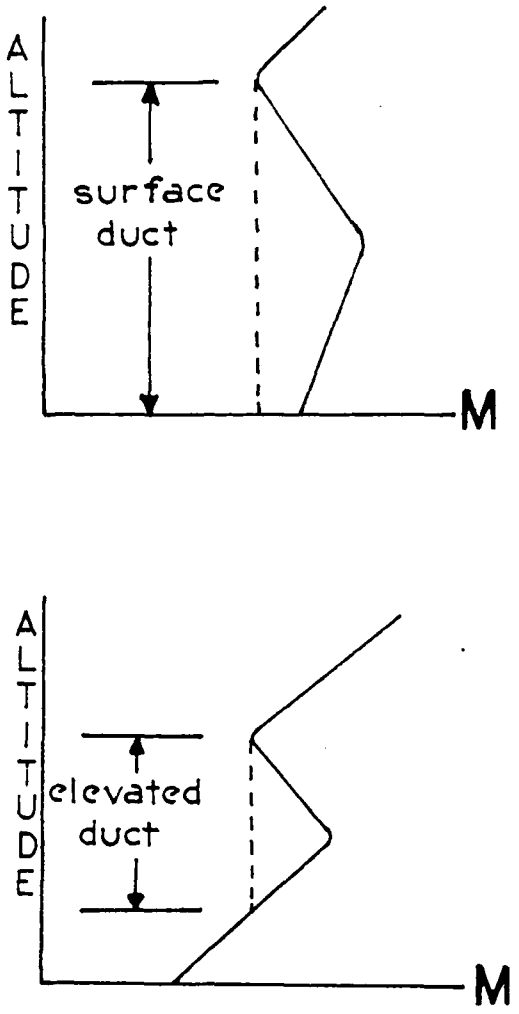

FIGURE 11

Duct Types

As shown by figure 12, the evaporation duct height, denoted by z_*, is the height at which dM/dz changes from negative to positive or (dM/dz = 0).

Paulus and Hitney (1979) have found that typical z_* values range from 10 to 20 meters, but have been noted as high as 30 meters. These ducts are thinner and weaker than other ducts and trap higher frequencies. However, significant over-the-horizon range extensions for some radars and even VHF/UHF communications can be realized.

Evaporation ducts are not dependent upon the large scale meteorological conditions necessary for the formation of surface and elevated ducts and, as such, will not be considered in this analysis. They can be evaluated from surface temperature, relative humidity and wind speed data. Additional information on evaluating evaporation ducts is given by Paulus and Hitney (1979).

D. MINIMUM TRAPPED FREQUENCY

A duct of thickness "d" can be compared to a wave guide of a specific thickness. The wave guide is manufactured to exact dimensions according to the proposed operating frequency. Likewise, a duct will trap certain frequencies depending upon its thickness.

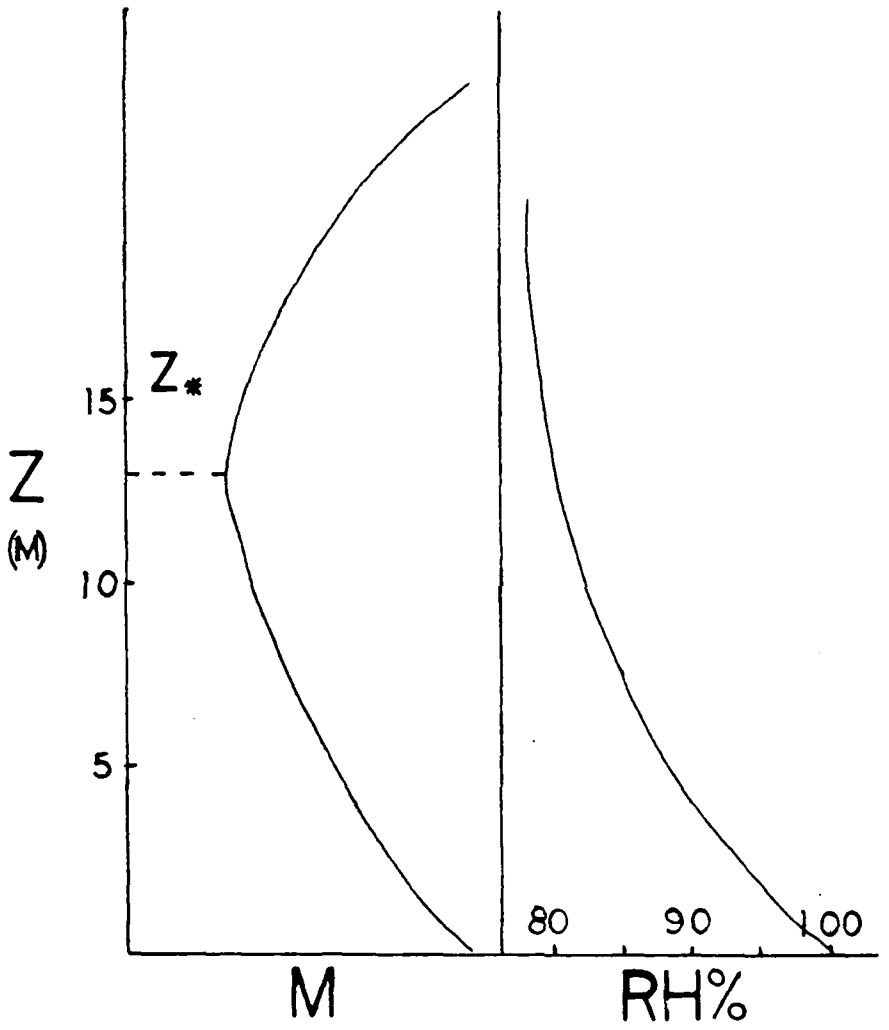

FIGURE 12

Evaporation Duct Refractive Profile
Adapted from IREPS Manual

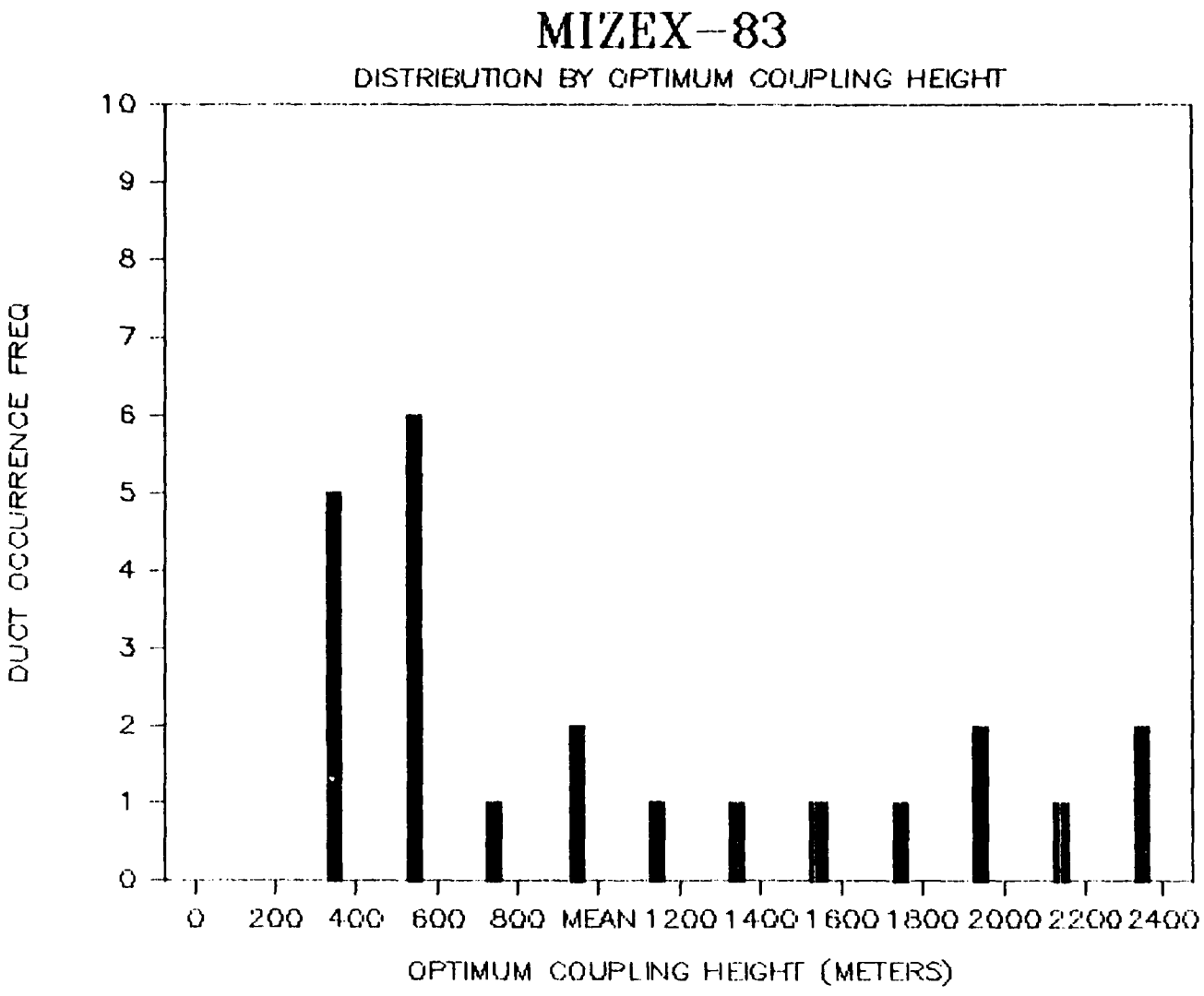

FIGURE 17

Optimum Coupling Height Histogram for Ducts Detected During MIZEX-83

TABLE 2

MIZEX-83 DUCT ANALYSIS DATA

	ASCENT NR	OPTIMUM COUPLING HEIGHT	DUCT THICKNESS (METERS)	DUCT INTENSITY (M UNITS)	WIND DIRECTION RELATIVE ICE POSITION
1	8	405.6	111	4.0	260/ON ICE
2	10	361.2	77	0.8	180/ON ICE
3	13	944.3	216	8.7	190/ON ICE
4	14A	392.7	51	1.2	197/ON ICE
5	14B	462.4	84	4.0	197/ON ICE
6	15	529.3	34	1.5	224/ON ICE
7	16A	795.8	217	17.3	248/ON ICE
8	16B	1717.1	109	6.0	248/ON ICE
9	17A	581.3	112	3.2	212/ON ICE
10	17B	2294.5	191	16.6	212/ON ICE
11	18	581.6	113	3.4	227/ON ICE
12	20	1488.5	58	0.2	158/ON ICE
13	22	285.2	81	5.3	077/OFF ICE
14	23	307.8	122	10.4	075/OFF ICE
15	34	2096.8	42	1.9	294/OFF ICE
16	67	397.5	31	0.3	300/OFF ICE
17	68	2308.5	69	2.5	230/ON ICE
18	77	1820.4	48	0.4	160/ON ICE
19	79	1992.8	53	0.9	155/ON ICE
20	85A	575.1	150	12.5	153/ON ICE
21	85B	1219.9	50	0.8	153/ON ICE
22	86	1182.9	123	2.6	100/ON ICE
23	88	922.1	76	0.8	160/ON ICE
MEAN		1028.84	96.43	4.58	
STND DEV		695.46	54.73	5.11	

number, for each sounding where a duct was detected. The first plot shows the overall modified refractivity profile over a broad altitude range and the second concentrates on the area of the duct. In four of the soundings, two ducts at different altitudes were detected. For these soundings, three plots were made; one overall profile and two detailed profiles with "A" indicating the lower duct and "B" indicating the upper duct.

C. ANALYSIS

Of the 88 soundings from the Polarbjorn which produced useful meteorological data, 19 contained ducts. Two ducts were present in four of these soundings bringing the total number of ducts used in this analysis to 23. Table 2 is a list of optimum coupling height, duct thickness, duct strength and the mean and standard deviation for each parameter for these 23 cases. Table 2 also lists the wind direction in degrees and assesses the wind as being either "on ice" or "off ice" for each of the cases. This is a broad assessment based on the Polarbjorn's position relative to the ice pack and wind direction. These parameters will be the basis for establishing a refractivity summary.

1. Optimum Coupling Height

Figure 17 is a frequency distribution by optimum coupling height of the 23 ducting cases. Figure 17 shows 14 of the 23 ducts occurred at an altitude below the mean

swing in the M profile. When this happens, the duct may be represented as stronger than it actually was. In the worst case, a non-existent duct can be indicated by the M profile. Some MIZEX-83 radiosonde data is questionable for this reason.

B. ANALYSIS APPROACH

A mainframe computer was used for initial processing of the Polarbjorn's radiosonde sounding data tape. Fortran routines were used to calculate and plot refractivity and modified refractivity profiles. This approach was adapted to allow for relatively quick processing of the voluminous amount of radiosonde data. Although the output was coarse, it provided a means for initial visual identification of ducts using the modified refractivity profile. Data sets for soundings containing ducts were then processed on a desk-top microcomputer using IREPS.

Although duct height and thickness can be read directly from the IREPS output, a more detailed plot of the modified refractivity profile is necessary to determine duct intensity. To obtain the necessary plots, modified refractivity was plotted against altitude on a Zenith Data Systems (Z-100) desk-top microcomputer. Duct optimum coupling height, duct thickness and duct intensity were read directly from these plots using the techniques described in Chapter III. Appendix B contains two plots, with corresponding ascent

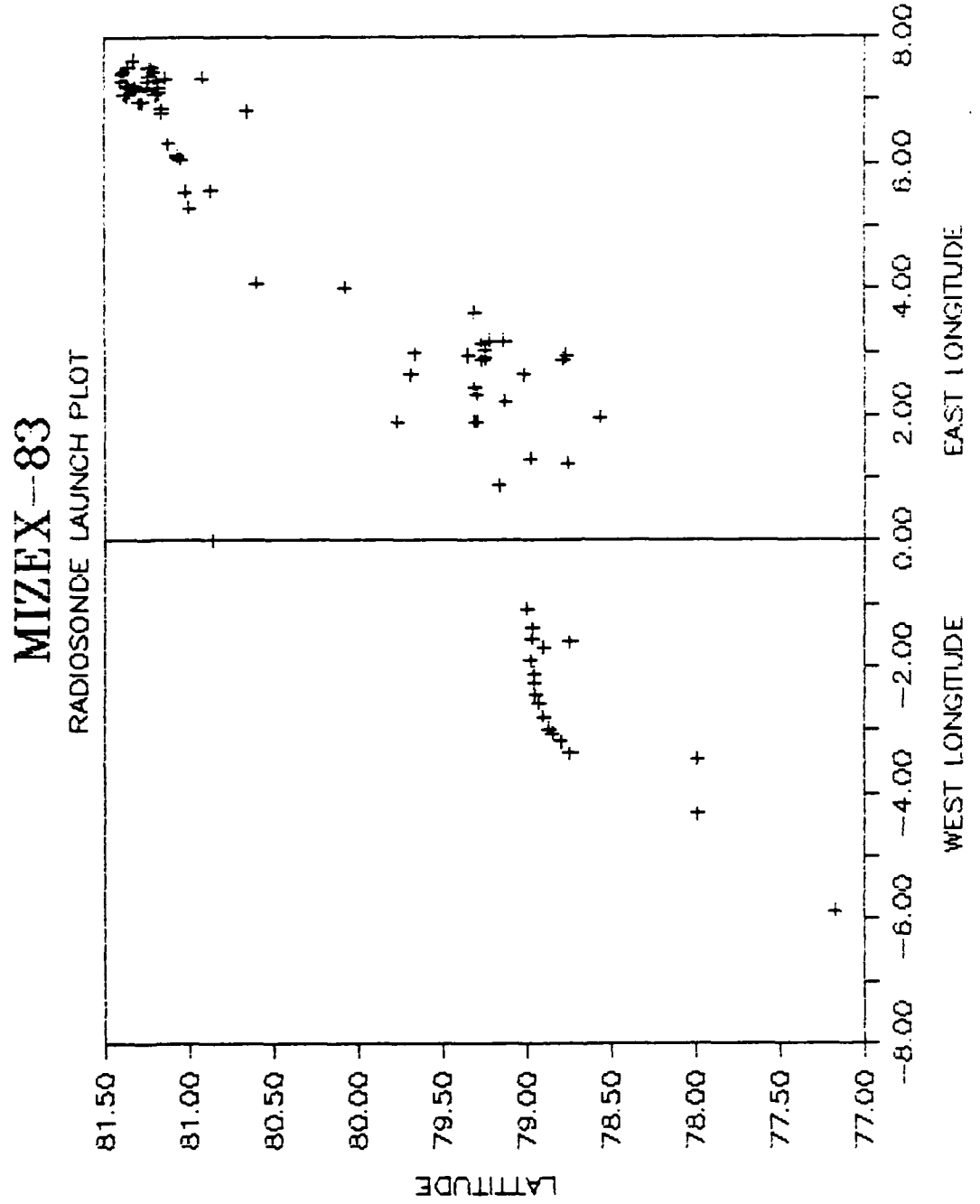

FIGURE 16

Scatter Plot of Radiosonde Ascents
Made During MIZEX-83

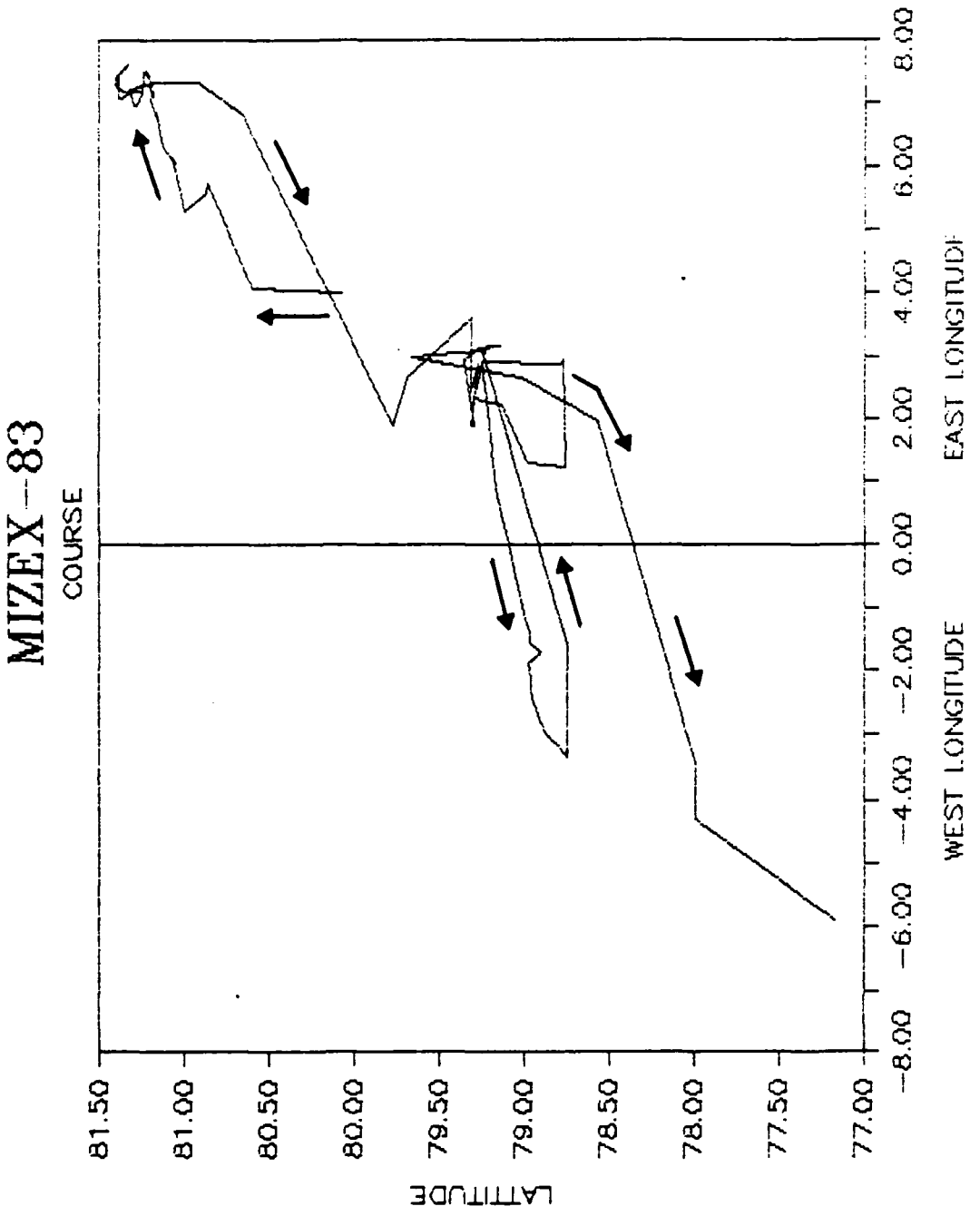

FIGURE 15

Detailed Course Plot for the Polarbjorn
During MIZEX-83

Although difficult to depict on figure 14, the Polarbjorn operated within or in close proximity to these ice floes throughout the exercise. Figure 15 is a more detailed plot of the Polarbjorn's course. These two figures will be referred to later to correlate refractivity conditions to surface meteorological conditions observed during the exercise.

Of the 103 radiosonde ascents made from the Polarbjorn, 88 provided usable data. Appendix A lists the time, position and surface observations of each of these 88 soundings. Figure 16 is a position plot of the 88 soundings and can be related to figures 14 and 15 for comparing meteorological and refractivity conditions.

In order to maximize vertical resolution, the ascent rates were kept low (120 to 150 meters/minute versus the normal 300 meters/minute. With temperature, humidity and pressure being measured and reported every 10 seconds and a 120 meter/minute ascent rate, a measurement is made every 20 meters.

Although radiosonde soundings generally provide reliable data, some conditions can lead to invalid results. For example, surface fog can saturate the humidity sensor. In this condition, high humidity level readings can occur in dry air well above the fog. When this sensor abruptly dries out, actual humidity is recorded leading to an abrupt decrease in the humidity profile and a corresponding negative

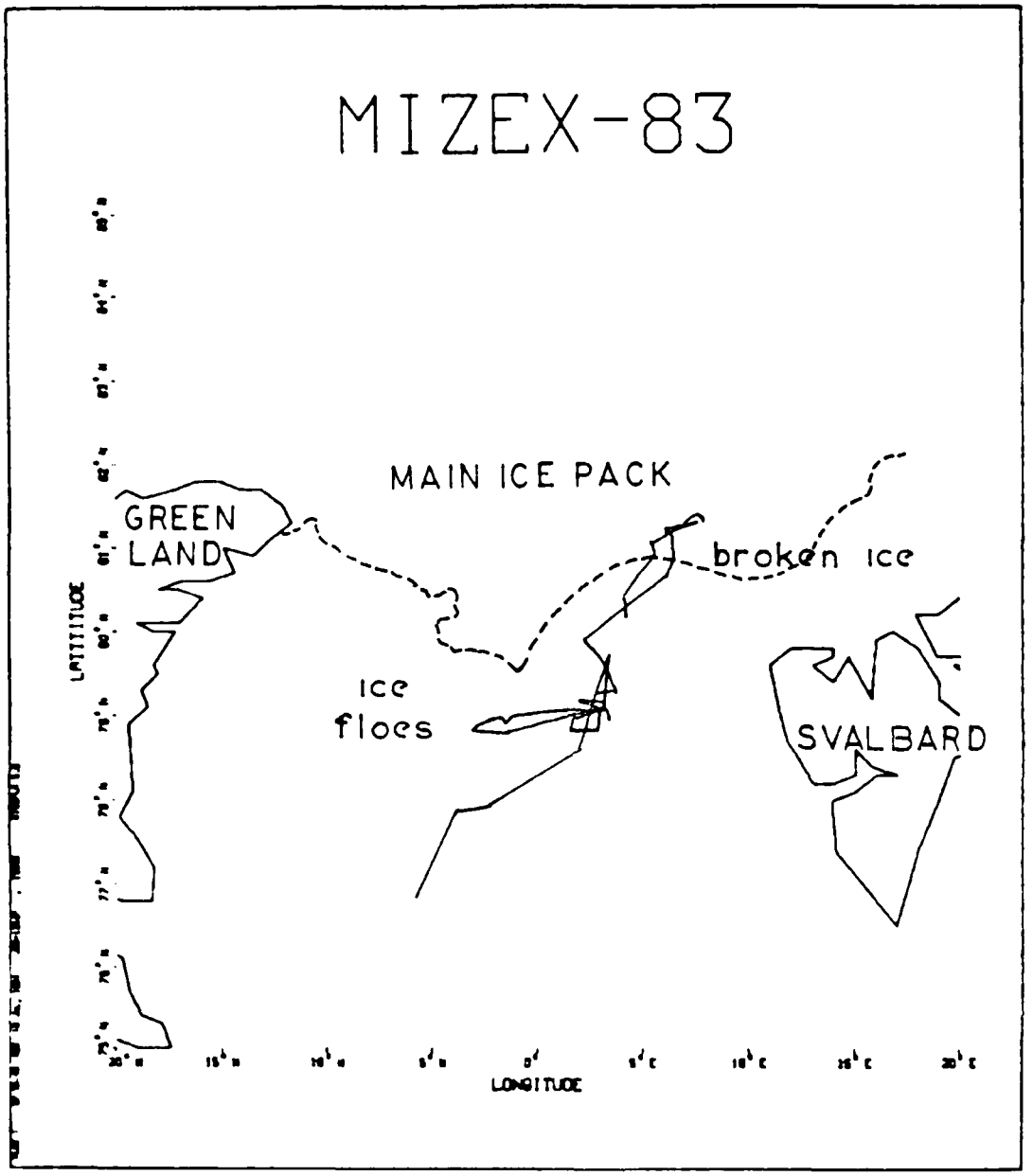

FIGURE 14

Polarbjorn's Course and Location of the Ice Pack

IV. ACQUISITION, ANALYSIS AND RESULTS

A. DATA ACQUISITION

1. Marginal Ice Zone Experiment (MIZEX)

MIZEX is a multi-year meteorological experiment designed to evaluate meteorological conditions in and around the Arctic marginal ice zone (MIZ). The MIZ is a zone of roughly 100 km width characterized by the transition from packed sea ice to broken ice to open ocean. MIZEX-83, conducted during July and August of 1983 in the East Greenland Sea, was the pilot experiment for the program. Data were gathered using meteorological and remote sensing aircraft and two research vessels (Polarbjorn and Polarstern). Radiosondes, sensors attached to a balloon which transmit measured meteorological data, were launched from the research vessels at various points in the MIZ. The radiosonde provides the information necessary to plot the refractivity gradients described in chapter III. This analysis will incorporate only radiosonde data taken from the Polarbjorn.

2. Radiosonde Data

Radiosonde observations on the Polarbjorn were made with the Vaisala Micro-Cora Upper Air sounding system using the RS-80 radiosonde. Figure 14 shows the course of the Polarbjorn and the boundary of the main ice pack. In summer, the main ice pack breaks up into floes at the edges.

will be used to produce an area refractivity summary based on the meteorological data gathered during MIZEX-83.

provide tactical commanders with a means to assess refractive conditions using available shipboard environmental data. Ultimately IREPS will be installed on all Navy aircraft carriers and used as an aid in adjusting tactics to compensate for and exploit atmospheric refractive effects, (Beach, 1979). IREPS processes vertical temperature and humidity profiles on the Hewlett-Packard model 9845 desk-top microcomputer to provide four basic product outputs:

1) a propagation condition summary of the existing refractive conditions for the location and time of the input data;

2) a coverage display profile of a specific system based on the systems specifications and an assessment of the input data;

3) a computer listing of the input data set;

4) a path loss display representative of the performance of a specified system for a given data set.

If on-scene refractivity data are not available, IREPS can generate products that show probable atmospheric effects on various electronic systems using a historic and geographical refractivity library. Hitney and Paulus (1979) give a detailed description of IREPS in the IREPS Interim User's Manual.

IREPS, designed to be an on-scene tactical refractivity assessment aid, was used to analyze part of the data gathered during MIZEX-83. In the following chapter, IREPS along with the other techniques described in this chapter

marine atmospheric boundary layer (MABL). Above the MABL, the air can be much warmer and dryer. At the boundary of these two layers, there is generally a sharp decrease in N and M. Ducts can form over land as well as water because the variations in temperature, pressure and humidity with increasing altitude are common to both these environments. Duct persistence, however, is enhanced by subsiding (sinking) air which is produced by trade wind circulation of relatively large, stable air masses in the area 20 to 30 degrees latitude north and south of the equator. Trade wind circulation is from east to west underneath a cap of warm dry subsiding air. This creates a trade wind inversion layer and the positive temperature and negative humidity gradients necessary to produce ducting conditions, (Neiburger, et al., 1982). These weather conditions occur more often over ocean areas. For the same reason, the persistence of ducting conditions in the extreme northern and southern latitudes is rare. Initial duct formation in these regions is based on smaller, mesoscale meteorological conditions such as surface flux and ice conditions.

G. ASSESSING REFRACTIVE CONDITIONS

The Naval Ocean Systems Center (NOSC), San Diego developed and continues to refine the Integrated Refractive Effects Prediction System (IREPS). The aim of IREPS is to

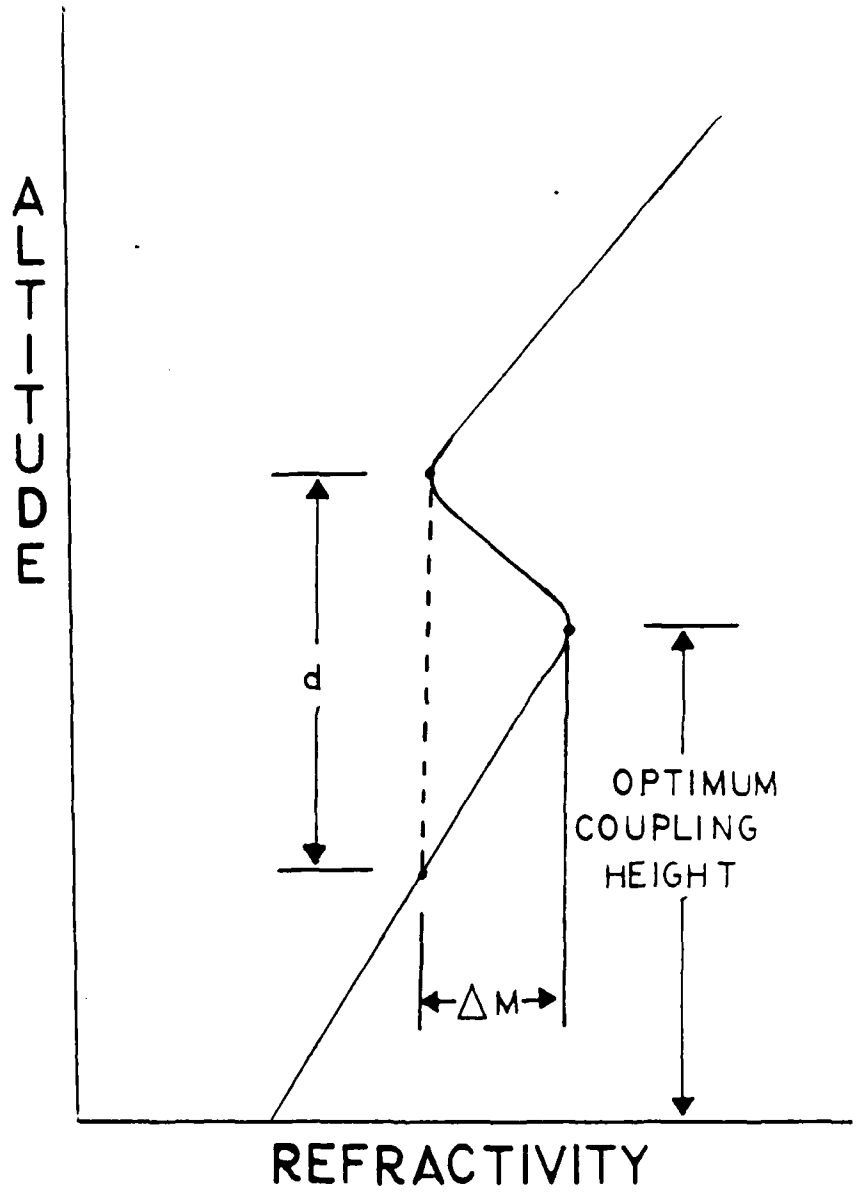

FIGURE 13

Duct Parameters

Based on experimental values, the minimum frequency in Hertz trapped by a duct of thickness d is:

$$f_{min} = 3.6033 \times 10^{11} \times d^{-(3/2)} \qquad (3.5)$$

Kerr (1951, Chapter 2) presents a detailed examination of duct frequency trapping.

It is important to note that f_{min} does not represent a cut-off frequency, but a frequency above which waves will be strongly guided. Frequencies below f_{min} can still be affected but to a limited degree.

E. DUCT CHARACTERISTICS

Knorr (1982) has described ducts by three physical parameters--duct thickness, intensity and optimum coupling height. Duct thickness d describes the vertical size of the duct and relates to minimum frequency trapped. Duct intensity or strength is described in M units and is the change in M units (Δ M) between the lower boundary of the duct and optimum coupling height. Optimum coupling height is the altitude for optimum trapping in the duct; altitude where the critical acceptance angle is the largest. Figure 13 shows the relationship between these parameters.

F. METEOROLOGICAL EFFECTS LEADING TO DUCTING

As previously stated, duct formation is dependent on the existence of two differing air masses or layers. Above the ocean, there normally exists a cool, moist layer called the

optimum coupling height of 1029 meters and 17 were within one standard deviation.

2. Duct Thickness

Figure 18 is a frequency distribution by duct thickness of the 23 cases. This figure shows a mean thickness of 96.43 meters with 19 of the 23 cases being within one standard distribution.

3. Duct Intensity

Figure 19 is a frequency distribution by duct intensity. This figure shows a large grouping below the mean intensity of 4.58 modified refractivity units. Again, 19 of the 23 cases are within one standard distribution.

D. RESULTS

Duct parameter comparisons made in this section are based on statistical information extracted from the GTE Sylvania report (Ortenburgher, et al., 1978). This data base contains the probability of occurrence and statistical parameters such as thickness, intensity and optimum coupling height of elevated ducts collected over a five year period at sounding stations around the world. For this analysis, comparisons were made with selected mid latitude sounding stations.

Figures 17, 18 and 19 reveal the following:

(1) Duct optimum coupling height in the MIZ for the

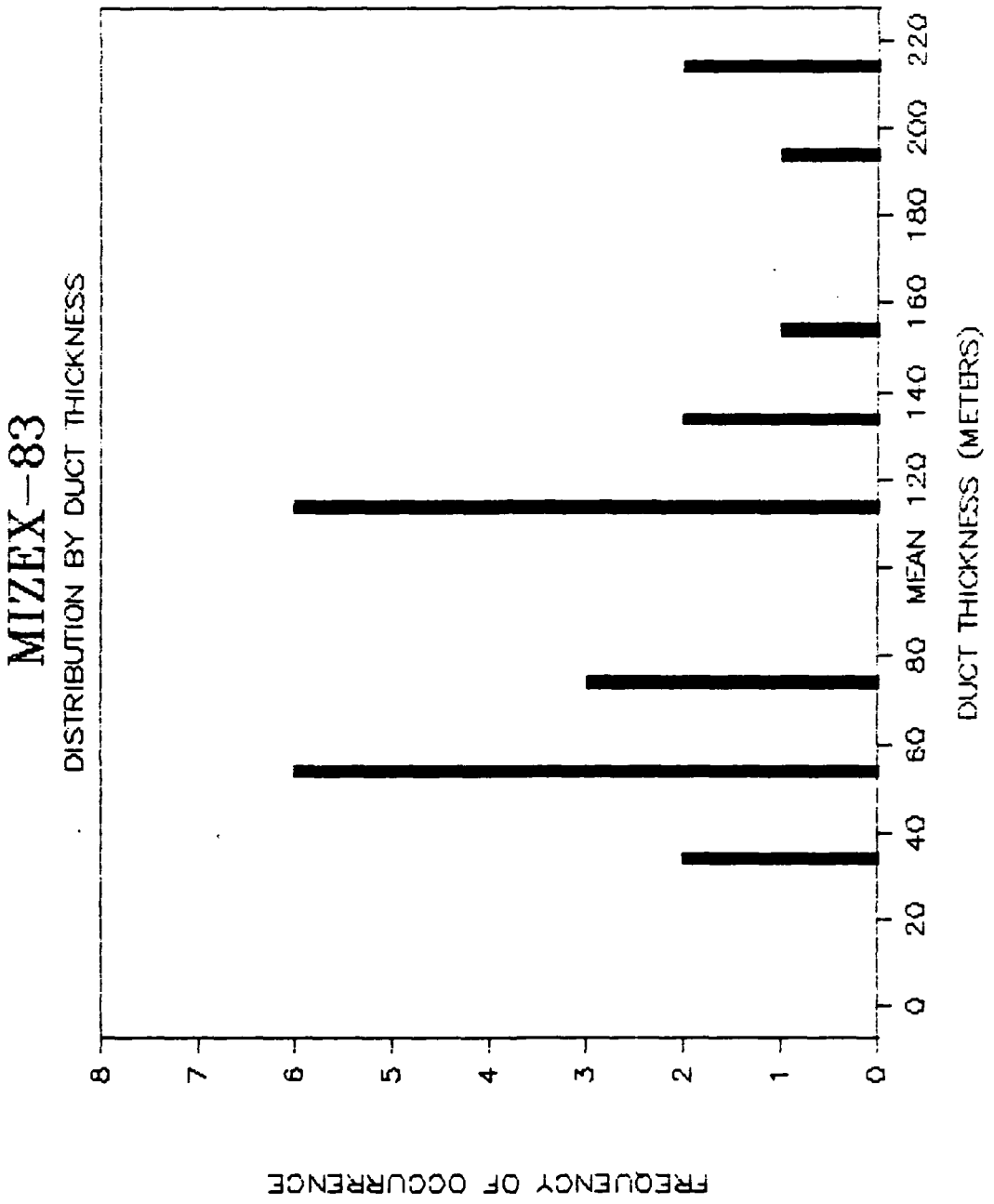

FIGURE 18

Thickness Histogram for Ducts Detected During MIZEX-83

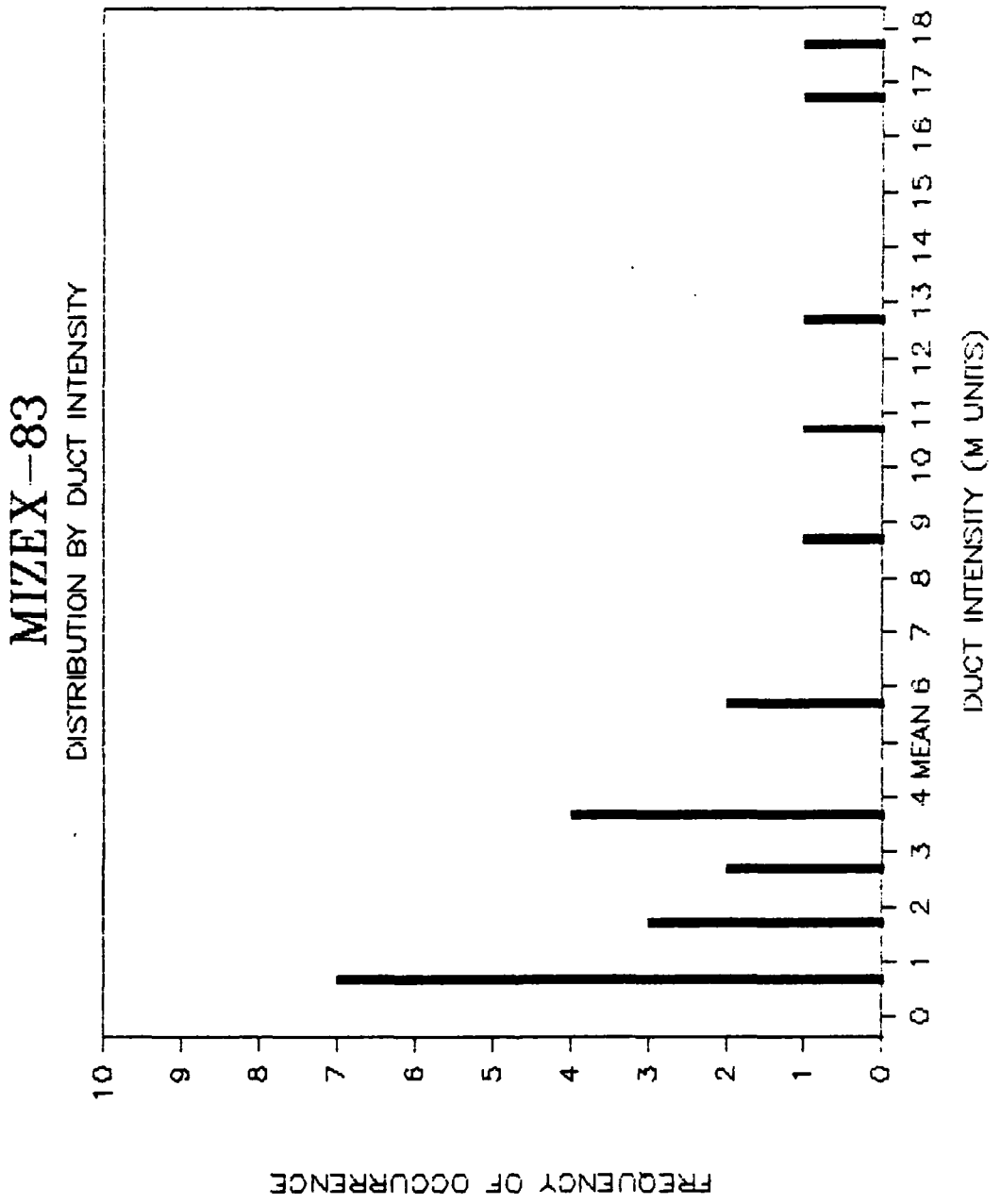

FIGURE 19
Intensity Histogram for Ducts Detected During MIZEX-83

observation period does not vary significantly when compared to selective mid latitude optimum coupling heights of 1209 meters at Birmingham, Alabama, 1136 meters at Baghdad, Iraq, and 727 meters at Qrendi, Malta. It is significant to note that no surface based ducts were detected.

(2) As stated, atmospheric ducts affect electromagnetic waves in the UFH, VHF and SHF frequency bands, and duct thickness determines minimum trapped frequency. Using the mean duct thickness of 96 meters and applying equation 3.5 yields a minimum trapped frequency of approximately 383 Mhz which is in the UHF band, see Table 1. Applying equation 3.5 to the largest and smallest detected ducts yields minimum trapped frequencies of approximately 110 Mhz (VHF) and 2.1 Ghz (SHF) respectively. However, selected mean duct thicknesses ranged from 139 meters in Birmingham, Alabama to 283 meters in Shreveport, Louisiana; all significantly thicker than in the MIZ.

(3) Mean duct intensity for the observation period compares favorably with many mid latitude regions of the world. However, there are mid latitude regions which average much stronger ducts. Compared to the mean intensity at Shreveport, Louisiana of 7 M units, ducts detected during the exercise do not seem very weak. However, when compared to Kenitra Morocco with a mean intensity of 16 M units, these ducts can be considered weak and not as efficient at

trapping and channeling energy as ducts in some parts of the world.

Inferences about the existing meteorological conditions can be made from the above observations. The optimum coupling height corresponds, roughly, to the height of the inversion layer and weak ducts result when the change in the refractive index is small. But, to get a change in refractivity requires a change in temperature and/or pressure and/or humidity. A major question to be answered by this analysis is what observable meterological conditions in the MIZ lead to ducting?

Figure 20 is a histogram of duct occurrence in time using optimum coupling height as a parameter. The time period is the length of the observation period or the duration of MIZEX-83 scaled to the launch or ascent number. Figure 21 is the same type of histogram using the actual number of days (36) in which ascents were made in place of the ascent number and reflects the time period more accurately. Since these histograms are designed to represent only the occurrence or non-occurrence of a duct at some point in time, only one of the ducts in each of the four cases where double ducts occurred has been considered. The determination of which duct to use in the analysis was based on the height of the stratus cloud layer which is a general indicator of the top of the inversion layer. A determination as

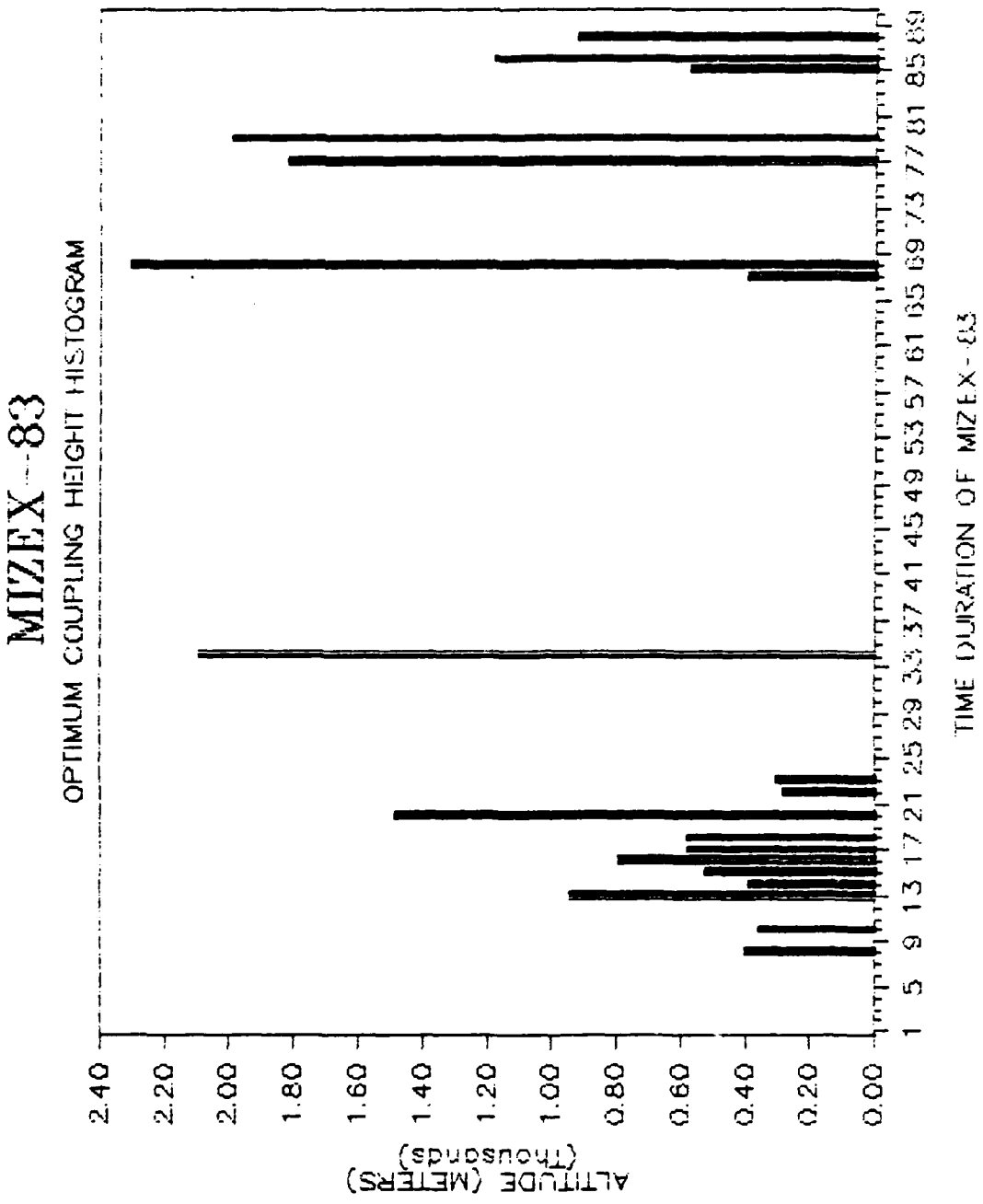

FIGURE 20

Histogram Showing Duct Occurrence over Duration of MIZEX-83 Using Optimum Coupling Height as a Parameter

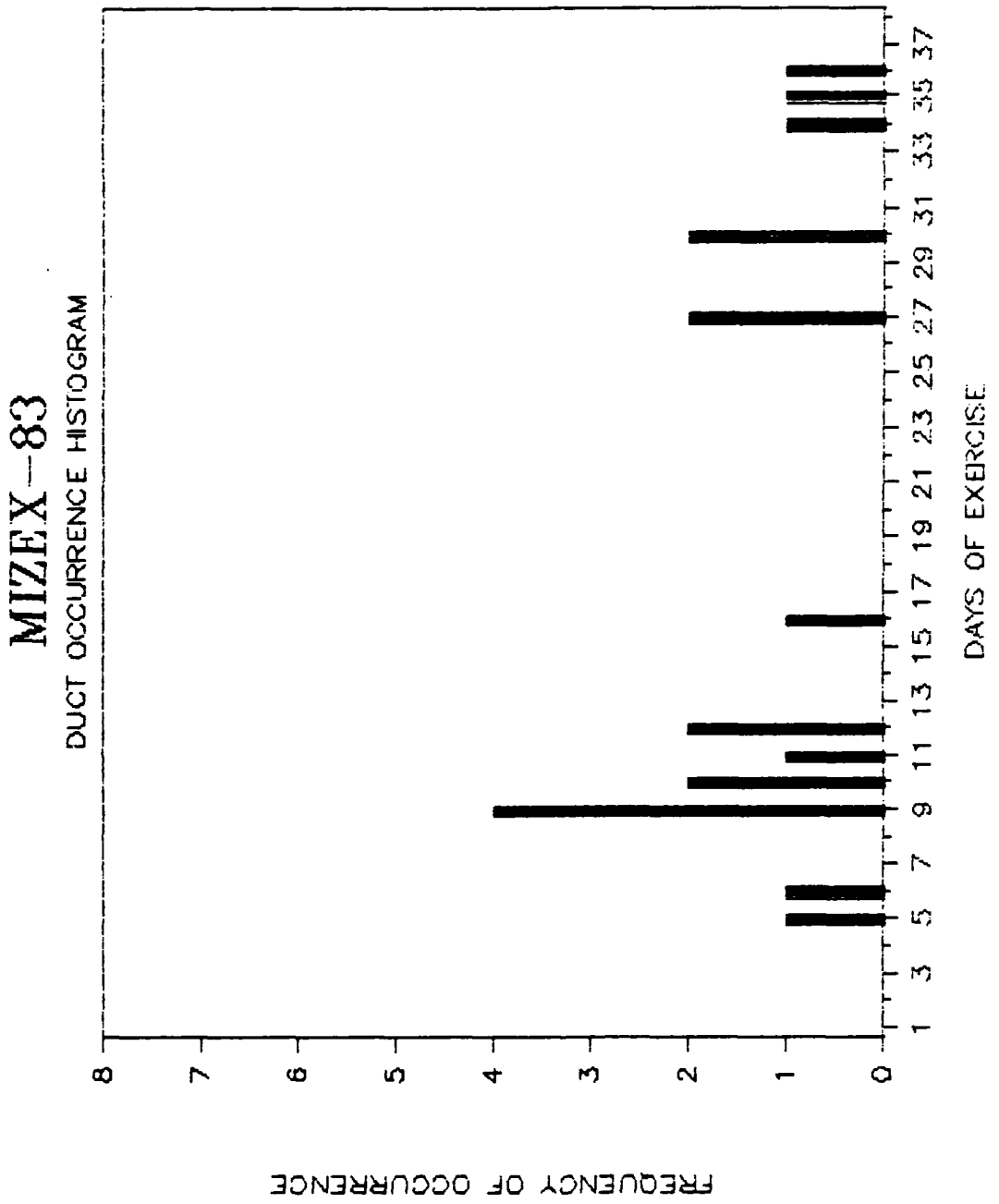

FIGURE 21

Histogram Showing Duct Occurrence Over the 36 Days of Radiosonde Ascents During MIZEX-83

to what meteorological factors caused the other duct in these four cases has not been made.

Figures 20 and 21 clearly show that ducts occurred in groups and that there were periods of time when no ducts were detected. Using Table 2, the following meteorological conditions can be correlated to the ducting and non-ducting periods indicated by Figure 20 and 21.

(1) Ducting conditions were prevalent during the period 1 to 4 July. Eleven soundings during these four days detected nine ducts. Ducts were also previously detected on 27 and 28 June. During this period, the Polarbjorn was in broken ice floes at the edge of the pack. Winds were light and predominantly from the south south-west onto the ice. Fog and stratus overcast dominated the period. Referring to Figure 16, these ducts were detected by the group of soundings indicated in the upper right corner of the radiosonde ascent plot.

(2) From 5 to 19 July, 43 soundings detected only one duct. As the Polarbjorn moved south and away from the main ice pack, ducts were no longer present. Meteorological conditions during this period were also characterized by stratus overcast and fog. Winds remained light and after 7 July, blew predominantly from the north off the ice. The soundings taken during this period are the group in the right center portion of Figure 16.

(3) Figure 20 shows another group of ducts that were detected during the period 20 to 29 July with the majority occurring after 23 July. From 23 to 29 July twelve soundings detected five ducts. The Polarbjorn was east of broken ice floes during this period with the wind blowing from the east and south onto the ice. This period was also characterized by fog and stratus overcast. This group of soundings can be seen in Figure 16 in the lower left portion of the plot.

SUMMARY AND RECOMMENDATIONS

A. SUMMARY

The optimum coupling height and thickness of ducts detected during MIZEX-83 do not vary significantly from ducts found in other parts of the world. However, these ducts do not tend to be as intense as ducts found in some mid latitude locations. In some cases, radiosonde data collected may not accurately reflect refractive conditions because of a fog saturated humidity sensor. This does not necessarily mean that the ducts did not exist, but that they may be represented as stronger than they actually were. L.N. Orthenburger (NOSC TD 260, 1979) states that radiosonde data tend to underestimate ducting occurrence because of time-lags and other inaccuracies in the humidity sensing element. This characteristic of the radiosonde may partially offset the inaccuracies caused by saturation, but may cause the rest of the ducts to be represented as weaker than they actually were.

During the period of this experiment ducting conditions occurred significantly more often when the wind blew from the open sea onto the ice. Based on this study, no other general or specific meteorological conditions have been correlated to the ducting and non-ducting periods. Light winds, fog, stratus overcast, drizzle and proximity to the ice were characteristic of the experiment. Although no

ducts were detected during the brief clear periods, the data set is too small to directly correlate these two conditions.

B. ELECTRONIC WARFARE ASSESSMENT

Of importance to a tactical commander operating in the MIZ would be the ability to assess atmospheric refractivity conditions to gain a tactical electronic warfare advantage. Of course, this assessment is made possible by real time assessment aids such as IREPS, but a knowledge of typical area conditions would enhance mission planning. For example, knowledge of the large scale ducting conditions in the Indian Ocean allows a tactical commander to stand off and monitor adversary VHF/UHF communications at a range well over the horizon. Since this analysis is a first step in analyzing and documenting refractivity conditions in the MIZ, only general statements about electronic warfare operations can be made. Therefore, the following observations should be considered in the context of the size of the data set and the time of year in which the data were taken.

The lack of surface based ducts will restrict over-the-horizon (OTH) electronic support measures (ESM) in the VHF/UHF/SHF frequency range from surface platforms. However, some OTH ESM may be possible if an evaporation duct is present. Likewise, if this is the case, a task force could propagate electromagnetic energy in these frequency

ranges without fear of OTH detection by an adversary operating on the surface.

Airborne ESM as well as electronic countermeasures (ECM) such as jamming, range gate pull-off and false target generation could be enhanced because of the existence of elevated ducts. Extended ranges could be exploited as well as radar holes by knowledge of the existence of and optimum coupling height of MIZ ducts. These ducts do not tend to be strong and seem dependent on an on-ice wind. Further, if this wind is caused by the sea-ice transition, ducts may not extend far from the boundary of the ice pack. These factors limit the possible tactical advantage. As in the case of surface operations, the opposite also exists for airborne platforms; MIZ ducts are capable of providing extended detection and exploitation ranges for an adversary.

C. RECOMMENDATIONS

This analysis has been limited by the size of the data set. The following recommendations address areas of analysis that were not considered or covered in sufficient detail.

1) The mesoscale meteorological conditions leading to ducting in the MIZ were only briefly mentioned here. However, this is the thesis of another analysis effort that will correlate MIZEX-83 radiosonde data with other data such as satellite photographs. This analysis should provide more

insight into the cause of the second duct in the double ducting cases and the actual effect of surface wind on MIZ duct formation.

2) Sufficient data were not available to accurately determine the spatial extent of the ducts detected during MIZEX-83. All soundings were taken in the proximity of the ice, therefore, it was not possible to determine if the ducts extended over the ice, the open water or both. Further, it could not be determined how far the ducts extended from the ice edge. Knowledge of the spatial extent of MIZ ducts would be extremely important in any electronic warfare planning. Data gathered in future MIZ experiments should take this into account and take soundings in open water at a distance from the ice.

3) Knorr (1982) proposes that there is a correlation between duct thickness and intensity and has presented methods to compute the power distribution of signals propagated through elevated ducts using the joint probability of elevated duct parameters. An analysis of this type on MIZEX-83 data would be valuable in determining expected range improvements when propagating in a duct.

4) MIZEX-84 has just recently been completed providing another data set which will reveal more information about the area. This should be added to MIZEX-83 results to increase the knowledge of refractive conditions in the MIZ.

APPENDIX A

MIZEX-83 RADIOSONDE ASCENTS DATA

ASNT NR	DATE	LAT	LONG	TIME GMT	PRES	TEMP CNTG	WIND DIR	WIND SPD
1	6/23	80.08N	4.02E	2330	999.1	3.1	180	4.0
	STRATUS, 1% ICE, WATER 1.0C							
2	6/24	80.60N	4.10E	1136	996.8	0.9	148	9.4
	STRATUS, LT SNOW, IN ICE, CEILING 200 METERS							
3	6/24	80.86N	5.37E	2339	1003.5	0.7	194	7.0
	STRATUS, FOG, IN ICE							
4	6/25	80.87N	5.58E	1139	1006.2	1.2	120	5.7
	STRATUS, NO WIND							
5	6/25	81.00N	5.30E	2333	1001.0	1.5	154	10.3
	FOG, DRIZZLE							
6	6/26	81.02N	5.56E	1135	999.6	0.0	210	4.2
	THIN FOG, IN ICE							
7	6/27	81.07N	6.12E	1138	1000.1	-0.7	220	3.0
	THIN FOG, BLUE SKY OVERHEAD, IN ICE							
8	6/27	81.05N	6.07E	2331	1000.2	-1.0	260	2.0
	FOG							
9	6/28	81.05N	6.07E	1135	1002.3	-2.1	330	1.4
	LOW THIN OVERCAST							
10	6/28	81.07N	6.11E	2331	1011.9	-3.7	180	3.5
	NONE							
11	6/29	81.12N	6.30E	2340	1012.1	-0.8	194	6.4
	CLEAR							
12	6/30	81.17N	6.86E	1133	1012.8	0.7	235	6.6
	STRATUS, CEILING 100 METERS							
13	7/01	81.17N	6.80E	0023	1013.2	0.5	190	4.5
	STRATUS							
14	7/01	81.20N	7.07E	0943	1010.1	-0.7	197	4.1
	THIN FOG, BLUE SKY OVERHEAD							

ASCENT 14B

7/01 81.20N 7.07E

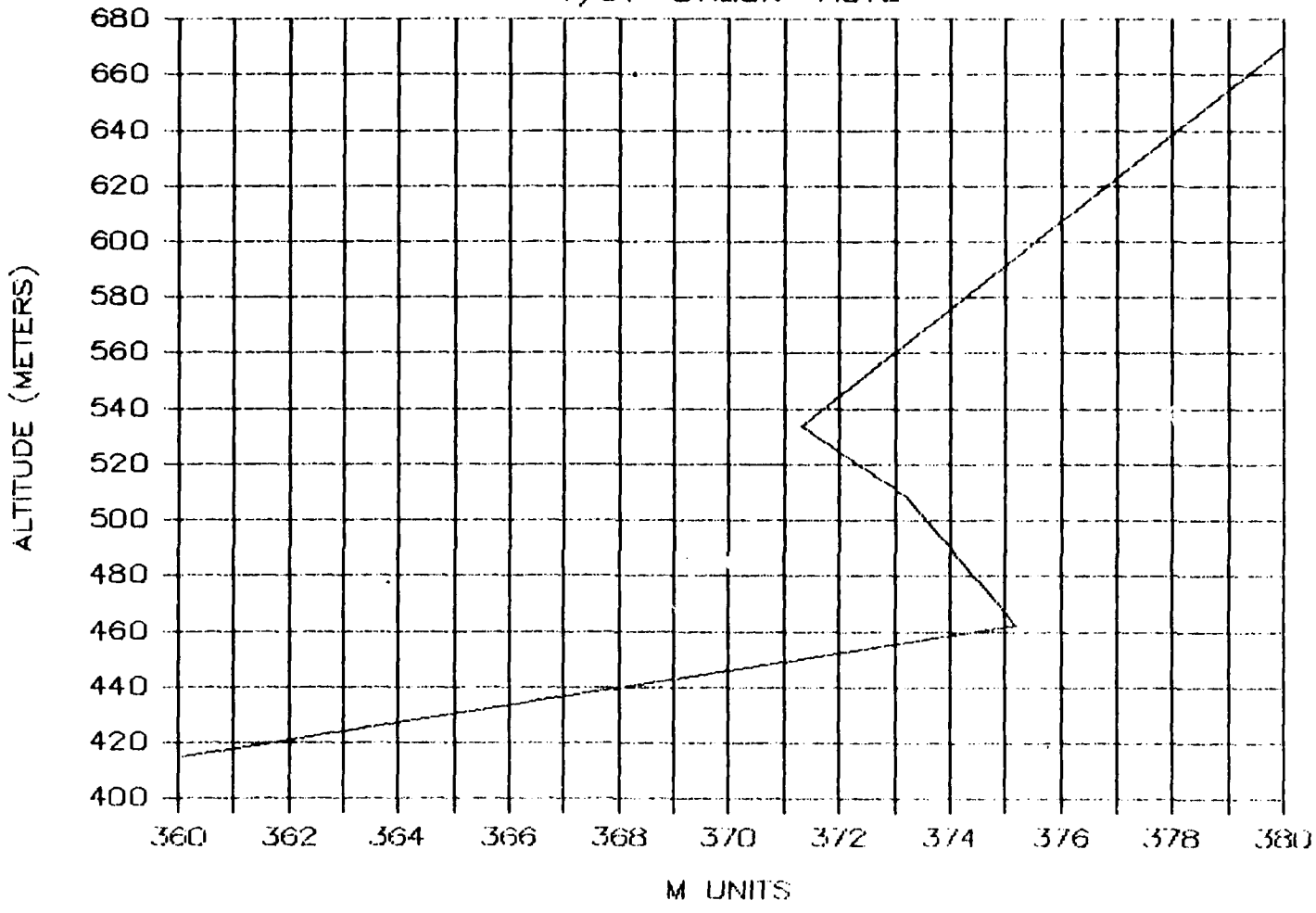

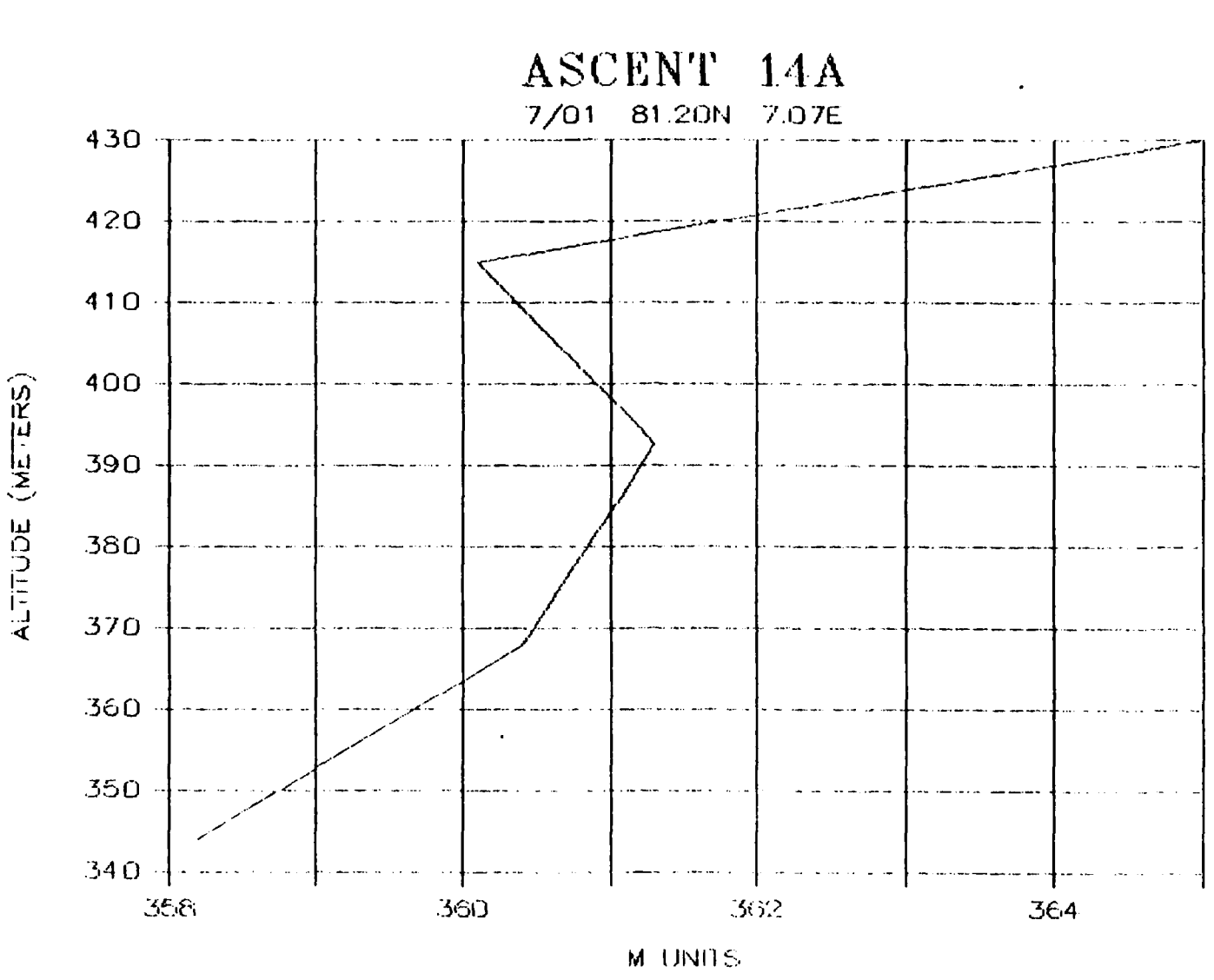
ASCENT 14A
7/01 81.20N 7.07E
430
420
410
400
390
380
370
360
350
340
ALTITUDE (METERS)
358
360
362
364
M UNITS

ASCENT 14

7/01 81.20N 7.07E

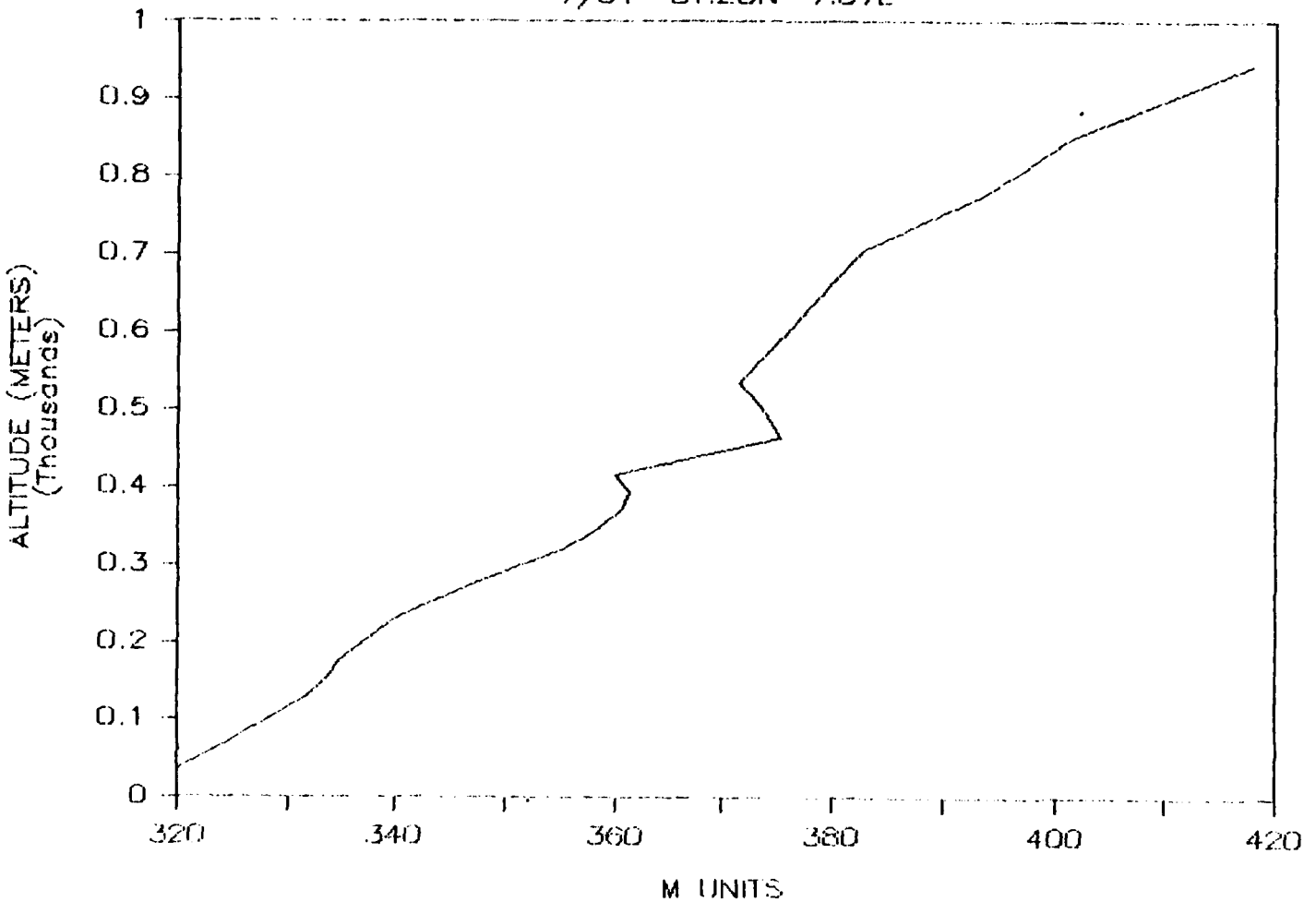

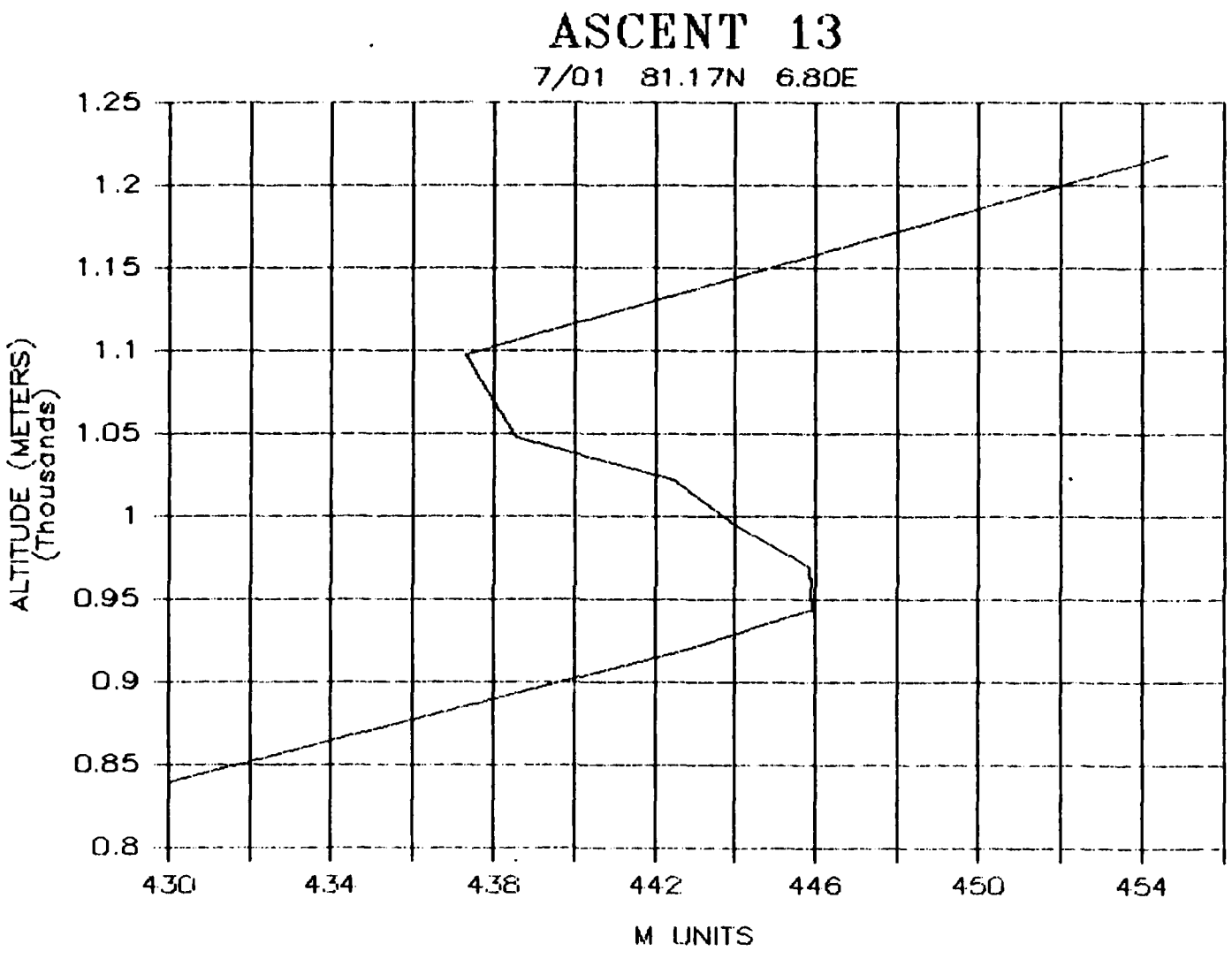
ASCENT 13
7/01 81.17N 6.80E
ALTITUDE (METERS)
(Thousands)
1.25
1.2
1.15
1.1
1.05
1
0.95
0.9
0.85
0.8
430
434
438
442
446
450
454
M UNITS

ASCENT 13

7/01 81.17N 6.80E

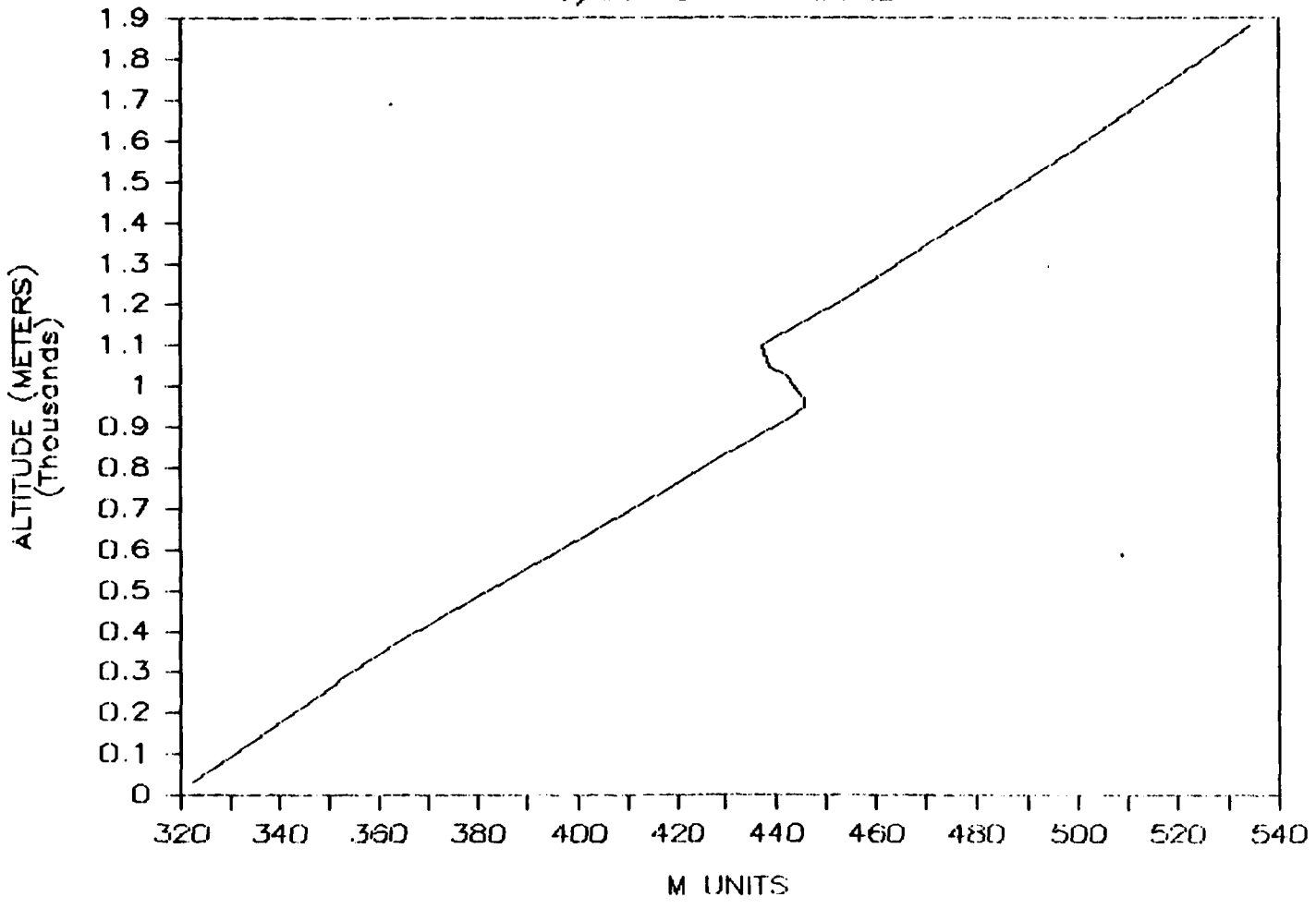

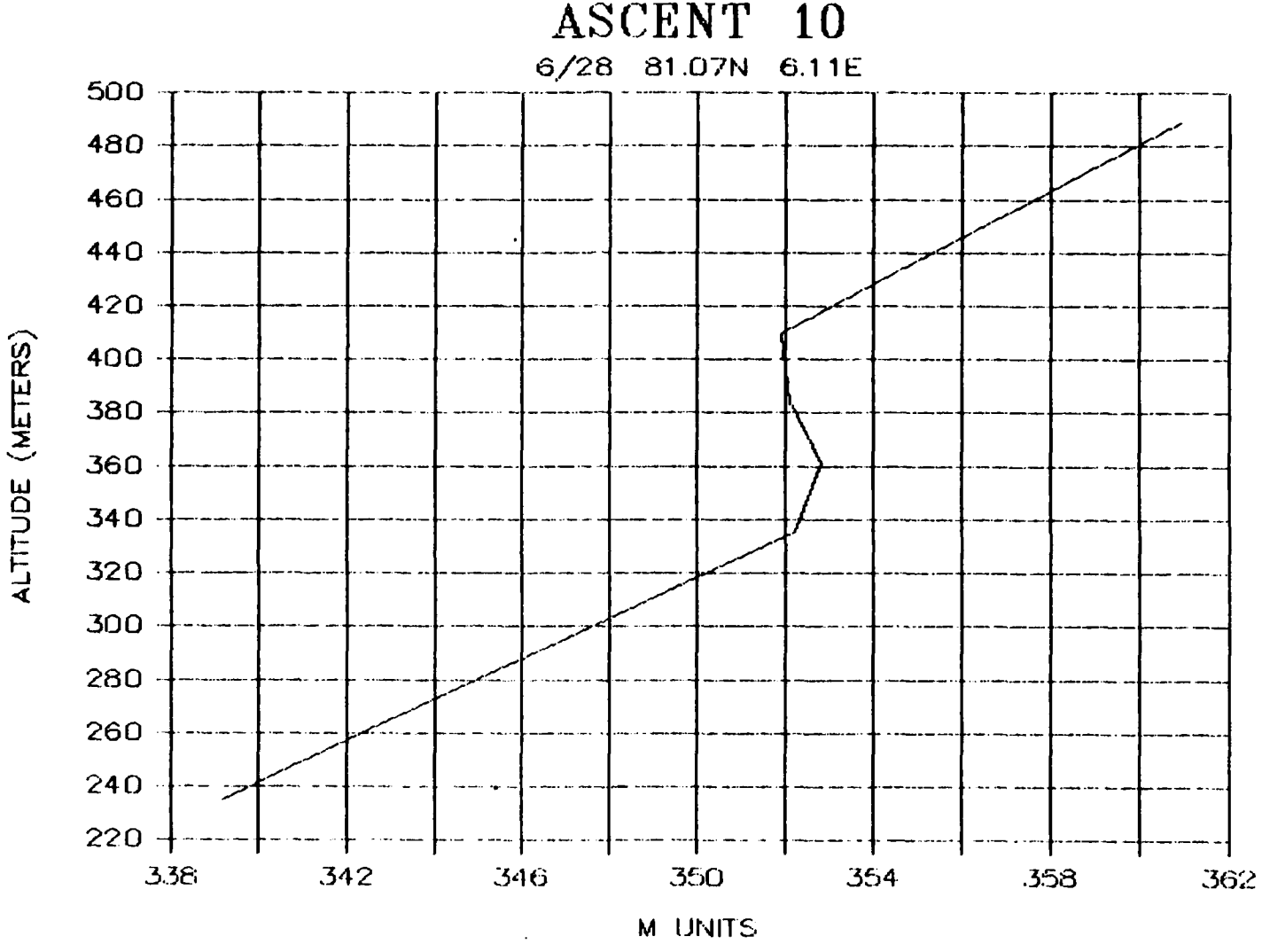
ASCENT 10
6/28 81.07N 6.11E
ALTITUDE (METERS)
500
480
460
440
420
400
380
360
340
320
300
280
260
240
220
338
342
346
350
354
358
362
M UNITS

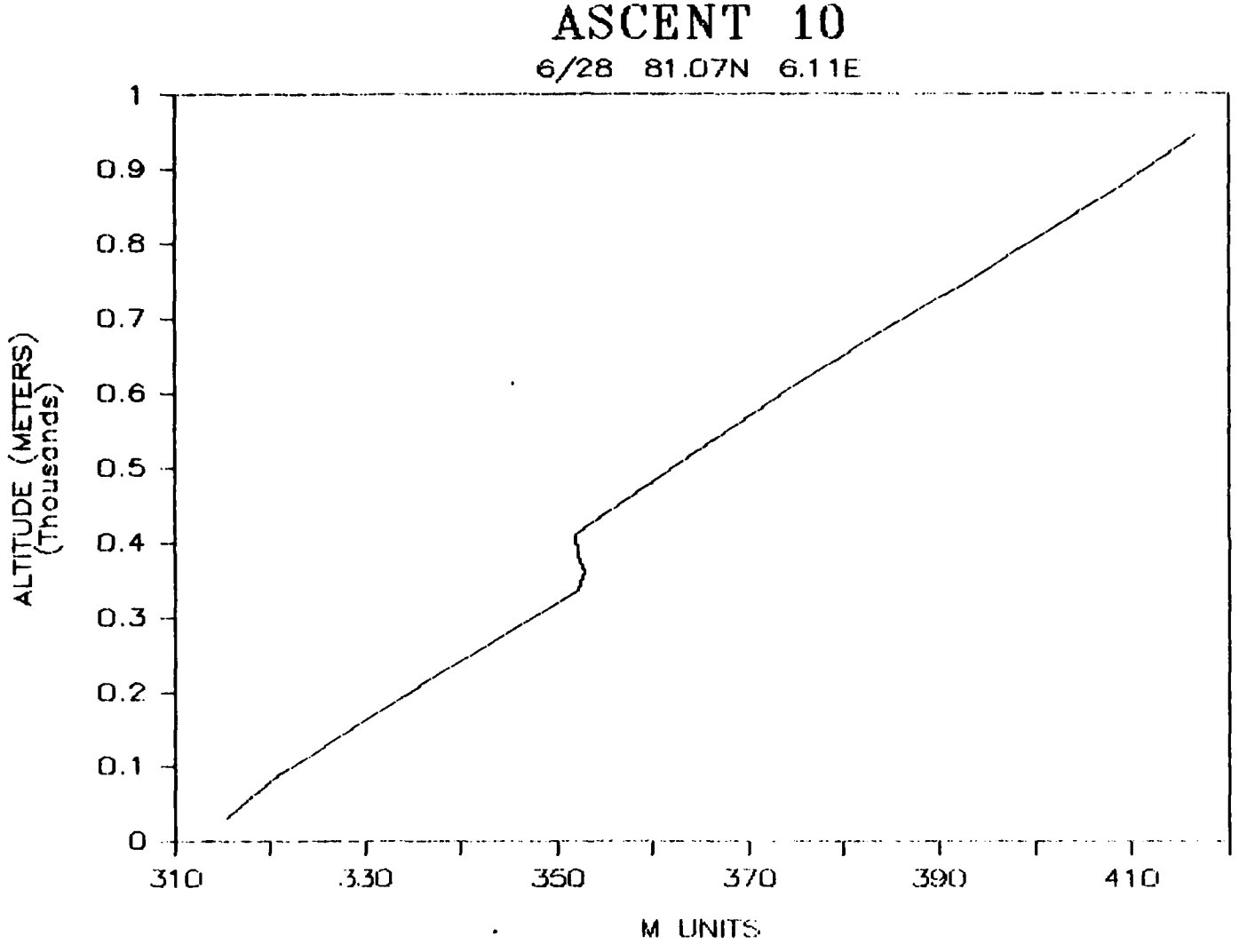
ASCENT 10
6/28 81.07N 6.11E
ALTITUDE (METERS)
(Thousands)
1
0.9
0.8
0.7
0.6
0.5
0.4
0.3
0.2
0.1
0
310
330
350
370
390
410
M UNITS

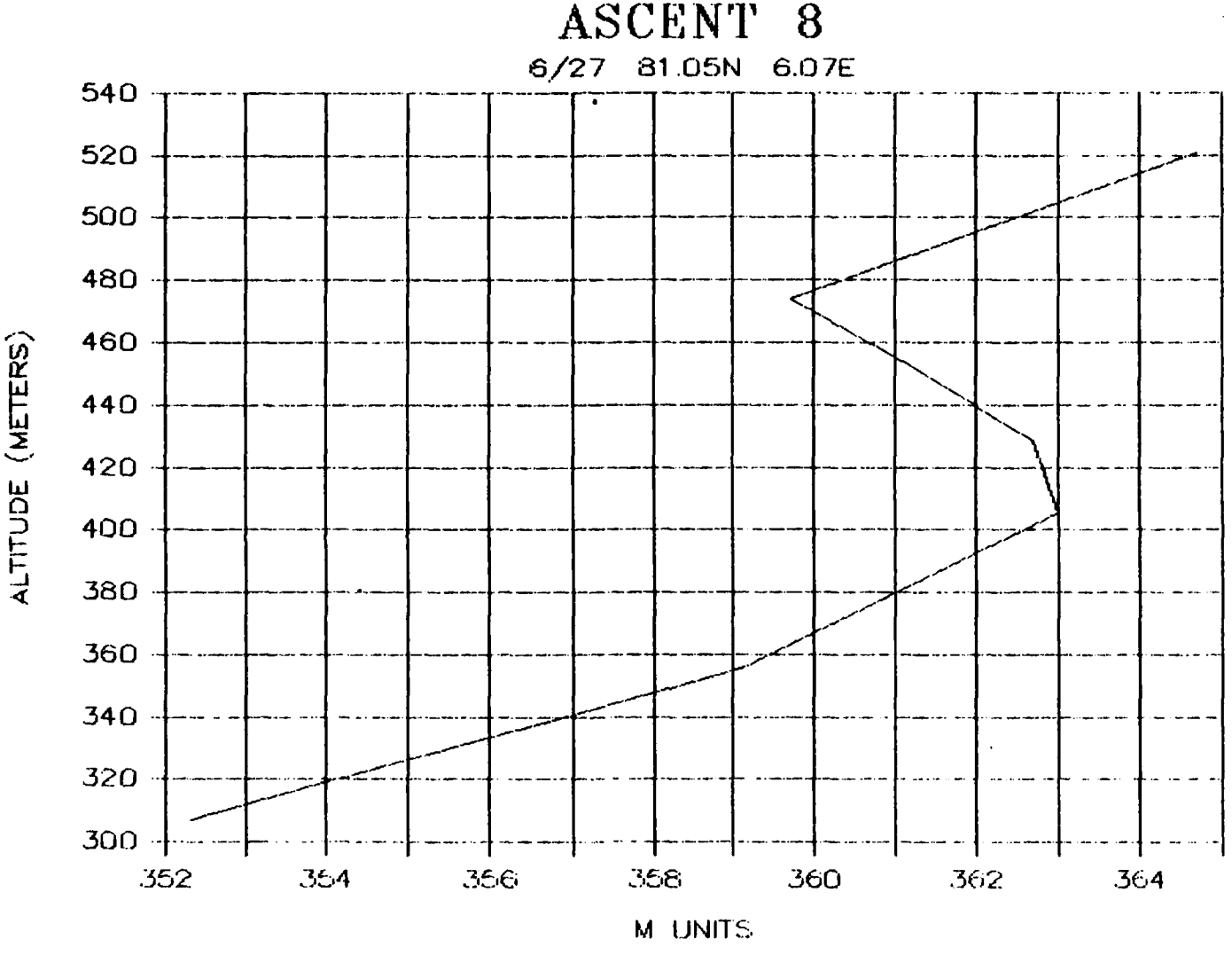
ASCENT 8
6/27 81.05N 6.07E
ALTITUDE (METERS)
540
520
500
480
460
440
420
400
380
360
340
320
300
352
354
356
358
360
362
364
M UNITS

APPENDIX B

DUCT PROFILES

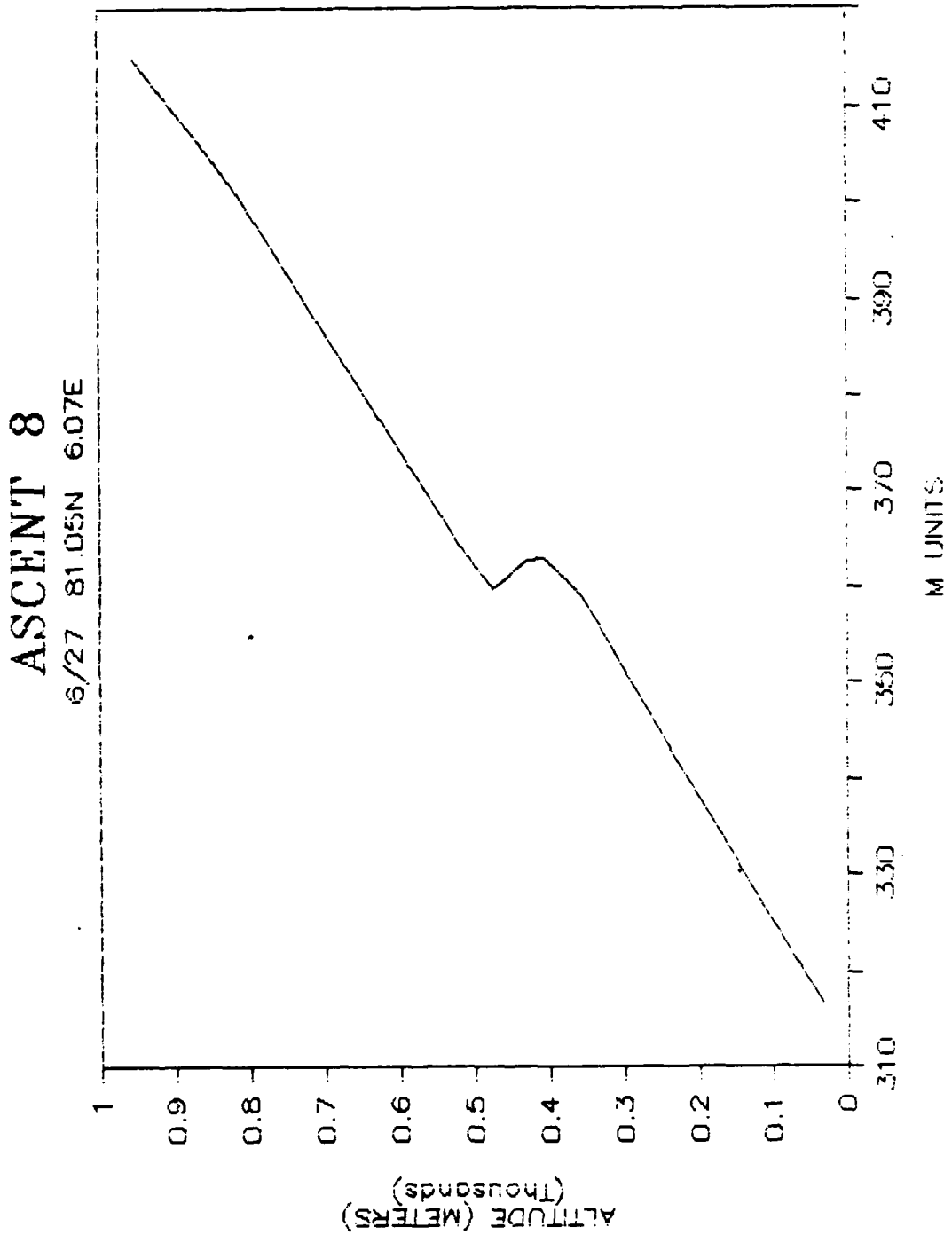

83	7/25	79.67N	2.98E	2332	1009.0	1.6	200	6.0
	STRATOCUMULUS							
84	7/26	79.02N	2.65E	1937	1016.4	0.1	240	3.0
	STRATUS, CEILING 80 METERS							
85	7/27	78.57N	1.96E	1404	1019.5	4.1	153	5.4
	STRATOCUMULUS, IN OPEN WATER, ICE TO THE WEST							
86	7/28	77.99N	-3.45E	1331	1013.1	1.8	100	5.0
	STRATOCUMULUS WITH BREAKS AND OCCASIONAL DRIZZLE							
87	7/28	77.99N	-4.32E	1737	1010.1	1.8	102	7.6
	HEAVY FOG							
88	7/29	77.18N	-5.87E	1329	1003.5	0.6	160	4.0
	STRATUS, CEILING 400 METERS							

66 7/19 79.17N 0.88E 2327 1010.3 -0.1 340 7.0
STRATUS, LT SNOW OR SLEET

67 7/20 79.00N -1.07E 1127 1013.5 -0.3 300 4.2
FOG

68 7/20 78.97N -1.39E 1805 1013.1 0.0 230 2.0
MOSTLY CLEAR, 1/8 ALTOCUMULUS TO THE WEST

69 7/20 78.97N -1.56E 2329 1013.1 -0.3 230 2.0
SUNNY, CLEAR

70 7/21 78.90N -1.70E 0450 1013.6 -0.3 185 3.4
CLEAR

71 7/21 78.98N -1.90E 1131 1014.8 1.1 200 2.0
SUNNY, ALTOCUMULUS AND ALTOSTRATUS TO THE SOUTH

72 7/21 78.96N -2.10E 1730 1014.5 1.7 200 1.7
1/4 ALTOCUMULUS TO THE SOUTH AND WEST

73 7/21 78.96N -2.24E 2330 1014.5 0.9 032 2.5
7/8 ALTOCUMULUS

74 7/22 78.95N -2.45E 0546 1013.4 0.8 235 4.2
ALTOCUMULUS OVERCAST

75 7/22 78.93N -2.58E 1128 1012.5 1.0 030 5.0
7/8 ALTOCUMULUS IN LAYERS, BLUE SKY OVERHEAD

76 7/22 78.90N -2.79E 1729 1011.0 1.3 053 4.3
1/4 ALTOCUMULUS

77 7/23 78.87N -2.97E 0135 1010.2 0.6 160 1.0
FOG, MIST

78 7/23 78.85N -3.06E 0640 1010.0 0.0 251 8.0
HEAVY FOG

79 7/23 78.80N -3.19E 1127 1009.5 0.3 155 0.6
FOG

80 7/23 78.75N -3.36E 2338 1010.0 -0.5 320 1.5
FOG

81 7/24 78.75N -1.60E 0957 1011.3 0.8 265 4.3
FOG

82 7/25 79.25N 3.01E 1427 1010.0 1.6 200 1.6
FOG, LT DRIZZLE

49 7/11 79.69N 2.65E 0901 1016.8 1.0 268 6.2
ALTOCUMULUS

50 7/13 79.31N 3.61E 0906 1008.1 -2.4 245 2.4
PATCHY FOG, STRATUS ABOVE

51 7/13 79.31N 2.43E 1703 1006.2 -0.6 317 2.1
THIN STRATOCUMULUS IN CELLS

52 7/13 79.27N 2.87E 2330 1005.5 0.1 333 3.7
STRATUS, LIGHT SNOW JUST ENDED, CEILING 200 METERS

53 7/14 79.31N 1.90E 1133 1005.6 -0.7 310 3.7
PATCHY FOG, CUMULUS OVERCAST, SNOW SHOWER AT 1330

54 7/14 79.30N 1.90E 2022 1002.4 -0.4 277 3.8
STRATOCUMULUS

55 7/14 79.35N 2.95E 2332 1001.5 -0.4 300 4.2
STRATOCUMULUS, SNOW SHOWERS, 3/8 ICE

56 7/15 79.27N 3.12E 1134 1002.7 0.5 247 2.2
LOW CUMULUS, 5/8 ALTOCUMULUS

57 7/15 79.14N 3.18E 2335 1006.5 2.0 020 4.1
CUMULUS AND ALTOCUMULUS

58 7/16 79.22N 3.17E 1147 1010.6 3.3 040 9.0
STRATOCUMULUS, IN OPEN WATER

59 7/16 79.30N 2.33E 1734 1012.2 0.9 010 8.7
STRATOCUMULUS, IN LOOSE BRASH AT ICE EDGE

60 7/16 79.13N 2.23E 2333 1011.8 0.8 000 9.8
STRATUS, AT ICE EDGE IN DENSE PACK

61 7/17 78.98N 1.31E 1415 1010.1 -0.5 340 8.0
1/4 CUMULUS, 1/4 ALTOCUMULUS, 1/4 CIRRUS, 1/4 ICE

62 7/17 78.76N 1.23E 2331 1006.6 -0.5 320 6.7
STRATOCUMULUS

63 7/18 78.77N 2.95E 1140 1004.4 0.9 345 5.5
STRATUS, IN OPEN WATER, ICE 10 KM TO N AND E

64 7/18 78.79N 2.89E 2336 1005.2 1.0 007 5.0
STRATUS, IN OPEN WATER, ICE 10 KM TO N AND E

65 7/19 79.25N 2.91E 1141 1005.2 0.8 006 3.8
OVERCAST, LT DRIZZLE, PATCHY FOG, IN OPEN WATER

32	7/07	81.35N	7.18E	0530	996.1	1.4	158	3.1
	STRATUS, LOW DRIZZLE							
33	7/07	81.37N	7.24E	1726	997.1	0.0	250	5.6
	THIN OVERCAST							
34	7/08	81.40N	7.30E	0539	1000.4	-0.2	294	0.2
	STRATUS, LIGHT DRIZZLE							
35	7/08	81.40N	7.40E	1134	1003.0	0.0	195	3.2
	STRATUS							
36	7/08	81.33N	7.65E	1802	1003.6	0.2	121	2.6
	FOG							
37	7/08	81.36N	7.52E	2342	1003.5	1.2	140	5.0
	FOG							
38	7/09	81.39N	7.45E	0535	1002.8	1.0	173	3.0
	STRATUS, DRIZZLE							
39	7/09	81.39N	7.09E	1454	1002.3	1.0	141	1.4
	FOG							
40	7/09	81.38N	7.10E	1553	1002.0	0.9	141	2.2
	STRATUS, CEILING 170 METERS							
41	7/09	81.37N	7.07E	1738	1001.9	1.0	136	2.9
	STRATUS, 7/8 ICE							
42	7/09	81.35N	7.14E	1904	1001.5	1.0	126	1.6
	FOG							
43	7/09	81.34N	7.17E	2330	1001.1	0.9	000	4.4
	FOG							
44	7/10	81.25N	7.32E	0236	1006.1	0.2	354	5.0
	STRATUS, DRIZZLE							
45	7/10	81.14N	7.36E	0535	1001.2	-0.2	342	5.4
	AT ICE EDGE, SCATTERED LOW CUMULUS, ALTOSTRATUS ABOVE							
46	7/10	80.92N	7.36E	0830	1001.8	-0.1	336	6.7
	FOG, NO ICE							
47	7/10	80.66N	6.83E	1132	1003.1	-0.3	326	7.1
	STRATUS							
48	7/10	79.77N	1.89E	2336	1012.6	1.0	300	6.2
	ALTOSTRATUS							

15	7/01	81.18N	7.18E	1553	1009.7	0.0	224	3.4
	CLEAR							
16	7/01	81.18N	7.11E	0123	1010.2	-0.4	248	1.0
	THICK FOG, DRY SPIKES ABOVE STRATUS							
17	7/02	81.21N	7.30E	1131	1010.3	0.9	212	4.5
	FOG							
18	7/02	81.19N	7.30E	2333	1010.0	0.0	227	3.1
	7/8 ALTOCUMULUS							
19	7/03	81.22N	7.52E	1134	1014.0	0.9	190	3.3
	SUNNY AND CLEAR							
20	7/03	81.21N	7.46E	2330	1015.4	0.6	158	3.2
	FOG							
21	7/04	81.24N	7.52E	0805	1015.1	-0.5	097	4.6
	FOG							
22	7/04	81.24N	7.38E	0415	1010.2	-0.5	077	5.2
	FOG							
23	7/04	81.25N	7.16E	0423	1006.4	-0.1	075	5.2
	FOG							
24	7/05	81.28N	6.97E	0511	1004.5	0.2	084	2.8
	FOG, LT DRIZZLE							
25	7/06	81.30N	6.97E	0022	1004.0	0.3	216	4.3
	FOG, LT DRIZZLE IN LAST HALF HOUR							
26	7/06	81.32N	7.23E	0815	1003.7	0.5	188	3.4
	STRATUS, DRIZZLE							
27	7/06	81.25N	7.18E	1615	1002.2	0.9	144	1.4
	STRATUS							
28	7/06	81.33N	7.18E	1818	1000.1	2.0	173	3.6
	STRATUS							
29	7/06	81.33N	7.18E	2046	999.4	1.7	153	3.9
	LOW STRATUS, DRIZZLE							
30	7/06	81.32N	7.18E	2333	998.0	1.6	171	3.8
	STRATUS							
31	7/07	81.33N	7.17E	0245	996.6	1.0	142	2.9
	STRATUS							

ASCENT 15

7/01 81.18N 7.18E

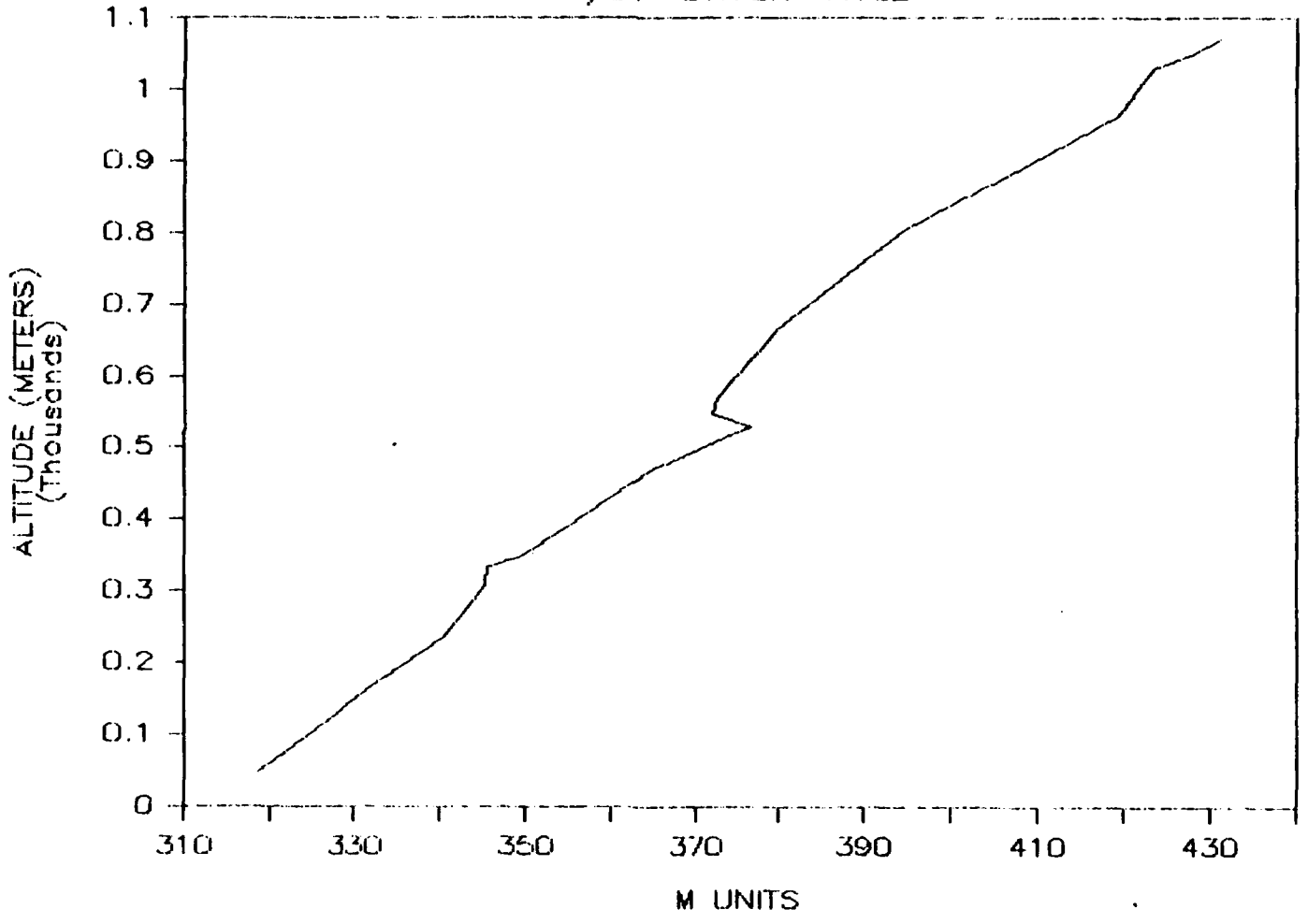

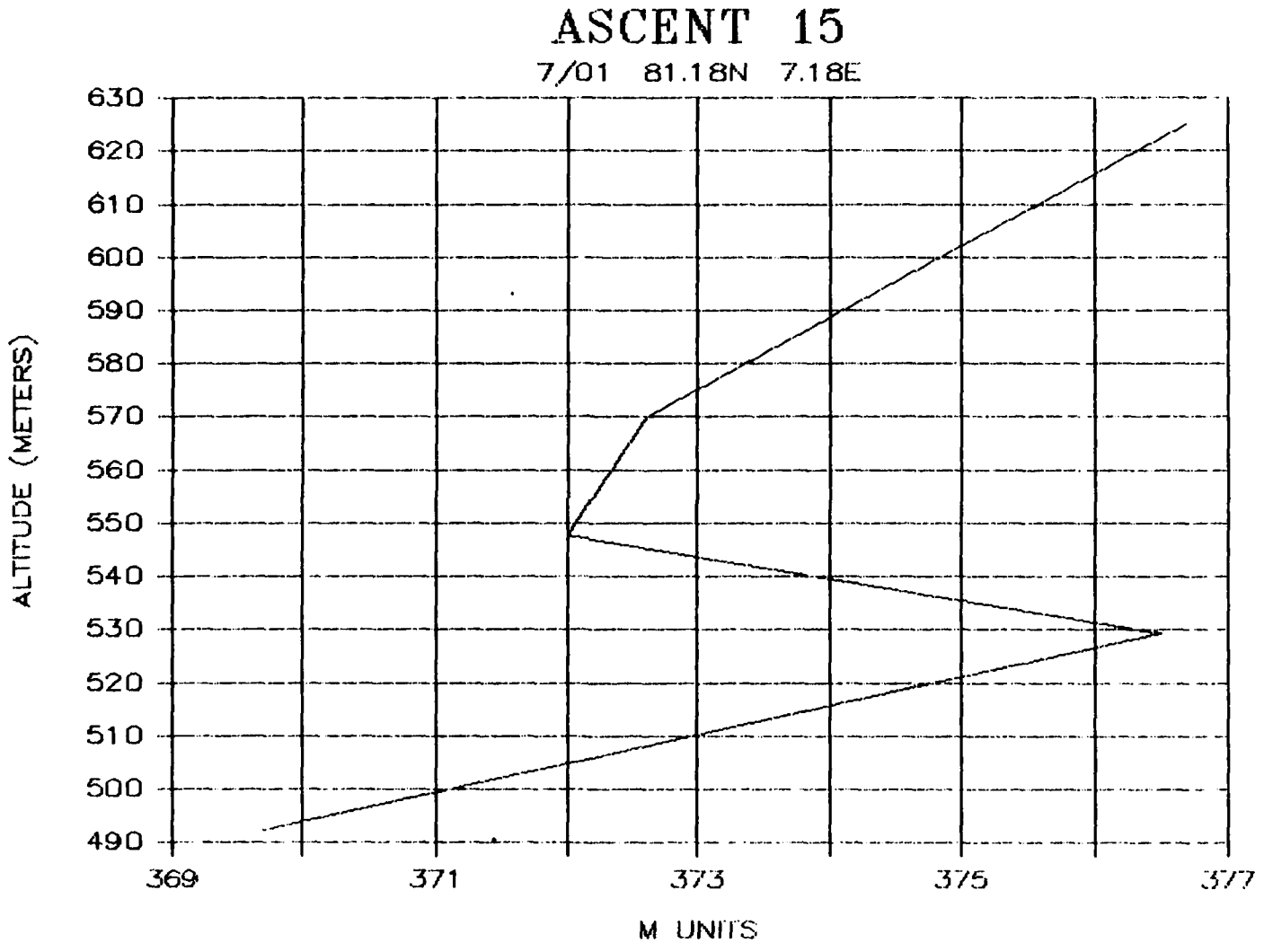
ASCENT 15
7/01 81.18N 7.18E
630
620
610
600
590
580
570
560
550
540
530
520
510
500
490
ALTITUDE (METERS)
369
371
373
375
377
M UNITS

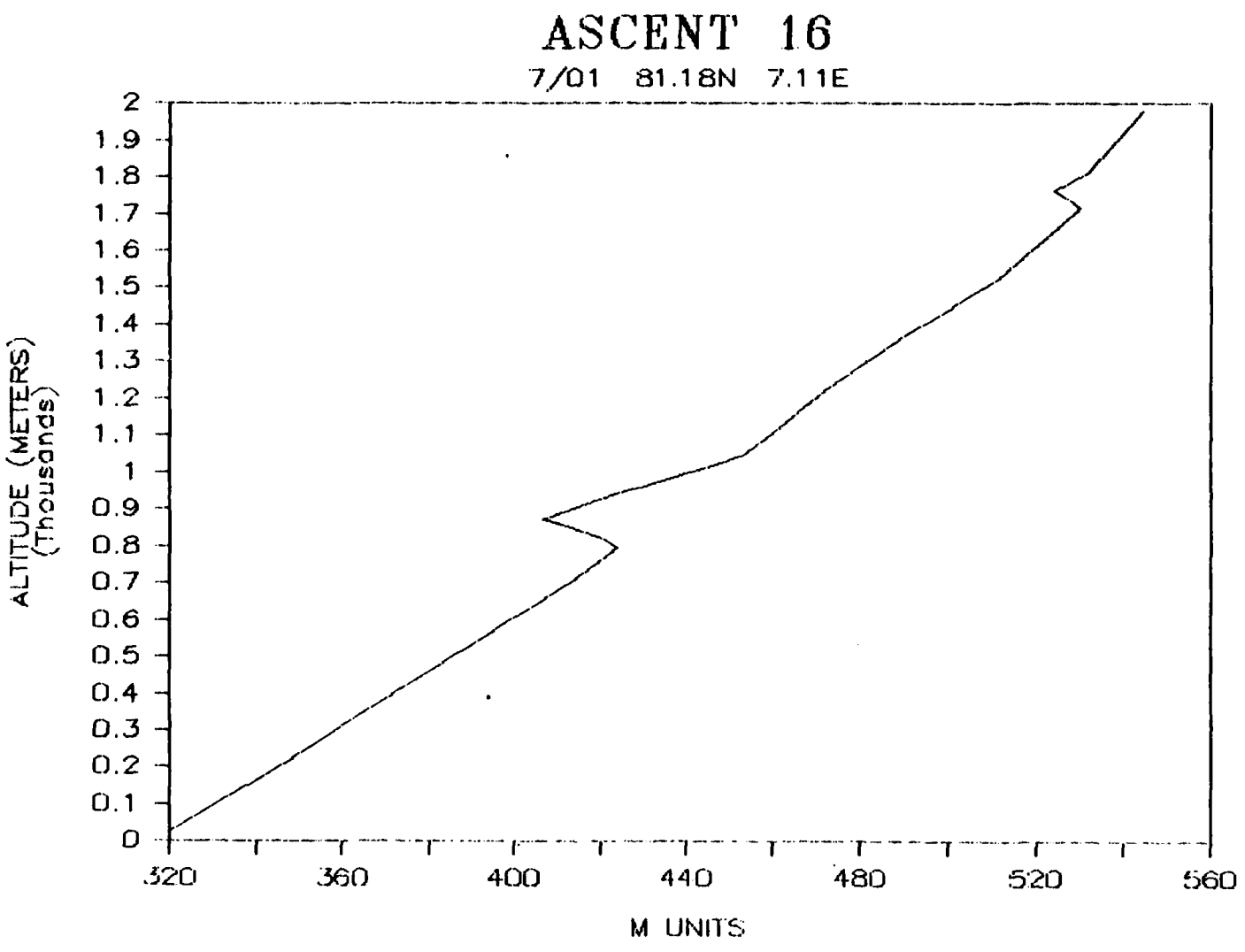
ASCENT 16
7/01 81.18N 7.11E
ALTITUDE (METERS)
(Thousands)
2
1.9
1.8
1.7
1.6
1.5
1.4
1.3
1.2
1.1
1
0.9
0.8
0.7
0.6
0.5
0.4
0.3
0.2
0.1
0
320
360
400
440
480
520
560
M UNITS

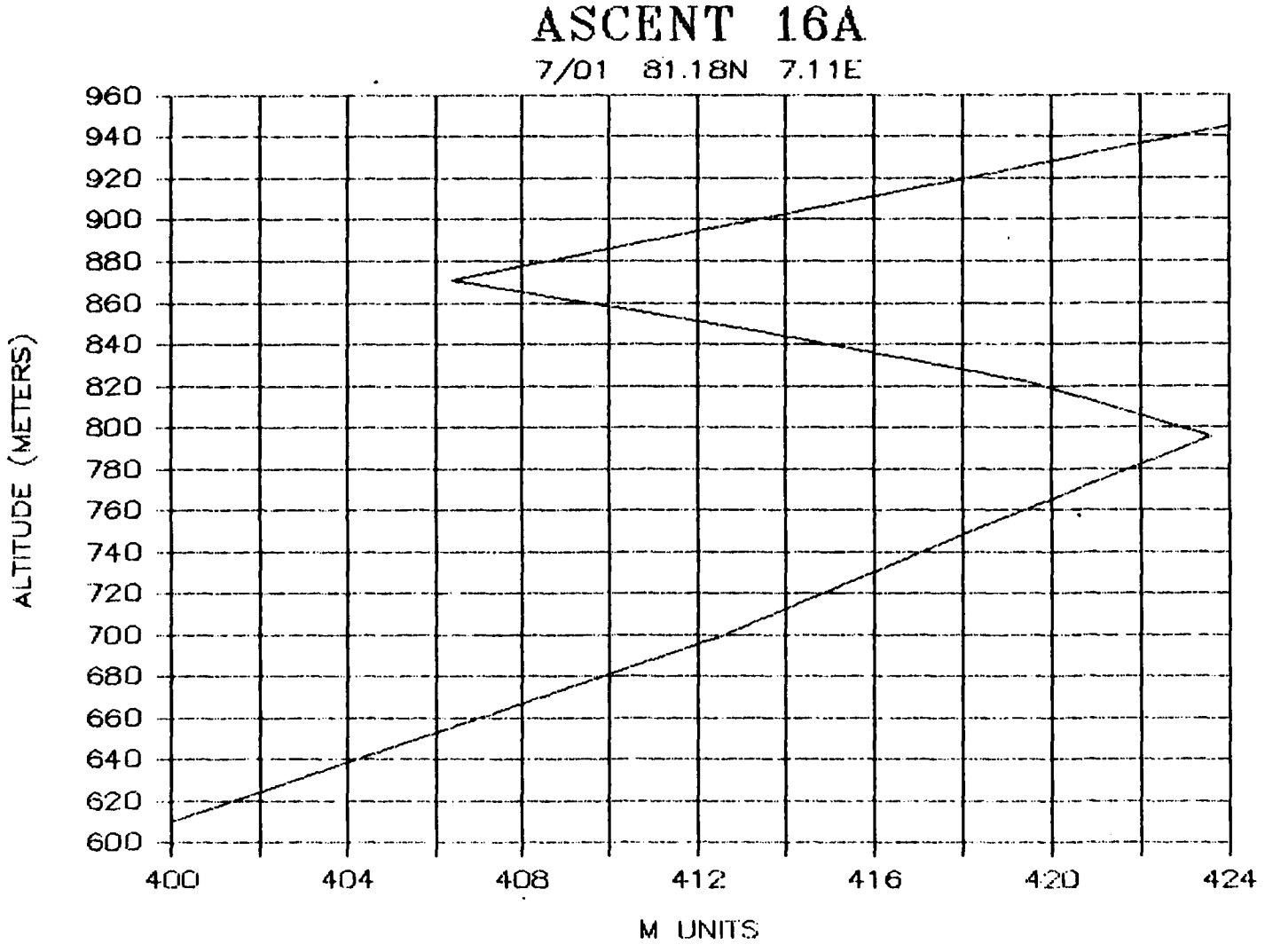
ASCENT 16A
7/01 81.18N 7.11E
960
940
920
900
880
860
840
820
800
780
760
740
720
700
680
660
640
620
600
ALTITUDE (METERS)
400
404
408
412
416
420
424
M UNITS

ASCENT 16B

7/01 81.18N 7.11E

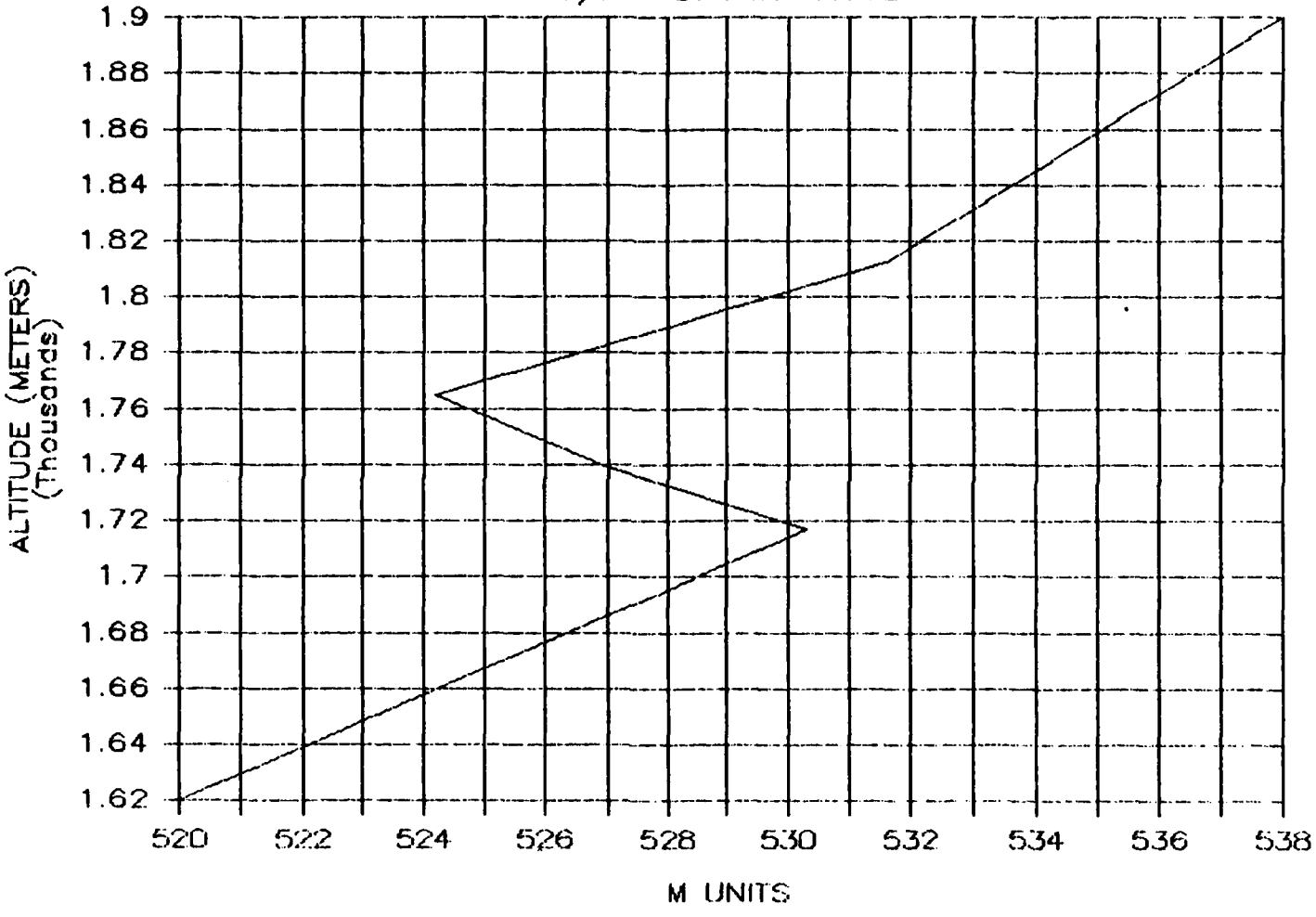

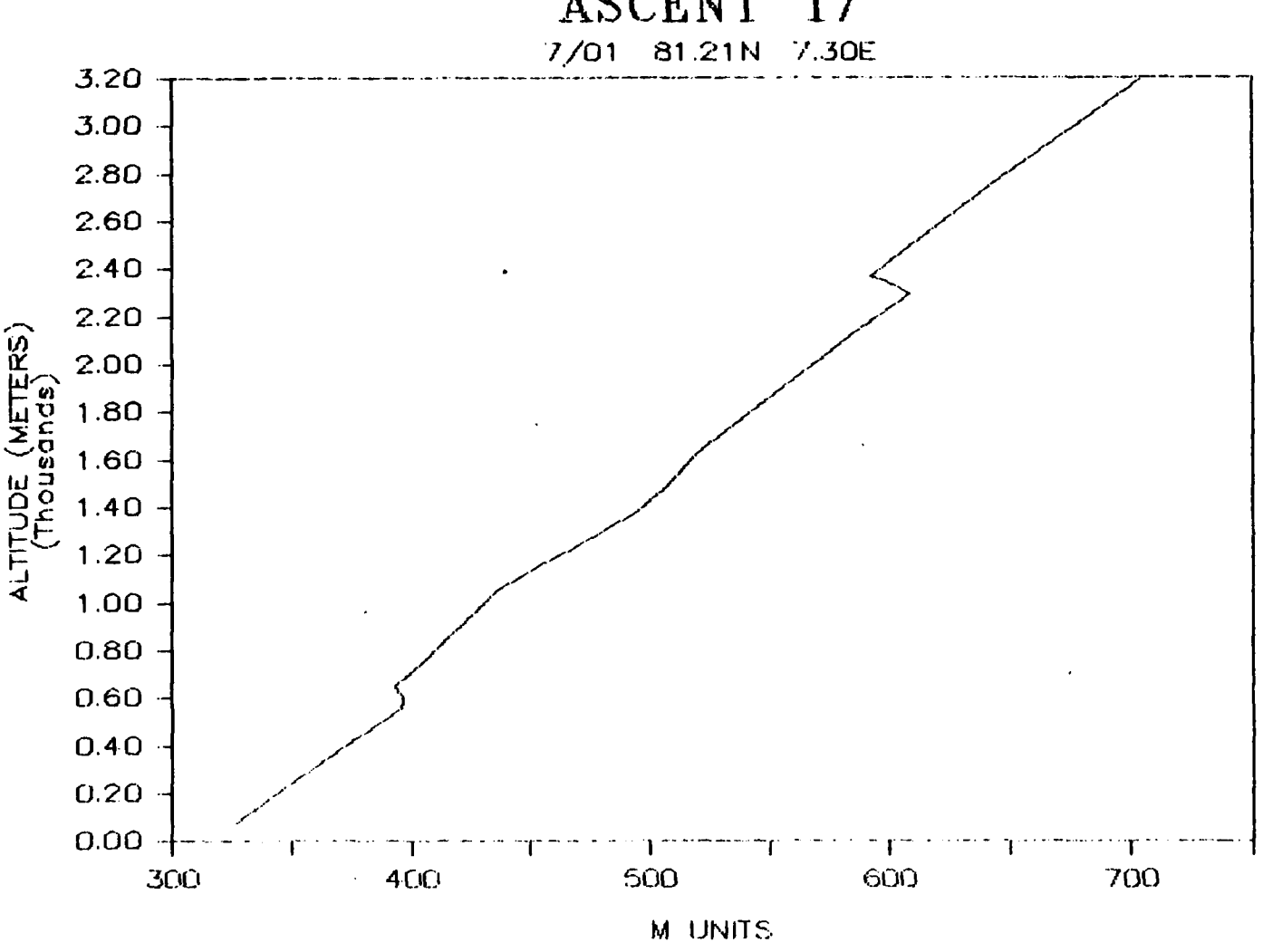
ASCENT 17
7/01 81.21N 7.30E
ALTITUDE (METERS)
(Thousands)
3.20
3.00
2.80
2.60
2.40
2.20
2.00
1.80
1.60
1.40
1.20
1.00
0.80
0.60
0.40
0.20
0.00
300
400
500
600
700
M UNITS

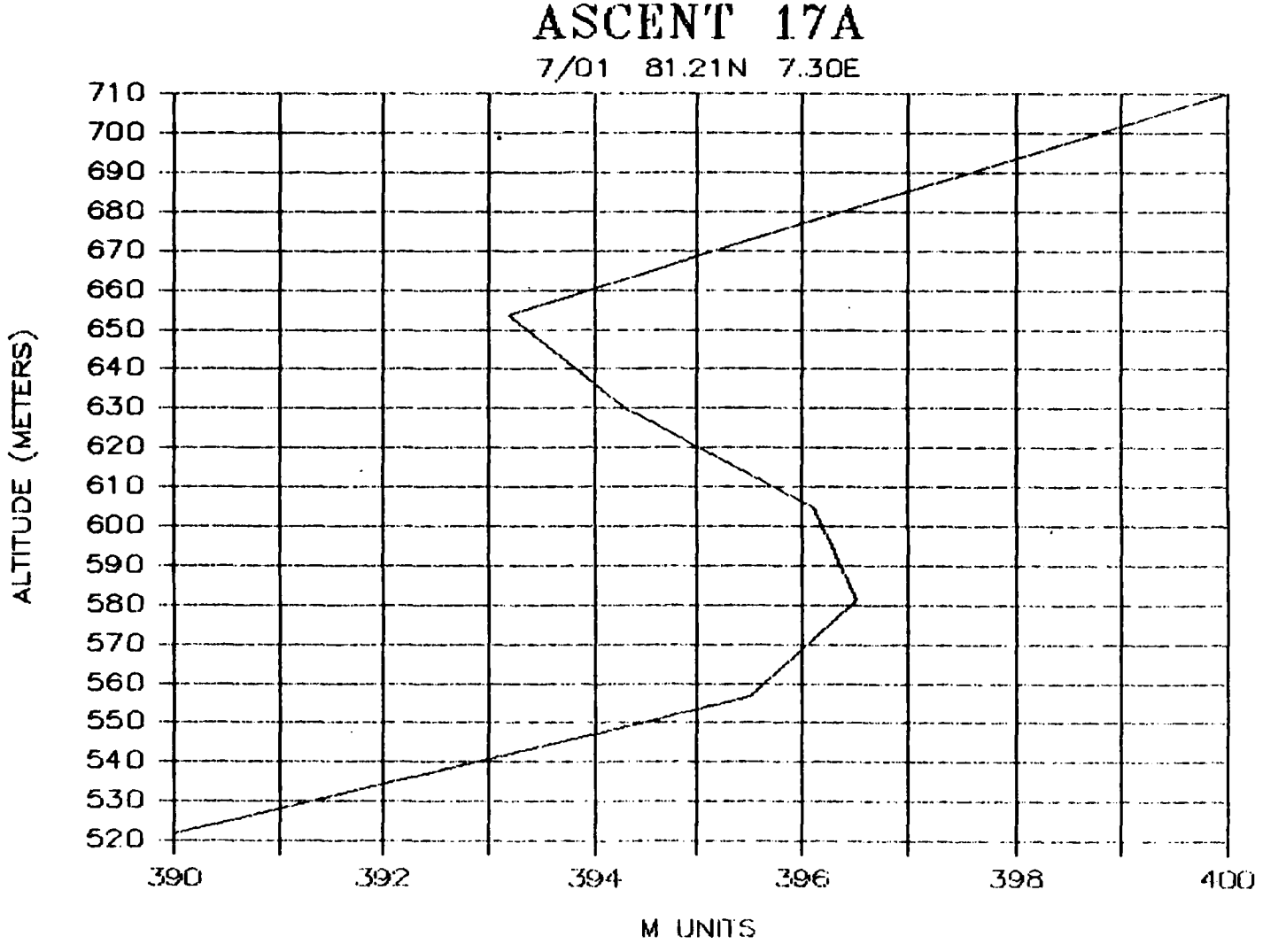
ASCENT 17A
7/01 81.21N 7.30E
ALTITUDE (METERS)
710
700
690
680
670
660
650
640
630
620
610
600
590
580
570
560
550
540
530
520
390
392
394
396
398
400
M UNITS

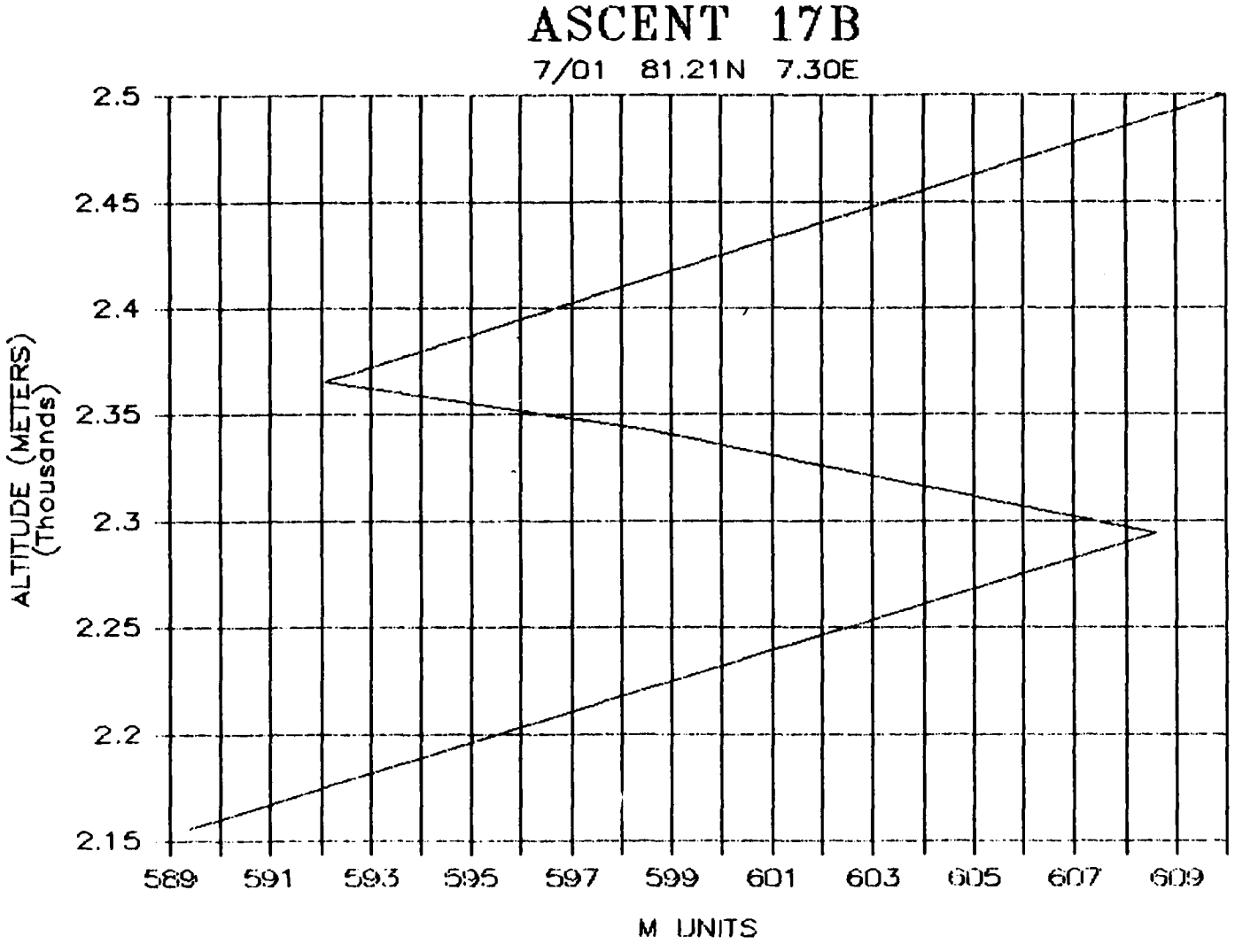
ASCENT 17B
7/01 81.21N 7.30E
ALTITUDE (METERS)
(Thousands)
2.5
2.45
2.4
2.35
2.3
2.25
2.2
2.15
589
591
593
595
597
599
601
603
605
607
609
M UNITS

ASCENT 18

7/02 81.19N 7.30E

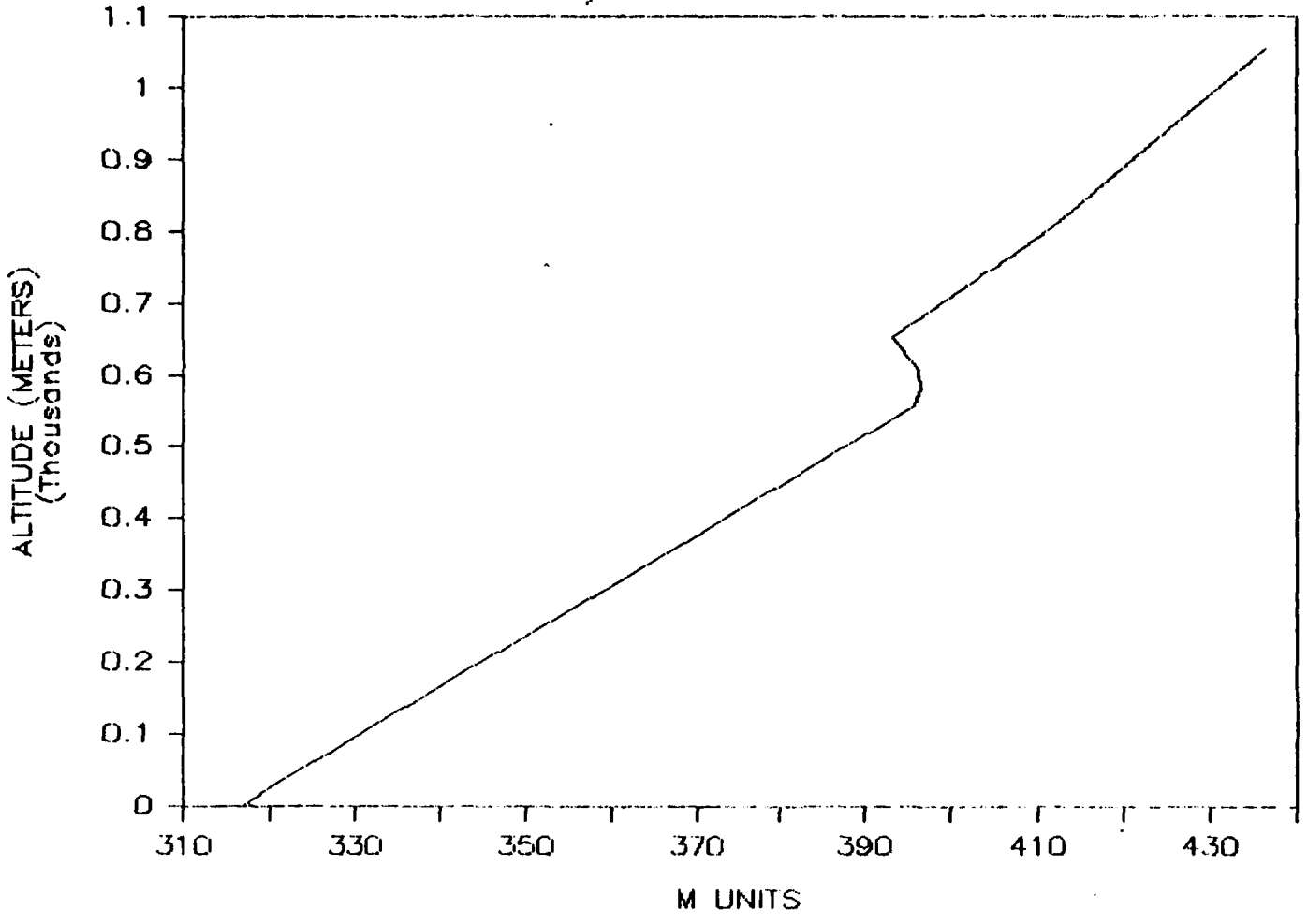

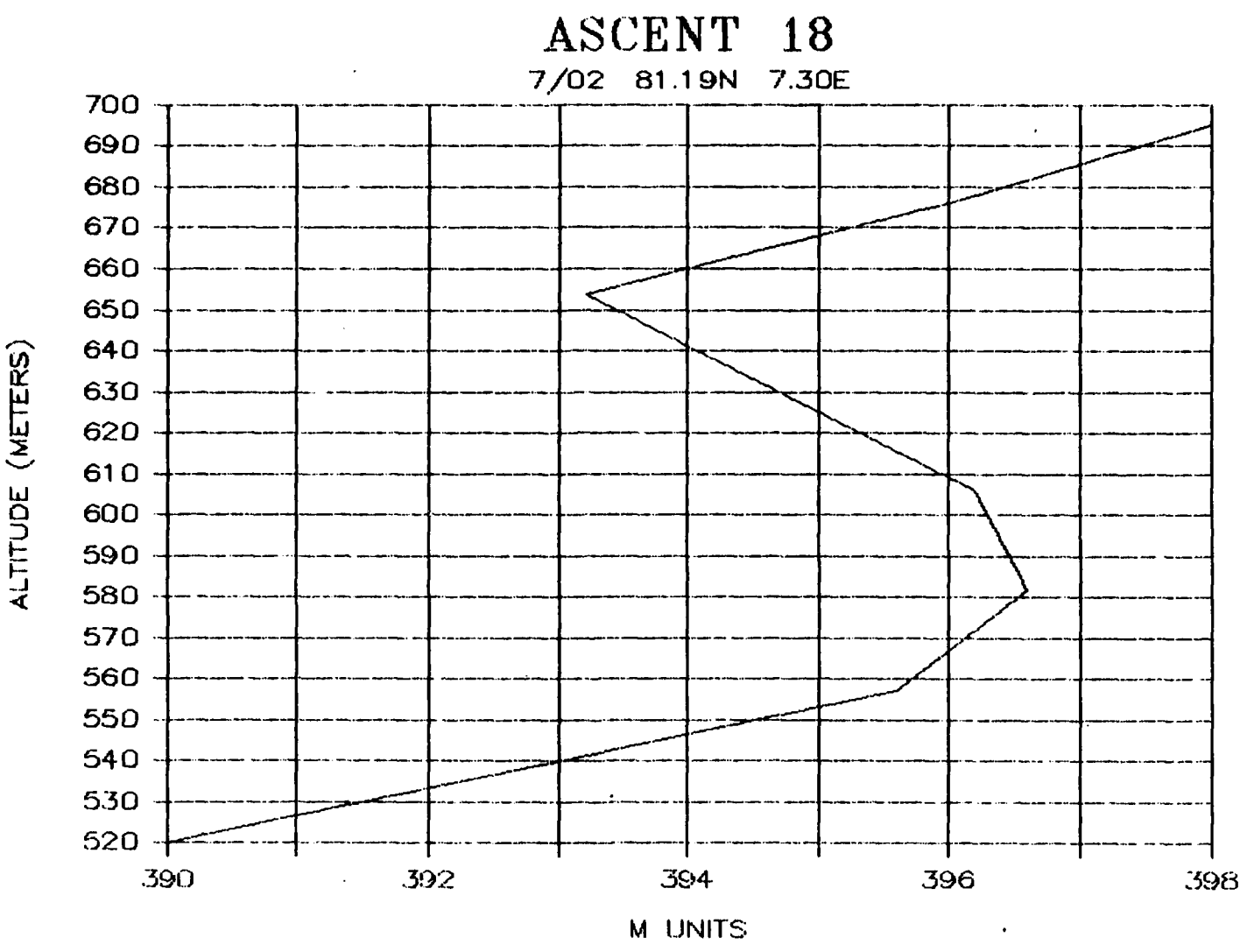
ASCENT 18
7/02 81.19N 7.30E
ALTITUDE (METERS)
700
690
680
670
660
650
640
630
620
610
600
590
580
570
560
550
540
530
520
390
392
394
396
398
M UNITS

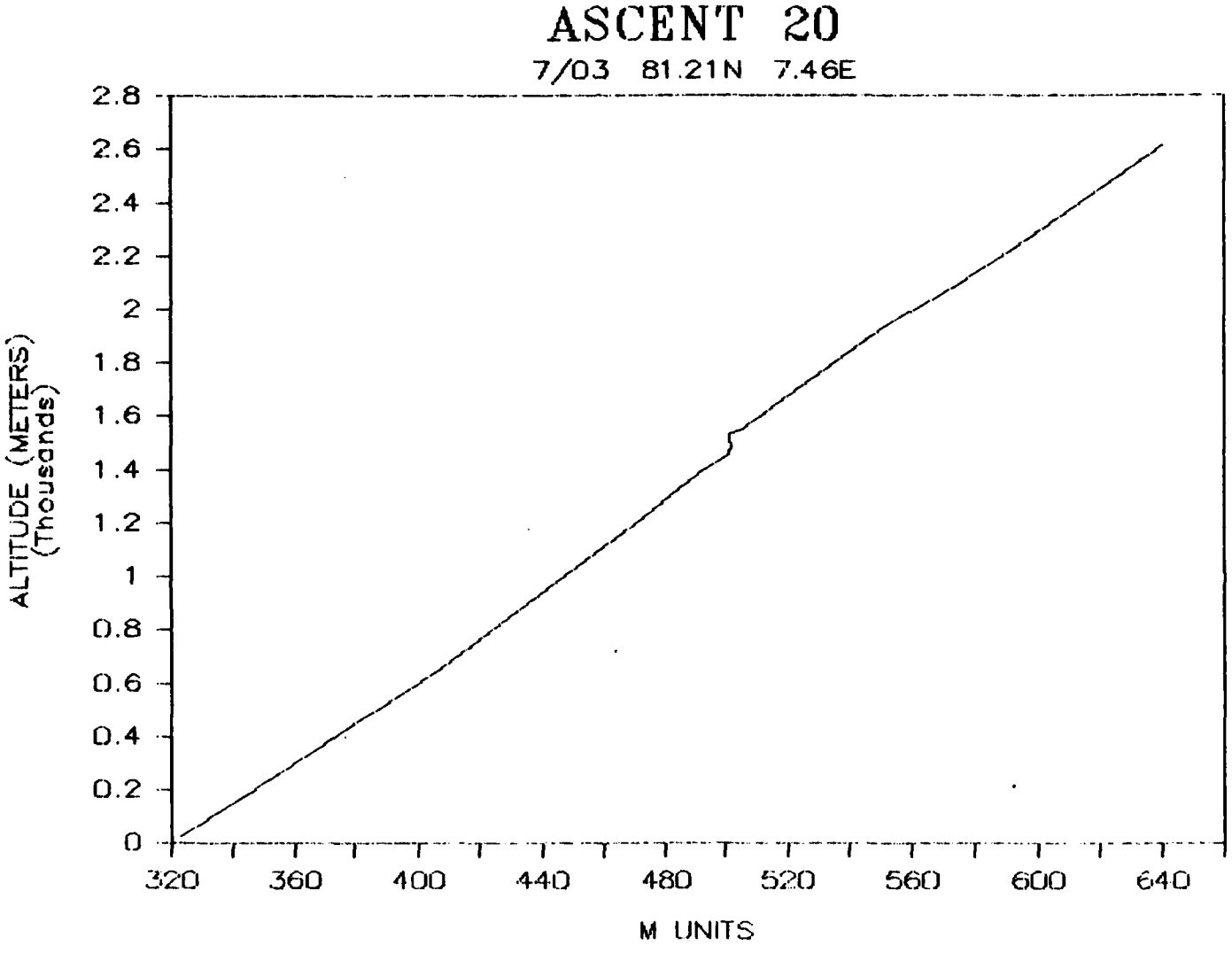
ASCENT 20
7/03 81.21N 7.46E
ALTITUDE (METERS)
(Thousands)
2.8
2.6
2.4
2.2
2
1.8
1.6
1.4
1.2
1
0.8
0.6
0.4
0.2
0
320
360
400
440
480
520
560
600
640
M UNITS

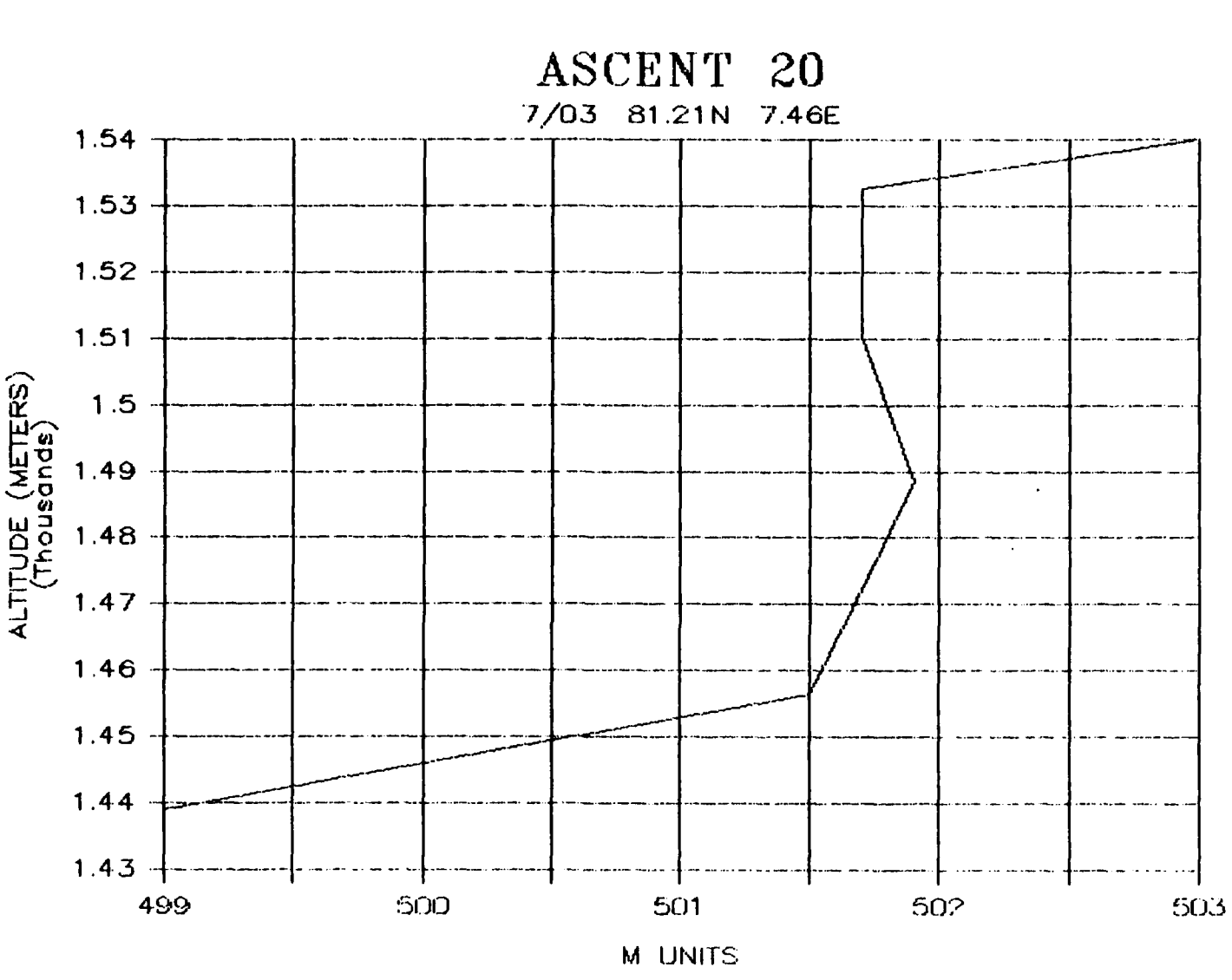
ASCENT 20
7/03 81.21N 7.46E
ALTITUDE (METERS)
(Thousands)
1.54
1.53
1.52
1.51
1.5
1.49
1.48
1.47
1.46
1.45
1.44
1.43
499
500
501
502
503
M UNITS

ASCENT 22

7/04 81.24N 7.38E

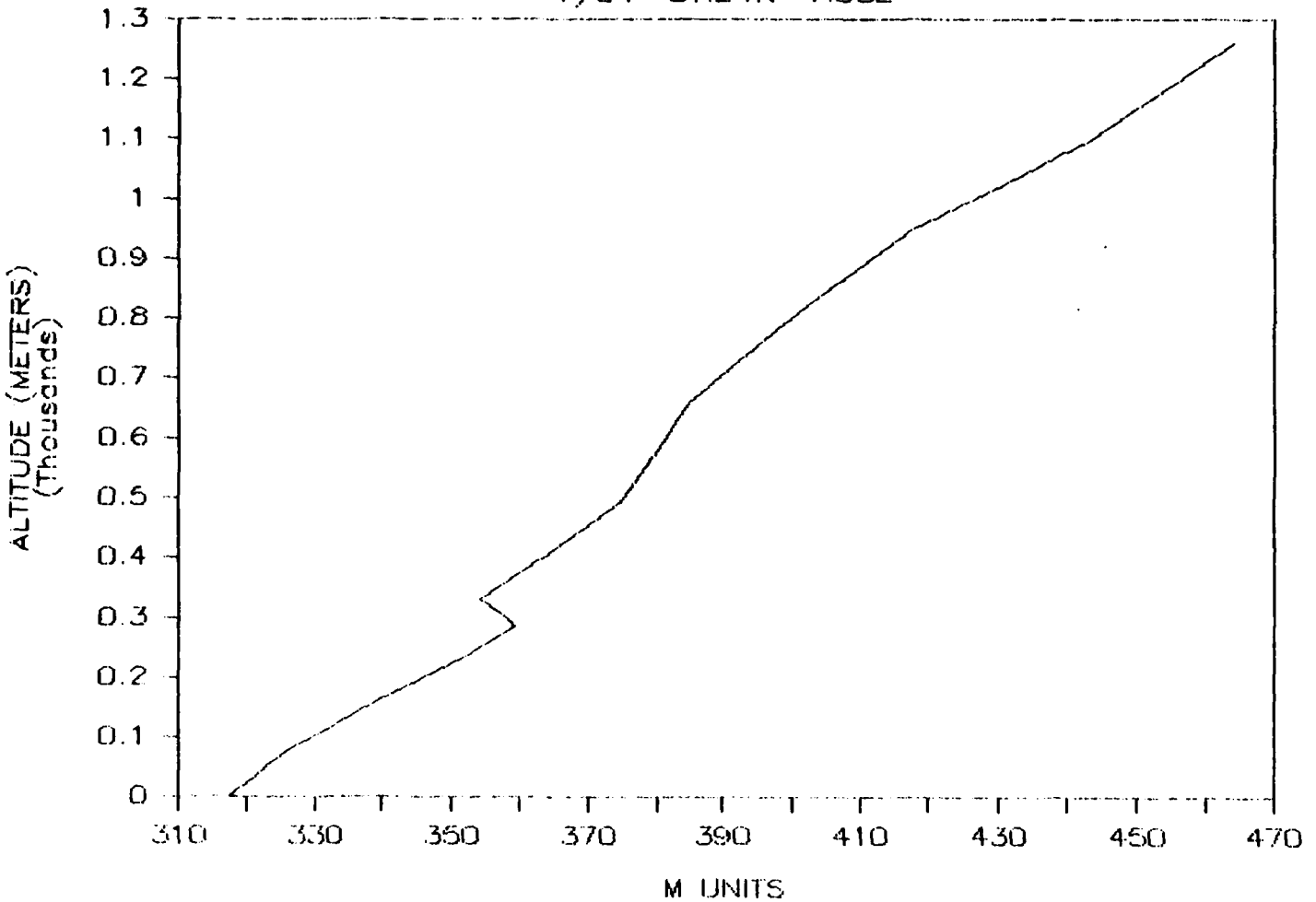

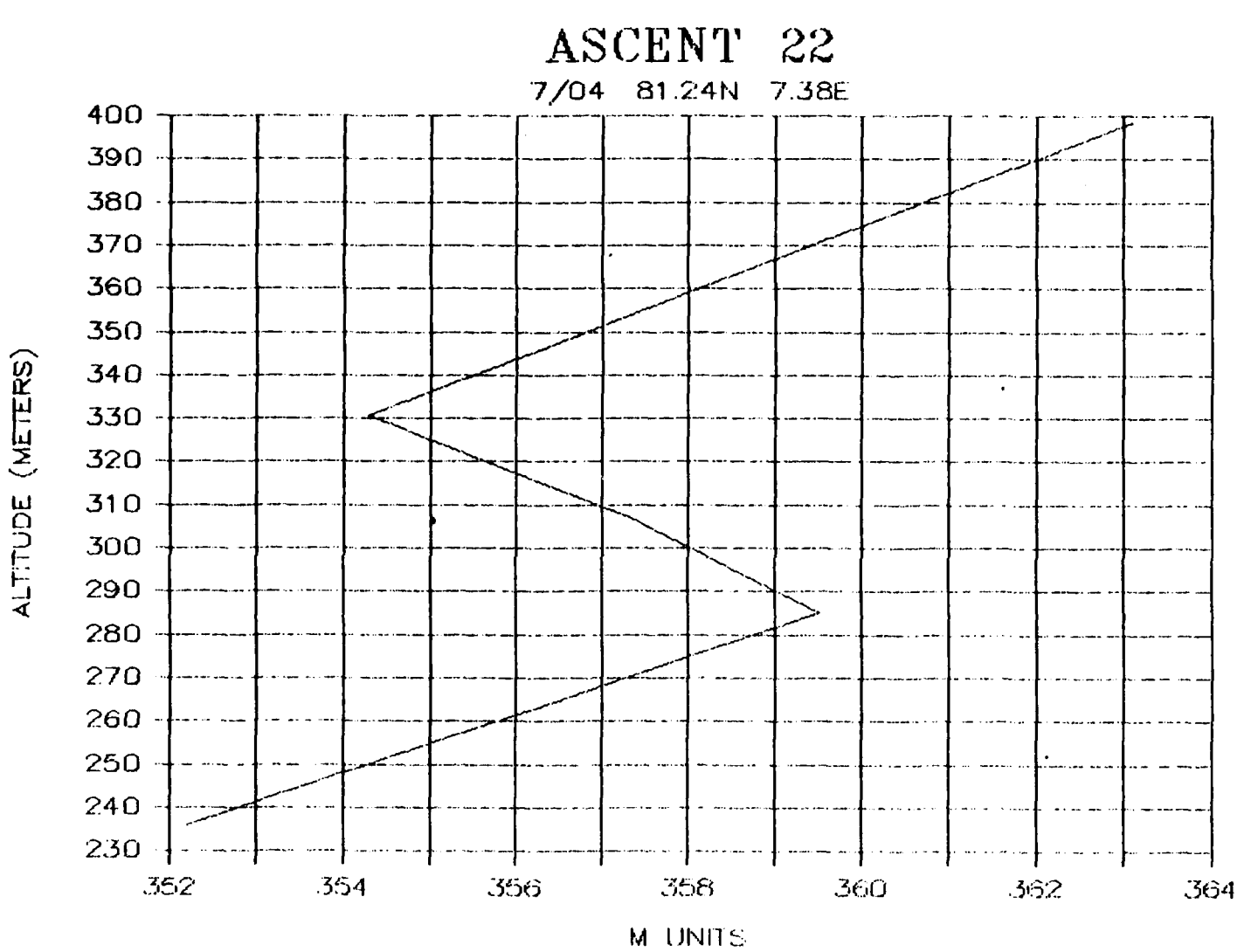
ASCENT 22
7/04 81.24N 7.38E
ALTITUDE (METERS)
400
390
380
370
360
350
340
330
320
310
300
290
280
270
260
250
240
230
352
354
356
358
360
362
364
M UNITS

AD-A152 346 AN ASSESSMENT OF ATMOSPHERIC REFRACTIVITY IN THE NORTHERN MARGINAL ICE ZONE(U) NAVAL POSTGRADUATE SCHOOL MONTEREY CA C T SUTHERLIN SEP 84 2/2

UNCLASSIFIED F/G 4/1 NL

END

FILMED

DTIC

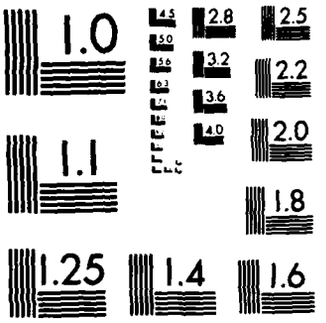

MICROCOPY RESOLUTION TEST CHART
NATIONAL BUREAU OF STANDARDS-1963-A

ASCENT 23

7/04 81.24N 7.16E

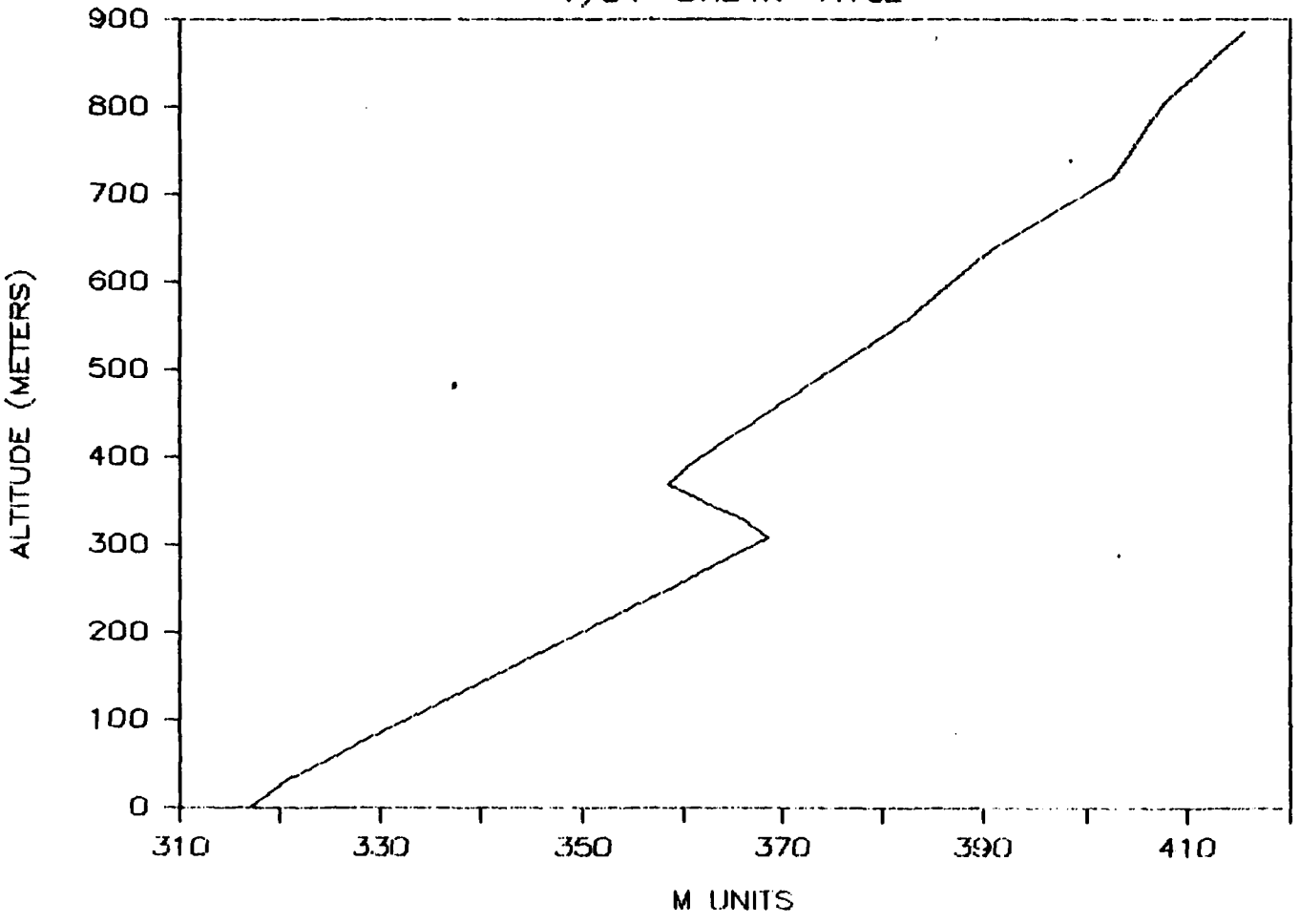

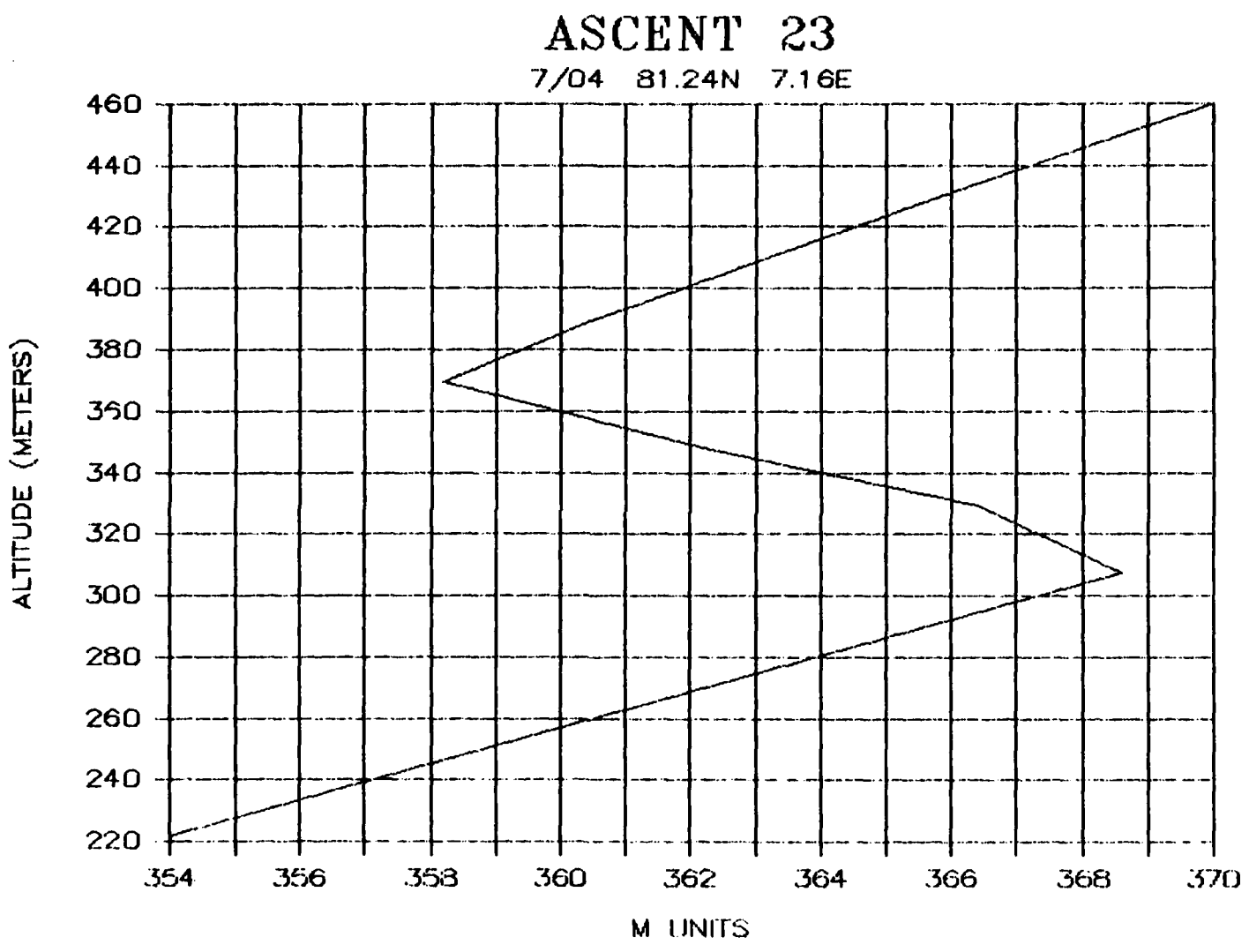
ASCENT 23
7/04 81.24N 7.16E
460
440
420
400
380
360
340
320
300
280
260
240
220
ALTITUDE (METERS)
354
356
358
360
362
364
366
368
370
M UNITS

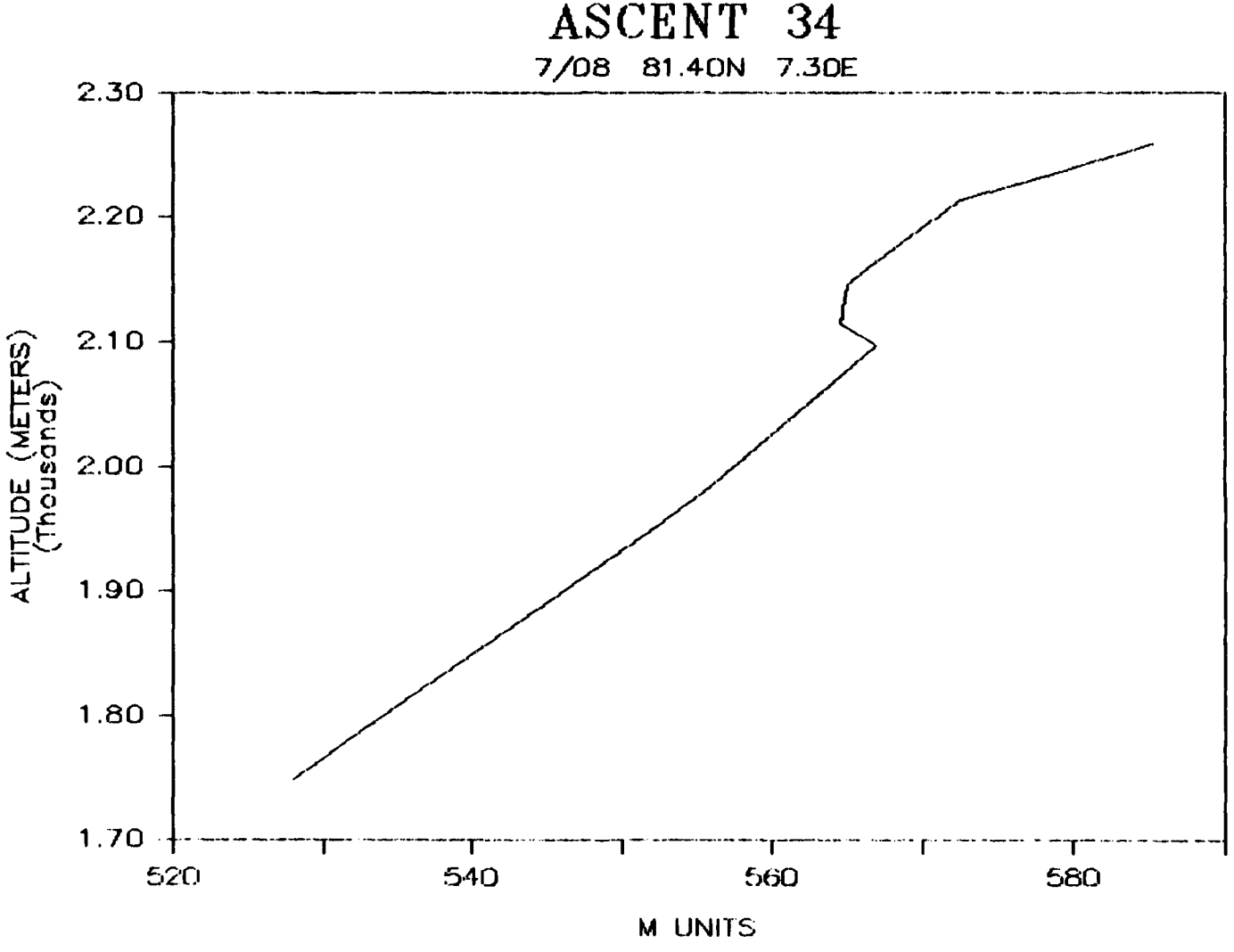
ASCENT 34
7/08 81.40N 7.30E
2.30
2.20
2.10
2.00
1.90
1.80
1.70
ALTITUDE (METERS)
(Thousands)
520
540
560
580
M UNITS

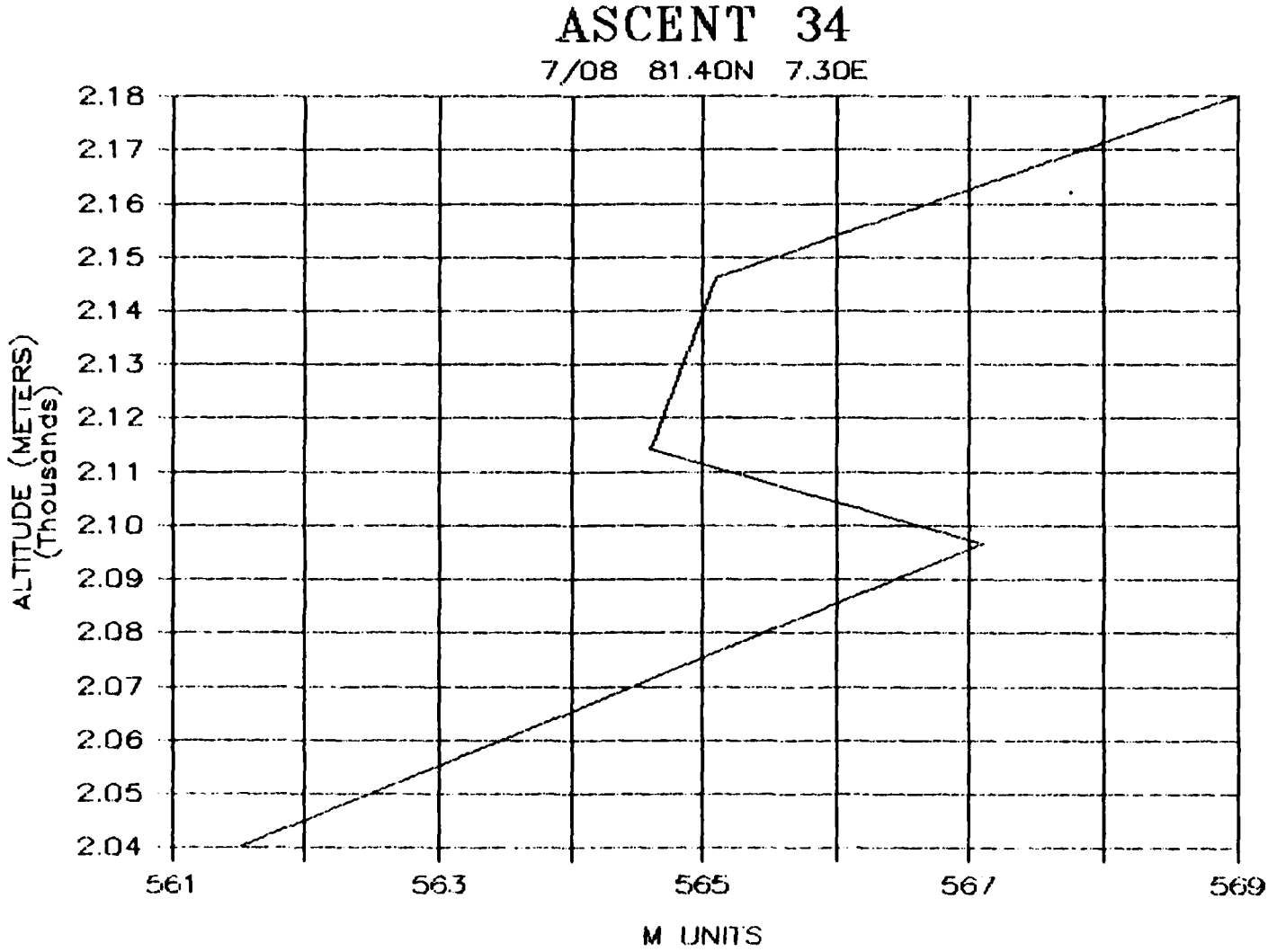
ASCENT 34
7/08 81.40N 7.30E
ALTITUDE (METERS)
(Thousands)
2.18
2.17
2.16
2.15
2.14
2.13
2.12
2.11
2.10
2.09
2.08
2.07
2.06
2.05
2.04
561
563
565
567
569
M UNITS

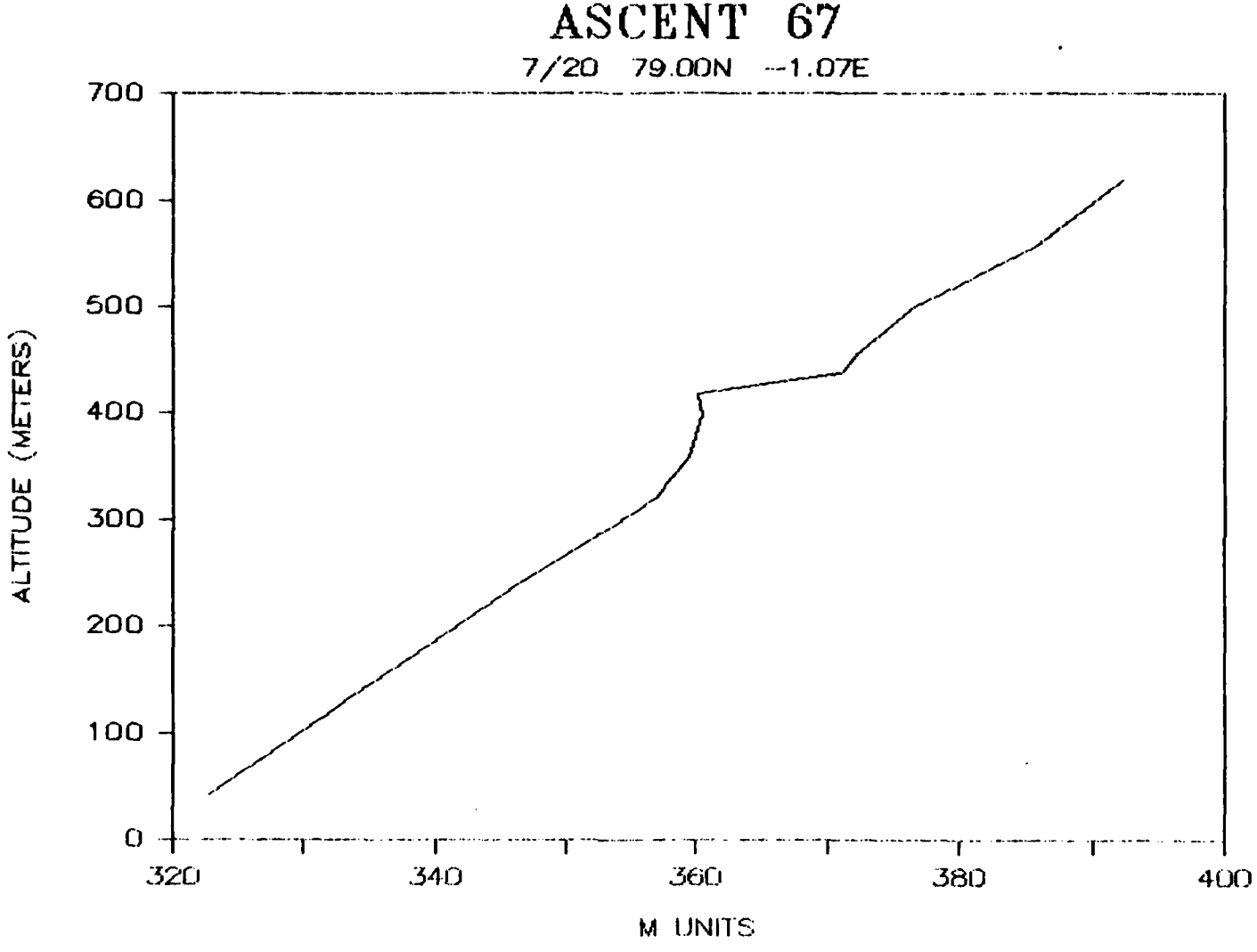
ASCENT 67
7/20 79.00N --1.07E
700
600
500
400
300
200
100
0
ALTITUDE (METERS)
320
340
360
380
400
M UNITS

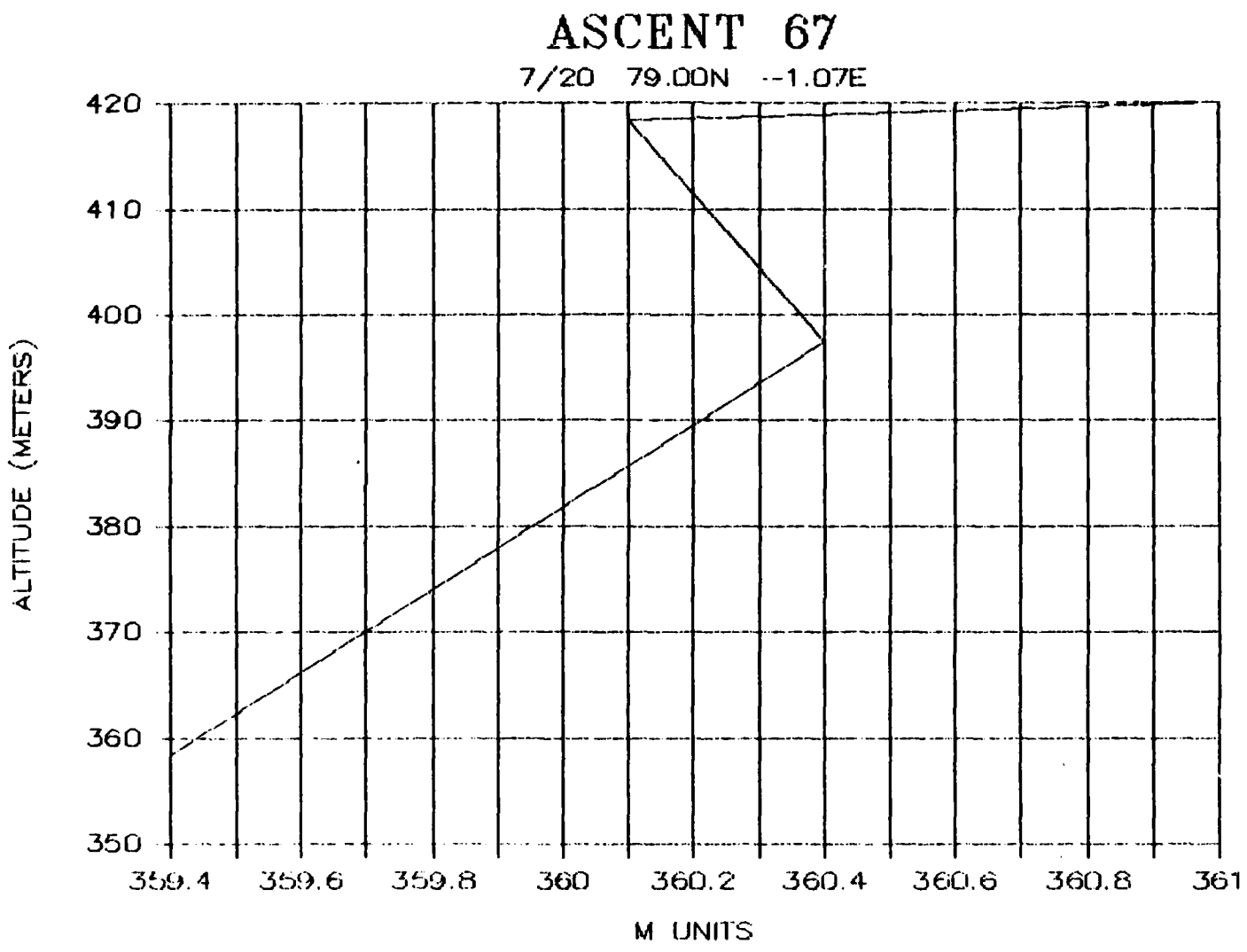
ASCENT 67
7/20 79.00N --1.07E
ALTITUDE (METERS)
420
410
400
390
380
370
360
350
359.4
359.6
359.8
360
360.2
360.4
360.6
360.8
361
M UNITS

ASCENT 68

7/20 78.97N -1.39E

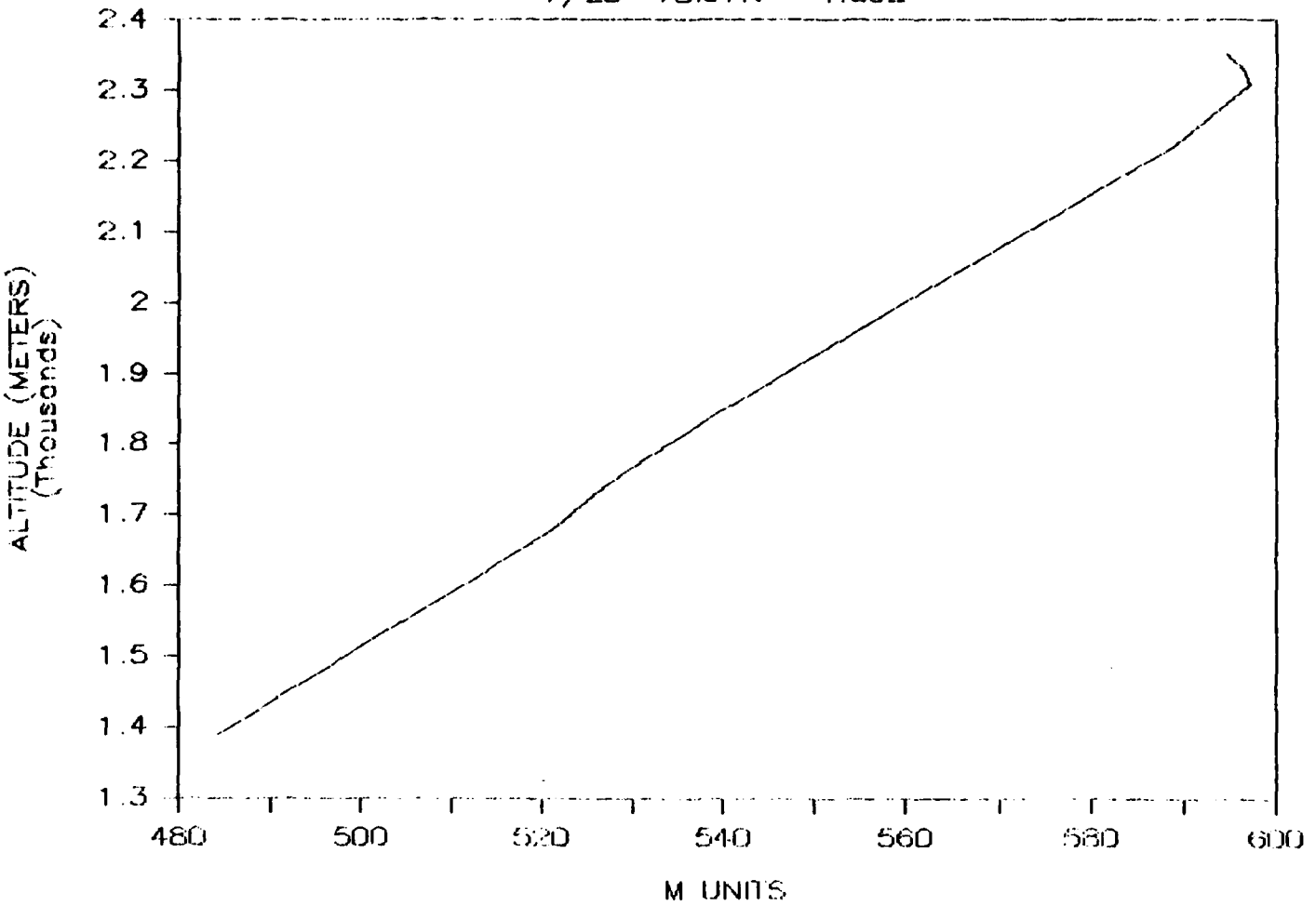

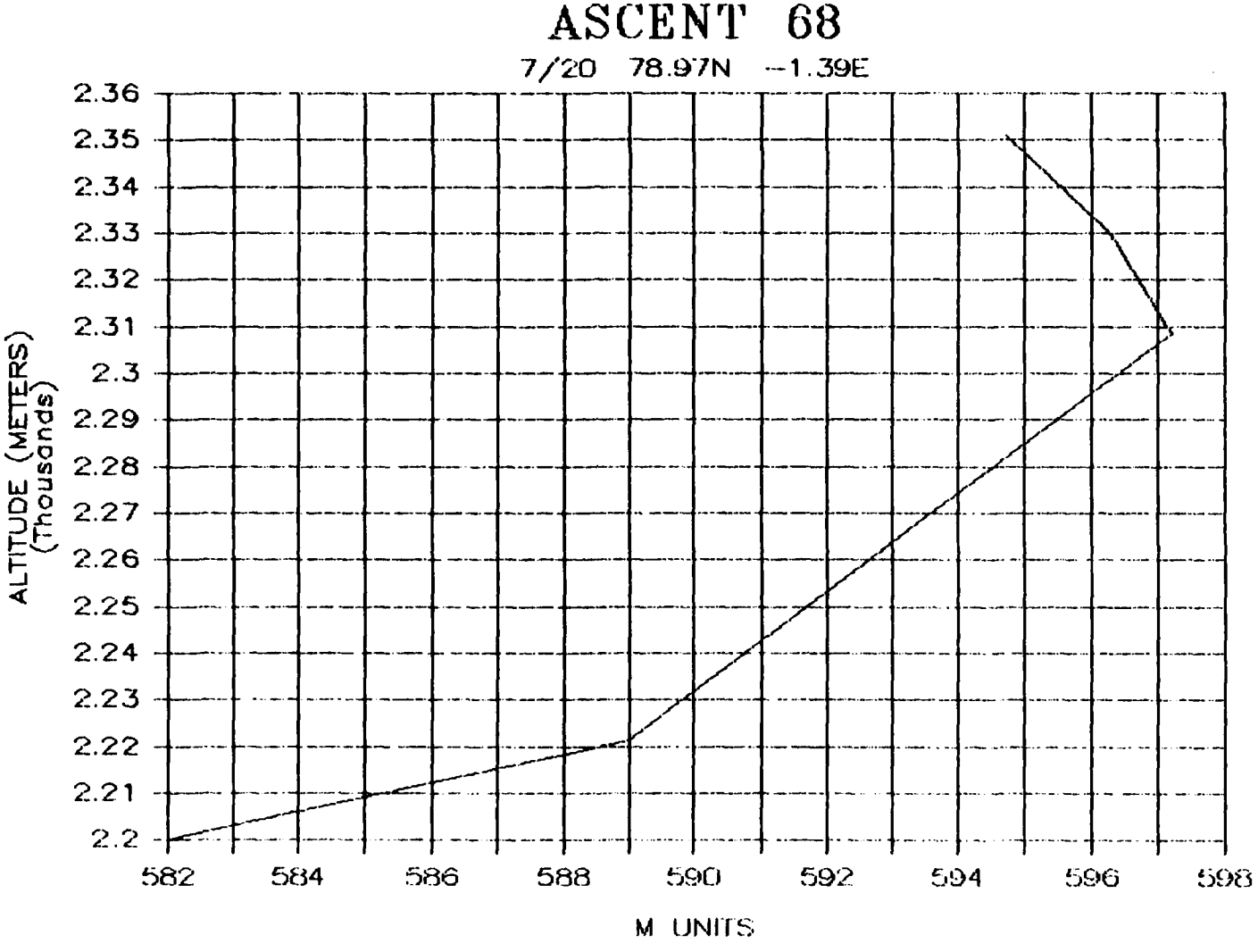
ASCENT 68
7/20 78.97N -1.39E
ALTITUDE (METERS)
(Thousands)
2.36
2.35
2.34
2.33
2.32
2.31
2.3
2.29
2.28
2.27
2.26
2.25
2.24
2.23
2.22
2.21
2.2
582
584
586
588
590
592
594
596
598
M UNITS

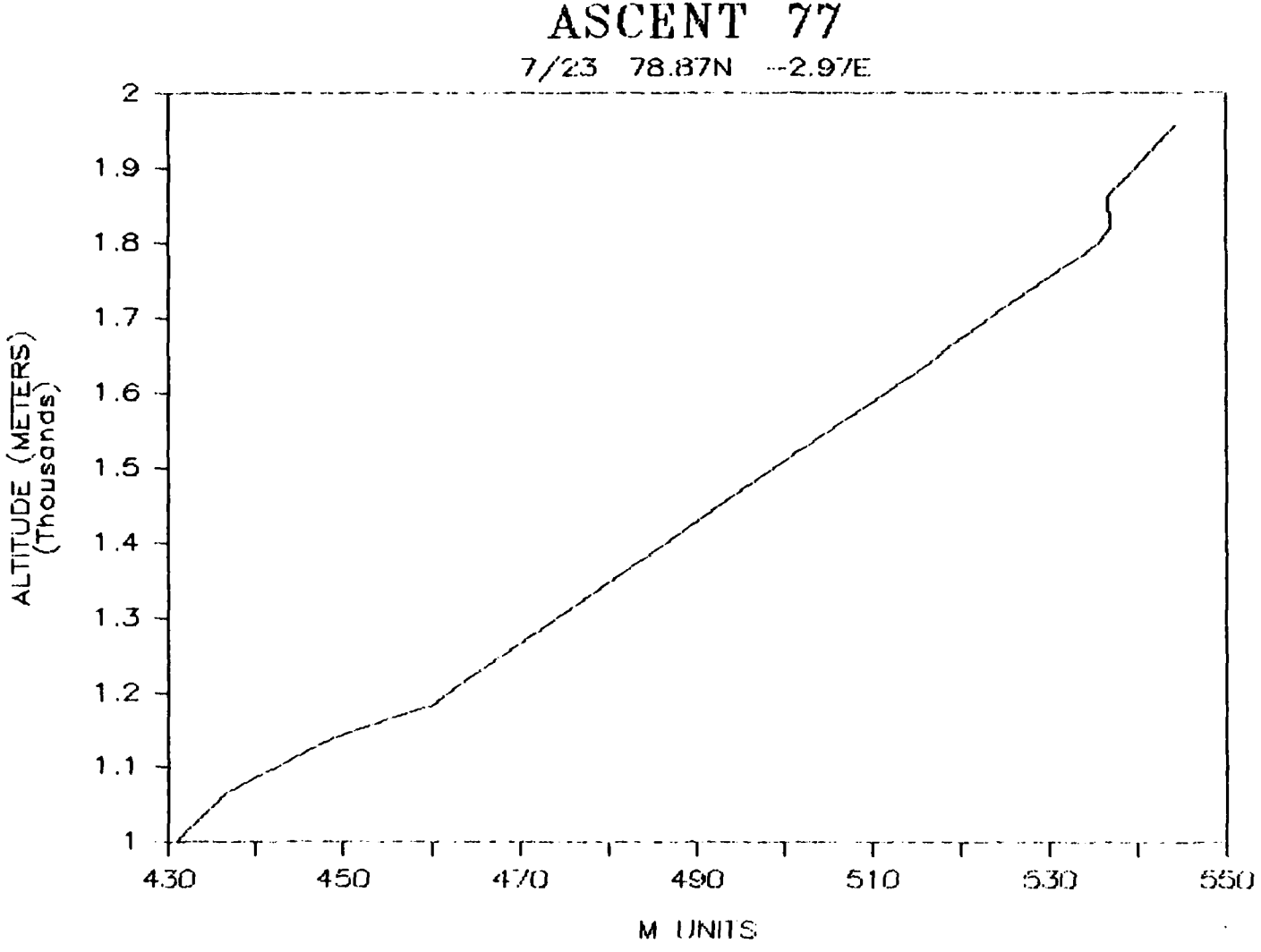
ASCENT 77
7/23 78.87N --2.97E
ALTITUDE (METERS)
(Thousands)
2
1.9
1.8
1.7
1.6
1.5
1.4
1.3
1.2
1.1
1
430
450
470
490
510
530
550
M UNITS

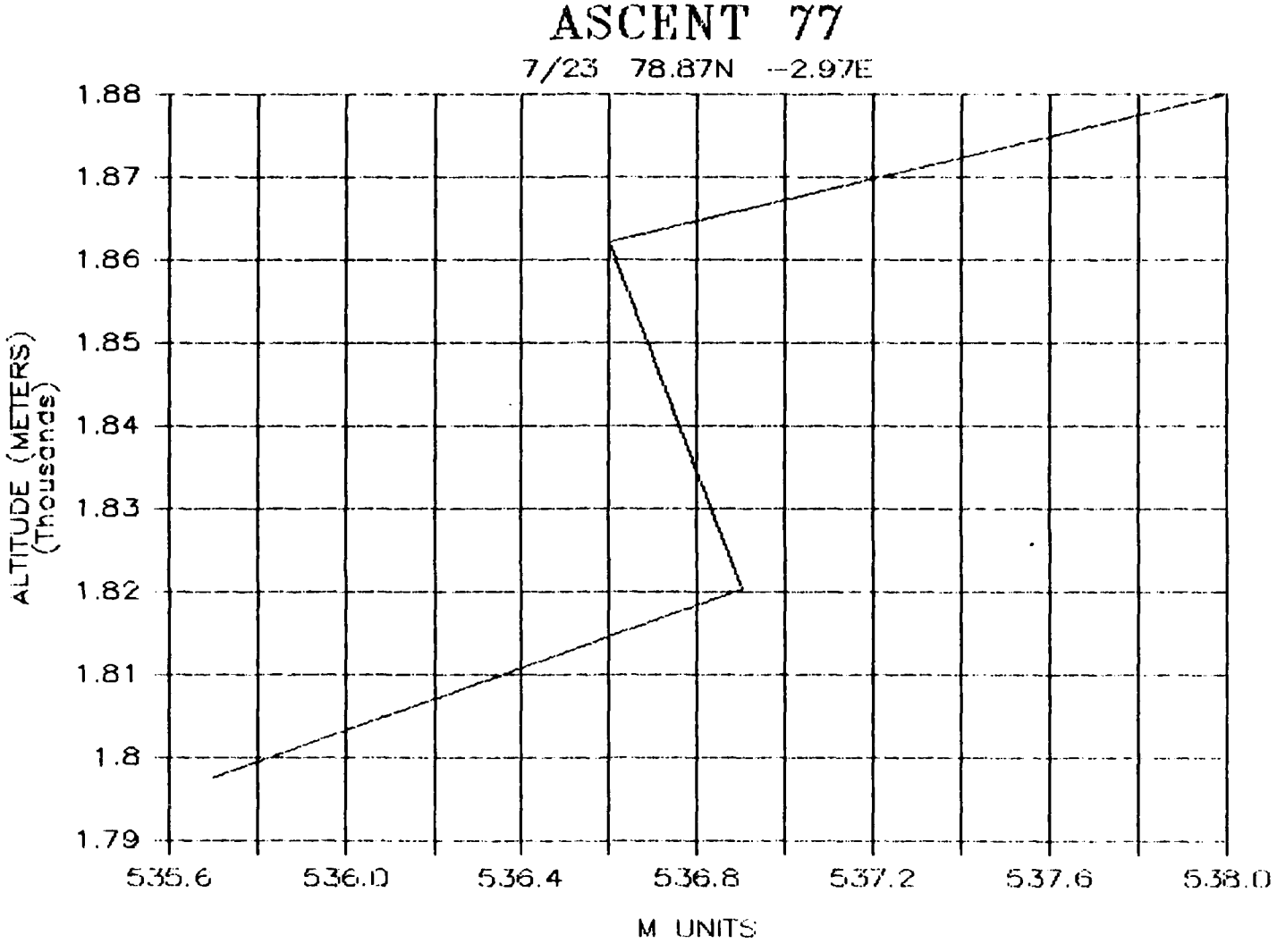
ASCENT 77
7/23 78.87N --2.97E
1.88
1.87
1.86
1.85
1.84
1.83
1.82
1.81
1.8
1.79
ALTITUDE (METERS)
(Thousands)
535.6
536.0
536.4
536.8
537.2
537.6
538.0
M UNITS

ASCENT 79

7/23 78.80N 3.19E

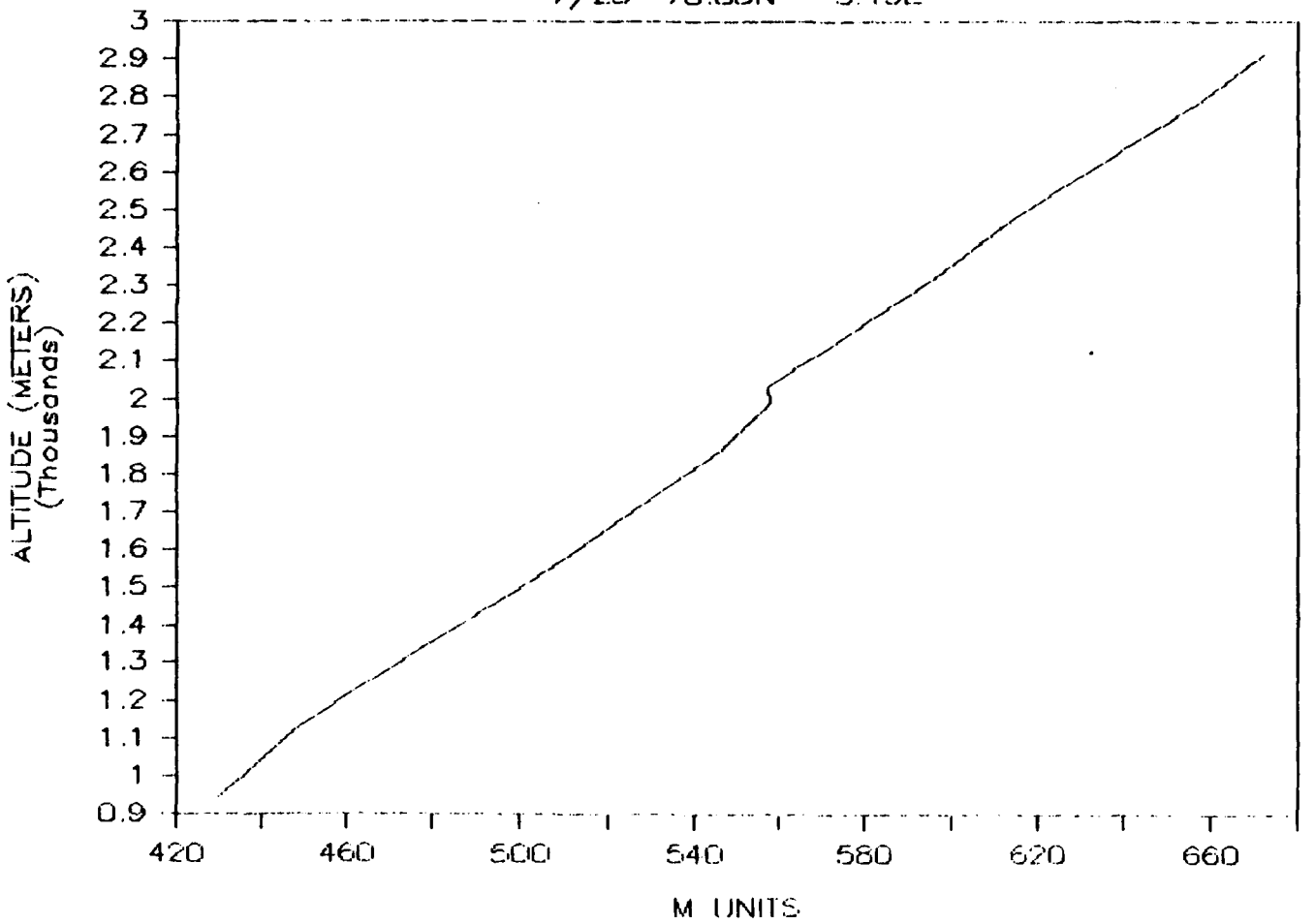

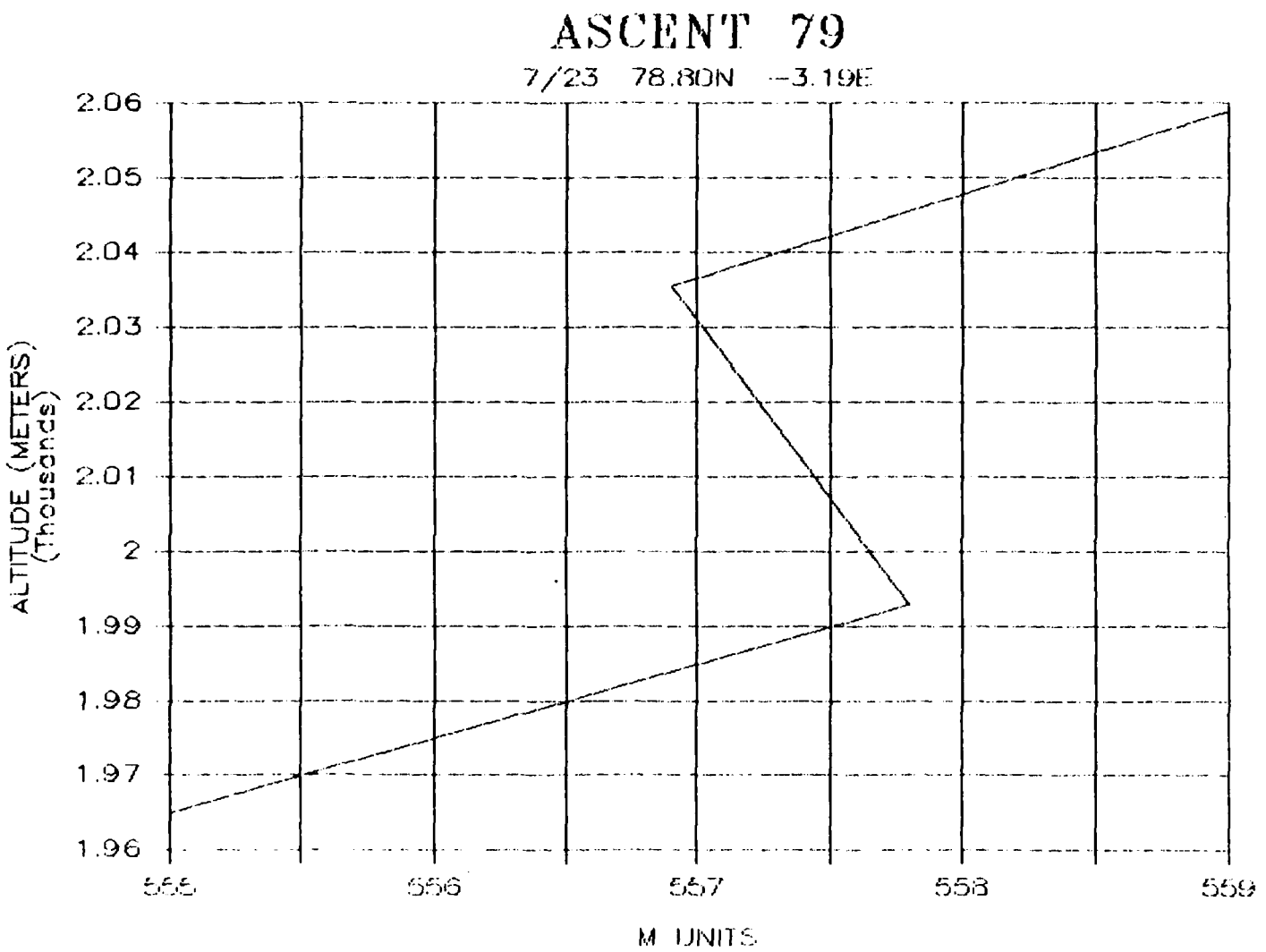
ASCENT 79
7/23 78.80N -3.19E
ALTITUDE (METERS)
(Thousands)
2.06
2.05
2.04
2.03
2.02
2.01
2
1.99
1.98
1.97
1.96
555
556
557
558
559
M UNITS

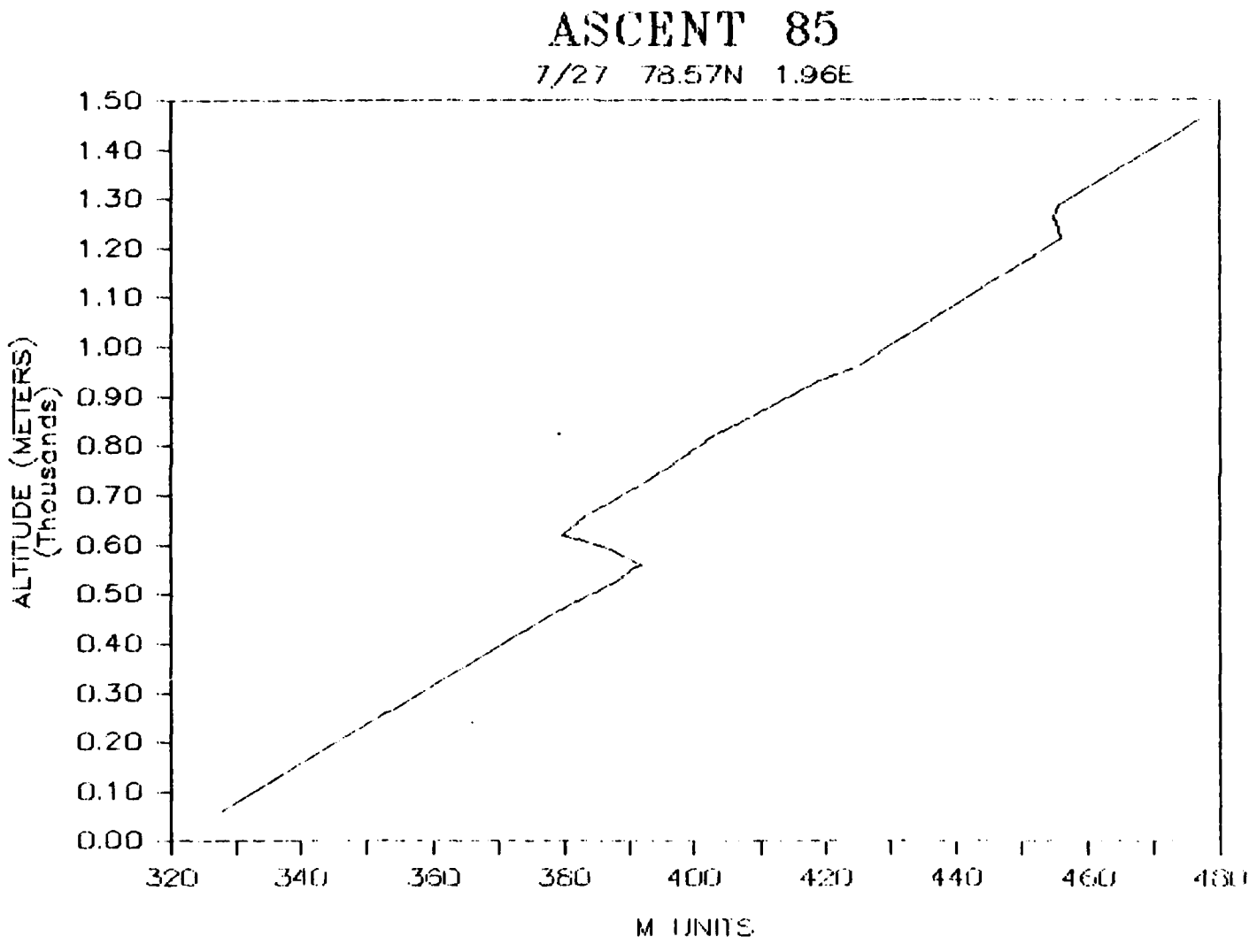
ASCENT 85
7/27 78.57N 1.96E
ALTITUDE (METERS)
(Thousands)
1.50
1.40
1.30
1.20
1.10
1.00
0.90
0.80
0.70
0.60
0.50
0.40
0.30
0.20
0.10
0.00
320
340
360
380
400
420
440
460
480
M UNITS

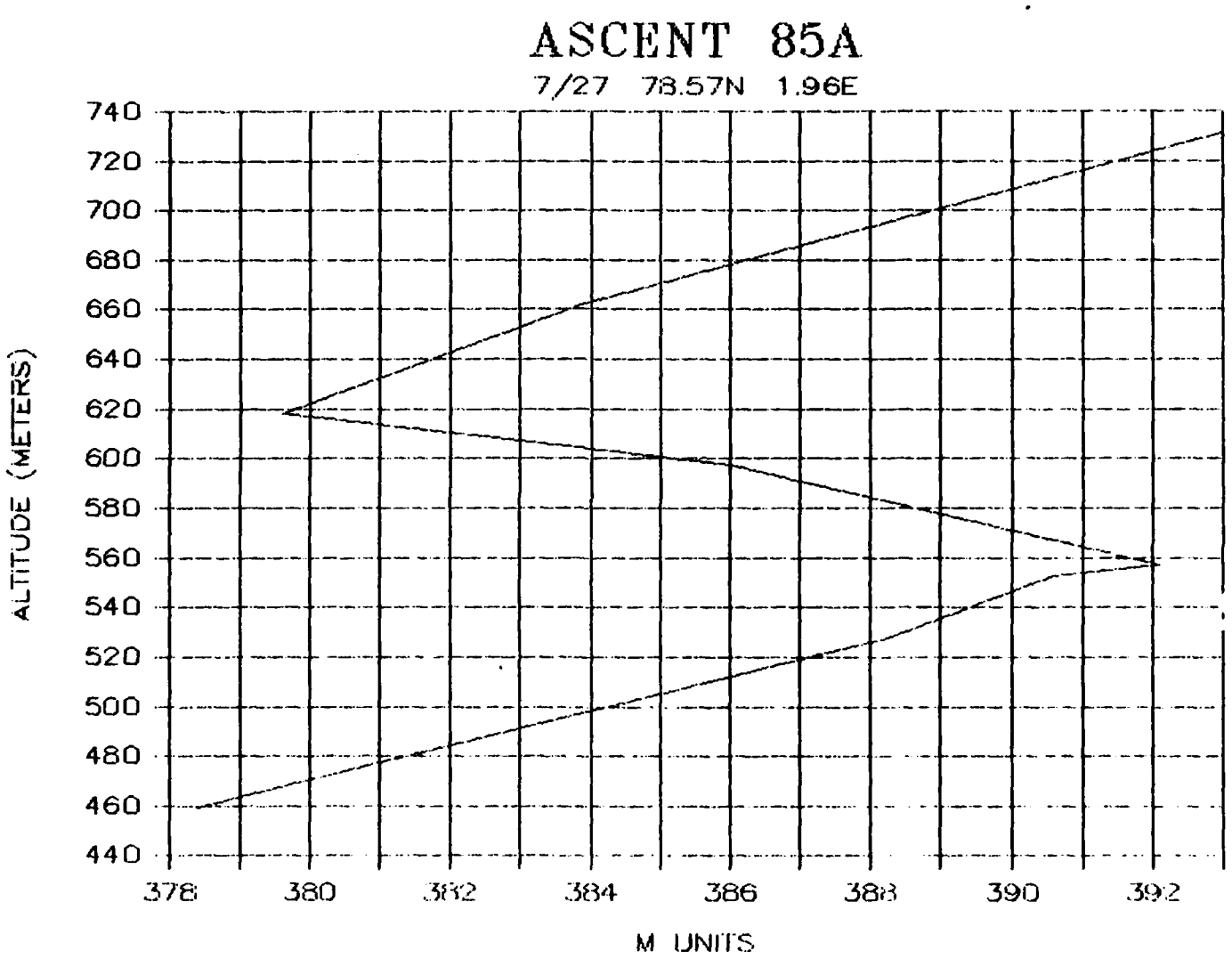
ASCENT 85A
7/27 78.57N 1.96E
ALTITUDE (METERS)
740
720
700
680
660
640
620
600
580
560
540
520
500
480
460
440
378
380
382
384
386
388
390
392
M UNITS

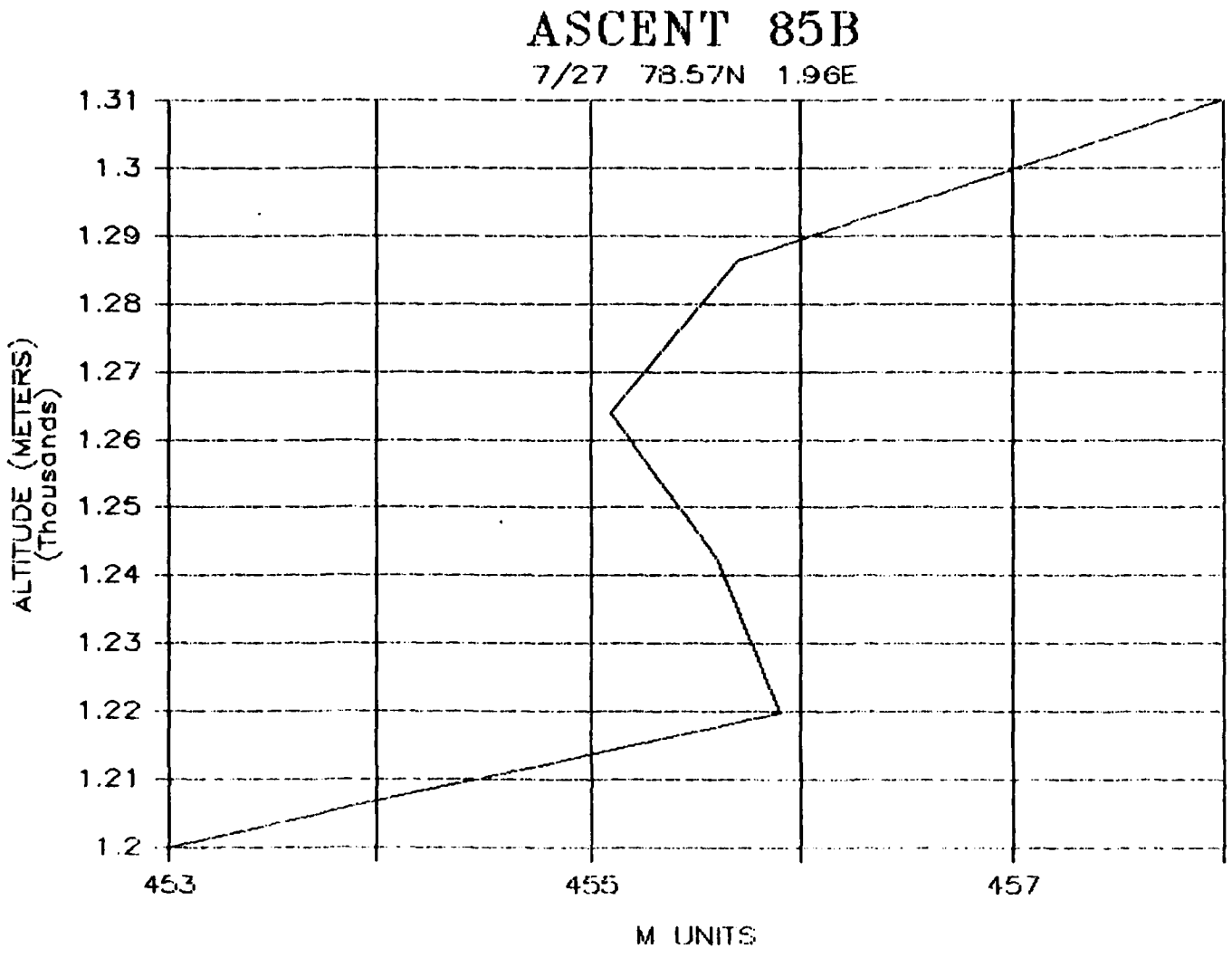
ASCENT 85B
7/27 78.57N 1.96E
1.31
1.3
1.29
1.28
1.27
1.26
1.25
1.24
1.23
1.22
1.21
1.2
ALTITUDE (METERS)
(Thousands)
453
455
457
M UNITS

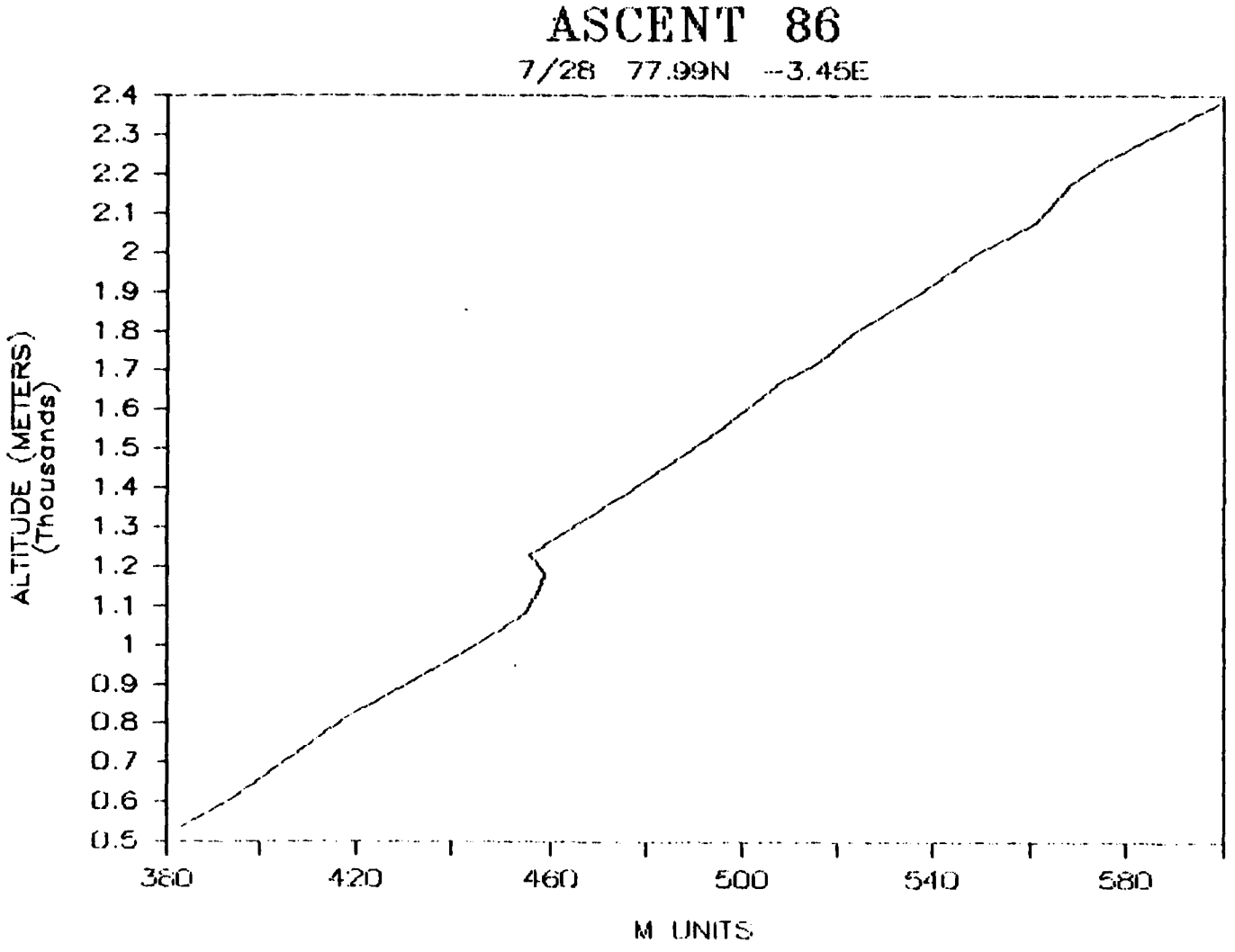
ASCENT 86
7/28 77.99N -3.45E
ALTITUDE (METERS)
(Thousands)
2.4
2.3
2.2
2.1
2
1.9
1.8
1.7
1.6
1.5
1.4
1.3
1.2
1.1
1
0.9
0.8
0.7
0.6
0.5
380
420
460
500
540
580
M UNITS

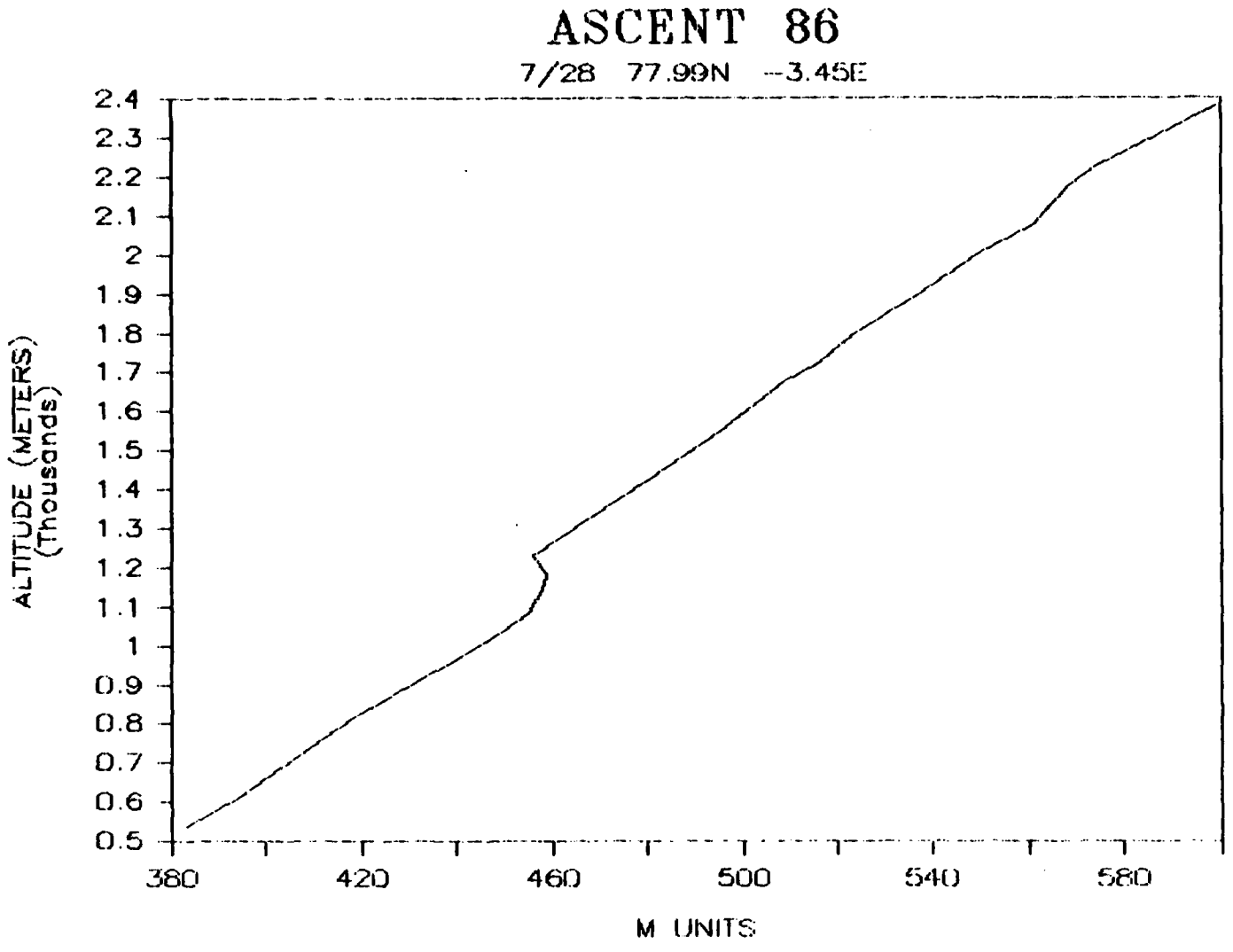
ASCENT 86
7/28 77.99N -3.45E
ALTITUDE (METERS)
(Thousands)
2.4
2.3
2.2
2.1
2
1.9
1.8
1.7
1.6
1.5
1.4
1.3
1.2
1.1
1
0.9
0.8
0.7
0.6
0.5
380
420
460
500
540
580
M UNITS

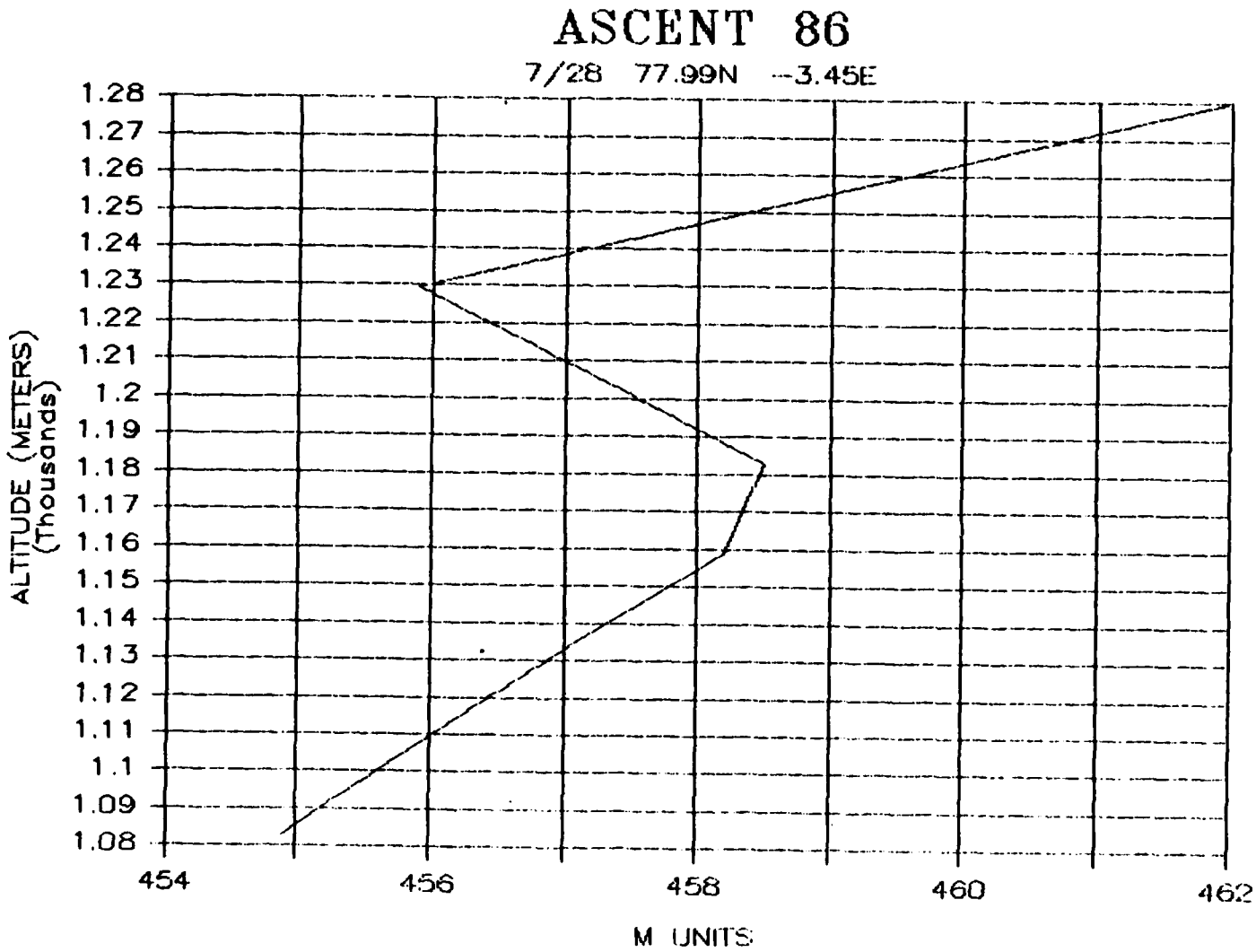
ASCENT 86
7/28 77.99N -3.45E
ALTITUDE (METERS)
(Thousands)
1.28
1.27
1.26
1.25
1.24
1.23
1.22
1.21
1.2
1.19
1.18
1.17
1.16
1.15
1.14
1.13
1.12
1.11
1.1
1.09
1.08
454
456
458
460
462
M UNITS

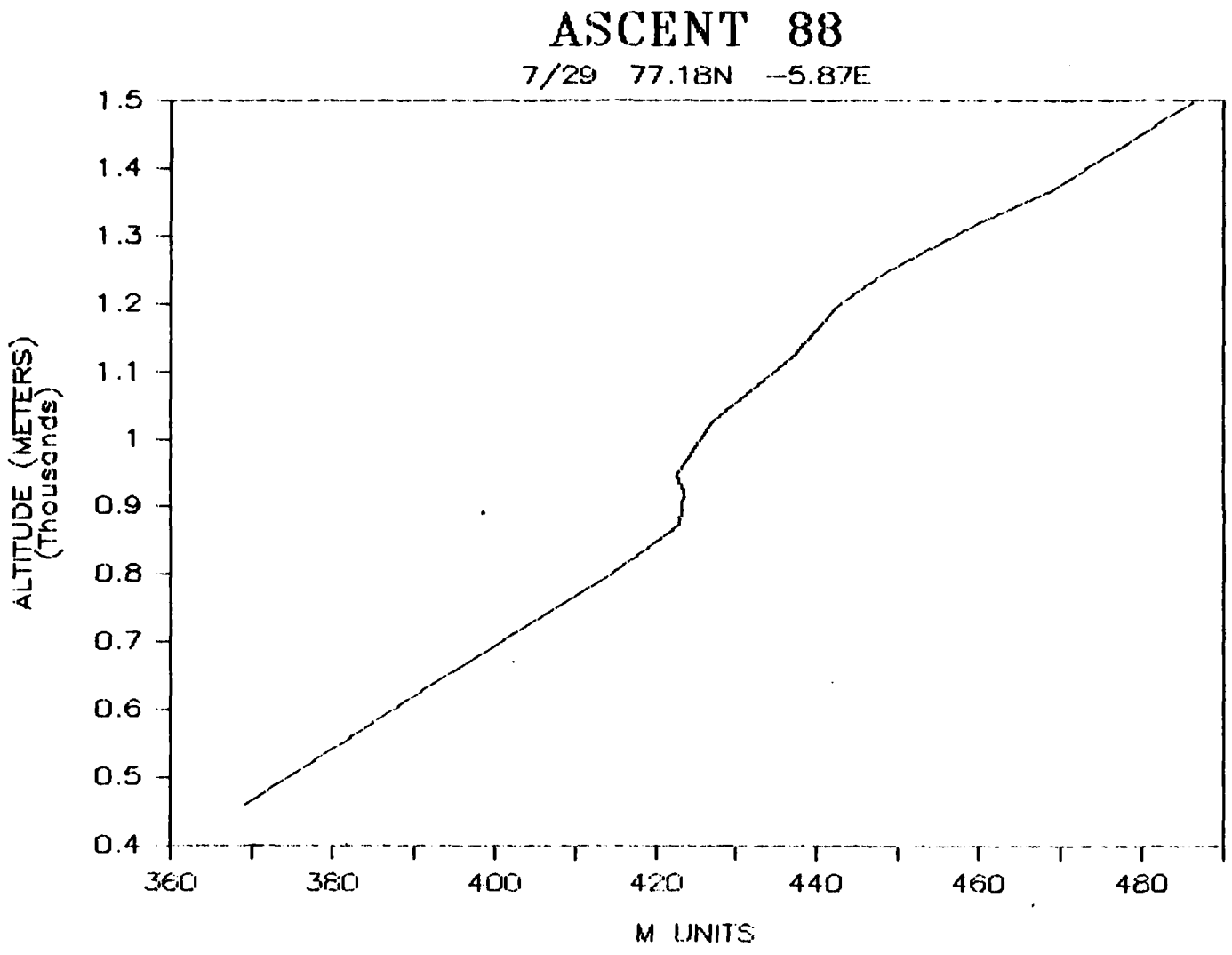
ASCENT 88
7/29 77.18N -5.87E
ALTITUDE (METERS)
(Thousands)
1.5
1.4
1.3
1.2
1.1
1
0.9
0.8
0.7
0.6
0.5
0.4
360
380
400
420
440
460
480
M UNITS

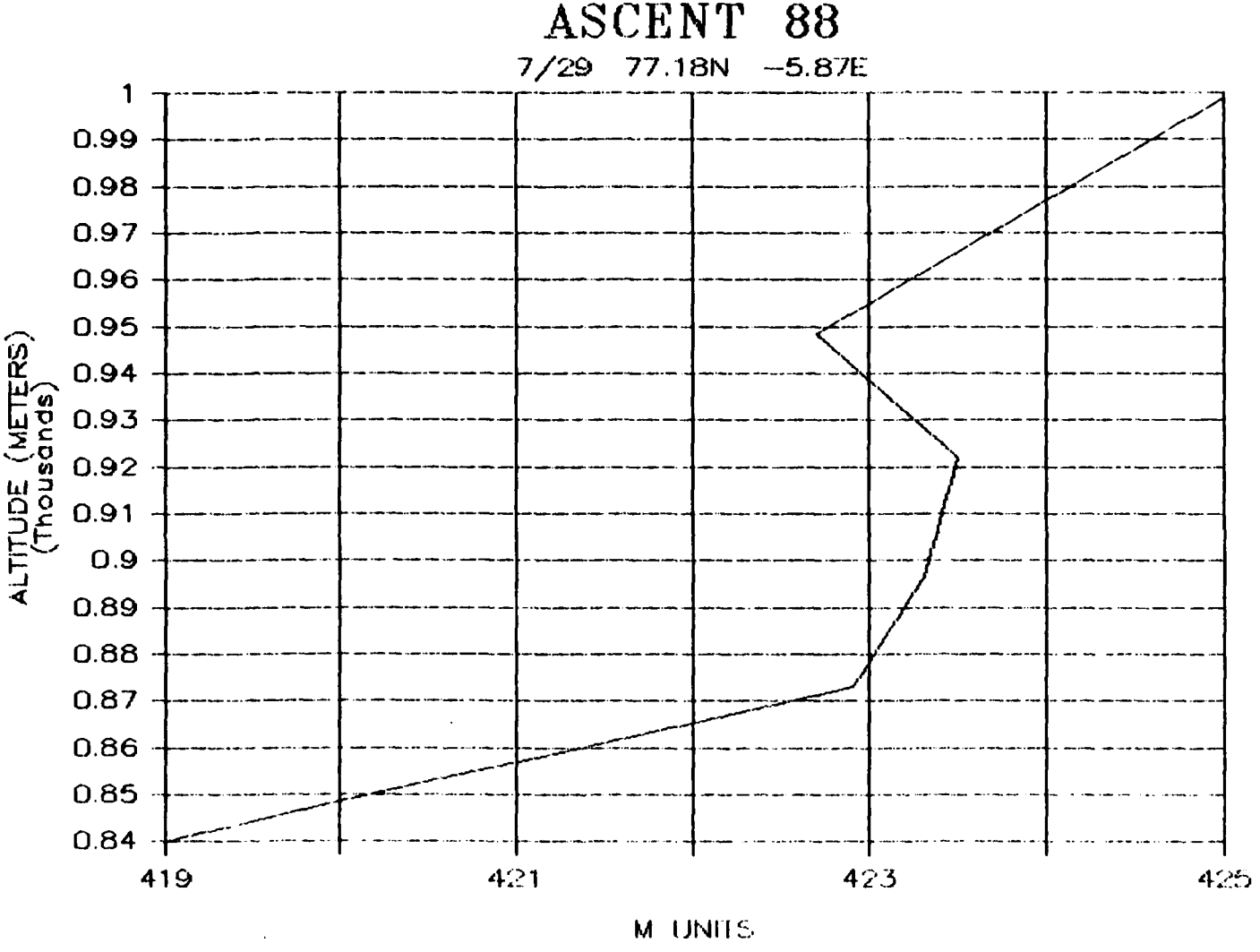
ASCENT 88
7/29 77.18N -5.87E
ALTITUDE (METERS)
(Thousands)
1
0.99
0.98
0.97
0.96
0.95
0.94
0.93
0.92
0.91
0.9
0.89
0.88
0.87
0.86
0.85
0.84
419
421
423
425
M UNITS

LIST OF REFERENCES

Beach, J.B., "Atmospheric Effects On Radio Wave Propagation", Defense Electronics Technology, vol. 11, no. 12, December, 1979.

Hecht, E., Zajac, A., Optics, Addison-Wesley Publishing Company, 1979.

Naval Ocean Systems Center Technical Document 238, Integrated Refractive Effects Prediction System (IREPS), Interim User's Manual, by H.V. Hitney and R.A. Paulus, March 1979.

Kerr, D.E., Propagation of Short Radio Waves, McGraw-Hill, 1951.

Macklin, S.A., "Wind Drag Coefficient Over First-Year Sea Ice in the Bering Sea", Journal of Geophysical Research, v. 88, p. 2845, 30 March 1983.

Knorr, J.B., Methodology for Computation of the Power Distribution of Signals Propagated Through Elevated Tropospheric Ducts, Technical Report Number NPS-62-82-044, Naval Postgraduate School, Monterey, Ca., September 1982.

Neiburger, M., Edinger J.G., and Bonner, W.E., Understanding Our Atmospheric Environment, Freeman and Co., 1982, pp. pp. 208-234.

Ortenburger, L.N., et al, Radiosonde Data Analysis II, GTE Sylvania Inc., February 1978.

Overland, J.E., et al, "A Model of the Atmospheric Boundary Layer Over the Marginal Ice Zone", Journal of Geophysical Research, v. 88, p. 2836, 30 March 1983.

Naval Ocean Systems Center Technical Document 260, Surface Duct Effects on Radio/ESM Detection Range, by Lt. R.A. Paulus and H.V. Hitney, 15 June 1979.

Naval Ocean Systems Center Technical Report 260, Procedings of Conference On Atmospheric Refractive Effects Assessment, by J.H. Richter, pp 165 -167, 15 June 1979.

Pacific Missile Test Center Technical Publication TP000005, Guide For Inferring Refractive Conditions From Synoptic Parameters, by R.A. Helvey and J.S. Rosenthal, 14 March 1983, p. 9.

Tipler, P. A., Physics, Worth Publishers, Inc., 1976, p. 832.

U.S. Army Cold Regions Research and Engineering Laboratory Special Report 84-7, MIZEX Bulletin, April 1984.

INITIAL DISTRIBUTION LIST

		No. Copies
1.	Defense Technical Information Center Cameron Station Alexandria, Virginia 22314	2
2.	Superintendent Attn: Library, Code 0142 Naval Postgraduate School Monterey, California 93943	2
3.	Commanding Officer Attn: LCDR C.T. Sutherlin Code 7501, Bldg 605, Rm 112 Naval Ocean Systems Center San Diego, California 92152	1
4.	Superintendent Attn: W.J. Shaw, Code 63 SR Department of Meteorology Naval Postgraduate School Monterey, California 93943	7
5.	Superintendent Attn: Chairman, Code 73 Electronic Warfare Academic Group Naval Postgraduate School Monterey, California 93943	1
6.	Superintendent Attn: CDR Don East Naval War College Newport, Rhode Island 02840	1

END

FILMED

5-85

DTIC